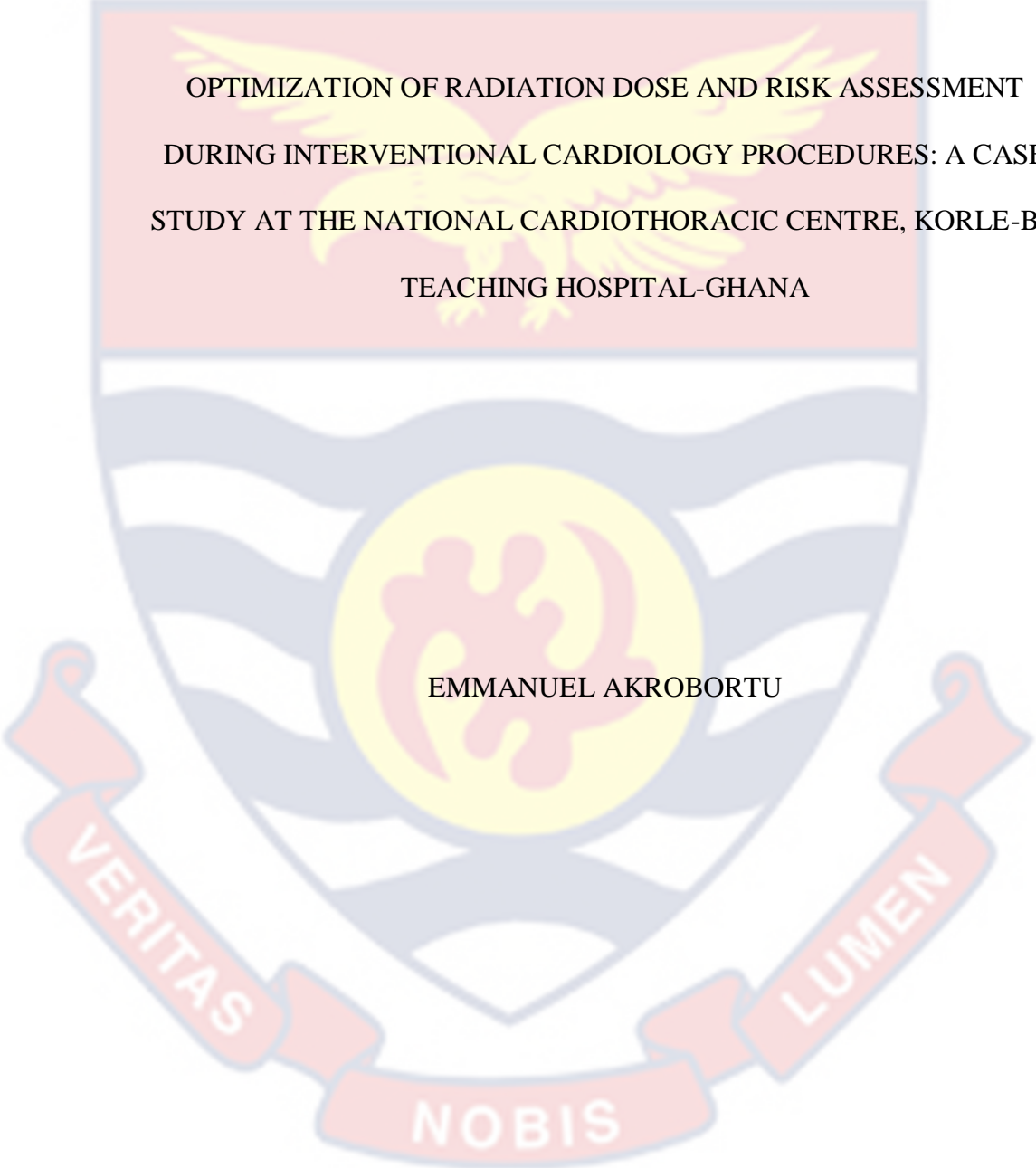


UNIVERSITY OF CAPE COAST

The background of the page features a large, faint watermark of the University of Cape Coast crest. The crest is a shield with a red top section containing a yellow eagle with wings spread. Below the eagle are blue and white wavy lines. In the center of the shield is a yellow circle containing a red stylized human figure. At the bottom of the shield is a red banner with the Latin motto "VERITAS LUMEN NOBIS" in white capital letters.

OPTIMIZATION OF RADIATION DOSE AND RISK ASSESSMENT
DURING INTERVENTIONAL CARDIOLOGY PROCEDURES: A CASE
STUDY AT THE NATIONAL CARDIOTHORACIC CENTRE, KORLE-BU
TEACHING HOSPITAL-GHANA

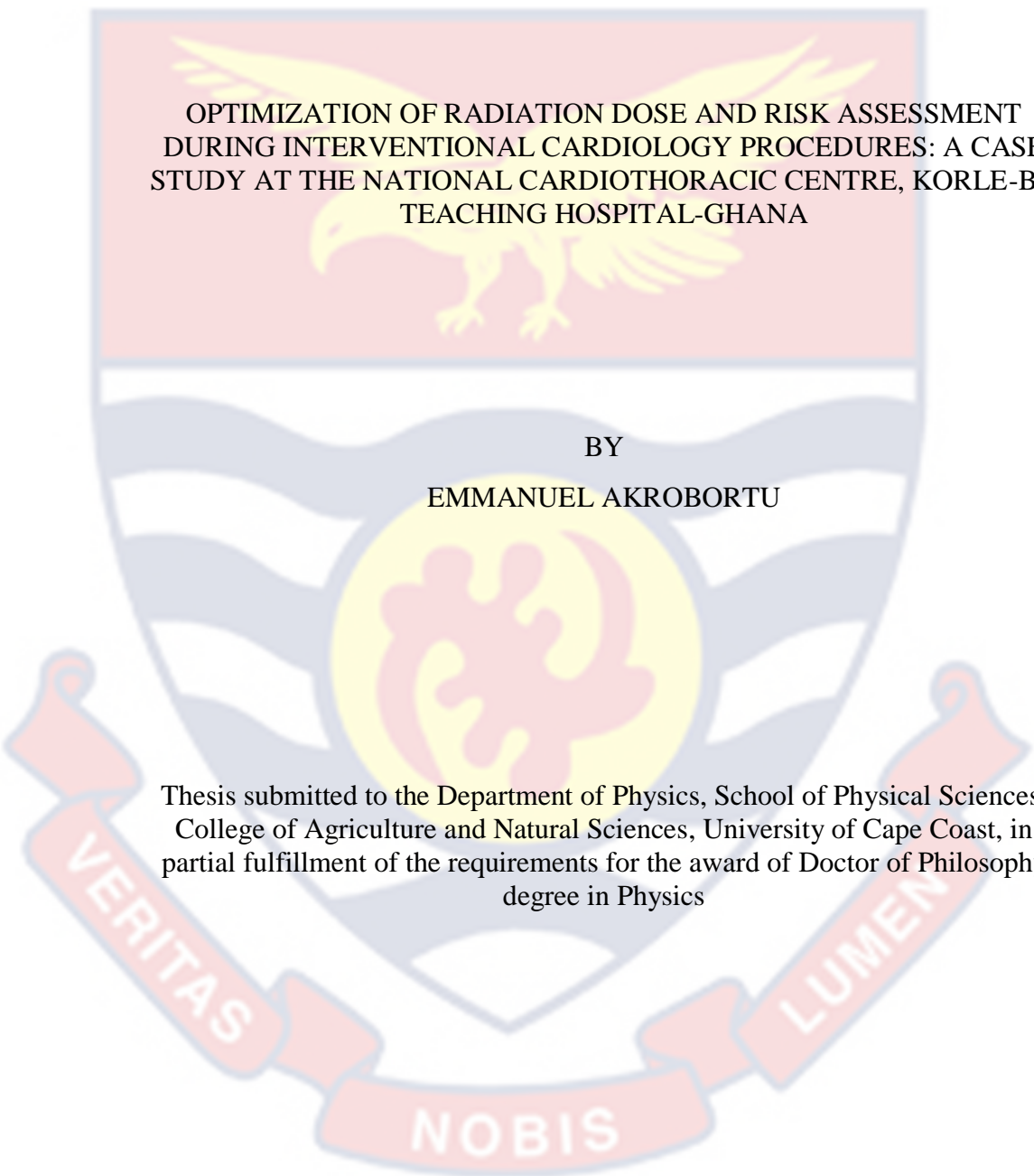
EMMANUEL AKROBORTU

2023



© Emmanuel Akrobortu
University of Cape Coast

UNIVERSITY OF CAPE COAST



OPTIMIZATION OF RADIATION DOSE AND RISK ASSESSMENT
DURING INTERVENTIONAL CARDIOLOGY PROCEDURES: A CASE
STUDY AT THE NATIONAL CARDIOTHORACIC CENTRE, KORLE-BU
TEACHING HOSPITAL-GHANA

BY

EMMANUEL AKROBORTU

Thesis submitted to the Department of Physics, School of Physical Sciences,
College of Agriculture and Natural Sciences, University of Cape Coast, in
partial fulfillment of the requirements for the award of Doctor of Philosophy
degree in Physics

AUGUST 2023

DECLARATION

Candidate's Declaration

I hereby declare that this thesis is the result of my own original research and that no part of it has been present in another degree in this university or elsewhere.

Candidate's Signature: Date:.....

Name: Emmanuel Akrobertu

Supervisors' Declaration

We hereby declare that the preparation and presentation of the thesis were supervised in accordance with the guidelines on supervision of thesis laid down by the University of Cape Coast.

Principal Supervisor's Signature:..... Date:.....

Name: Professor Mary Boadu

Co-Supervisor's Signature: Date:.....

Name: Professor George Amoako

ABSTRACT

Cardiac intervention procedures involve high radiation doses, hence the need to protect patients and staff from deterministic and stochastic effects. Patients' weight, height, age, and radiation exposure values were measured at the National Cardiothoracic Centre (NCTC), where a number of different interventional cardiology procedures were performed. Body Mass Index (BMI) was calculated from measured weight and height results. Dose data were collected for a total of 498 patients: comprising of 309 males and 189 females. The values for Dose Area Product (DAP) were measured using DAP meter for four cardiovascular examinations namely, Coronary Angiography (CA), Percutaneous Coronary Intervention (PCI), combine Coronary Angiography and Percutaneous Coronary Intervention (CAPCI) and Right Heart Catheterization (RHC). Occupational doses (staff effective doses) were calculated using three different double dosimetry algorithms with two dosimeters (TLDs) that were placed above and below the lead protective apron. Staff total detriment to radiation was estimated using risk coefficients for stochastic effect and the results obtained are $1.76 * 10^{-3}$ for surgeons $7.96 * 10^{-4}$ for nurses and $1.29 * 10^{-4}$ for operators. BMI obtained for females and males were $(29.92 \pm 5.51) \text{ kg/m}^2$ and $(27.14 \pm 4.03) \text{ kg/m}^2$, respectively. Male dose values obtained were $[(17.34 \pm 12.62), (74.77 \pm 11.20), (87.17 \pm 10.72), (34.87 \pm 37.48)] \mu\text{Gycm}^2$ and female dose values were $[(69.44 \pm 76.15), (133.49 \pm 94.37), (80.90 \pm 10.78), (34.27 \pm 35.02)] \mu\text{Gycm}^2$ for CA, PCI, CAPCI and RHC, respectively. Effective doses obtained ranged between $[0.54-2.20), (0.45-1.61), (0.52-1.04)] \text{ mSv}$ for cardiologists, nurses, and operators, respectively.

KEY WORDS

Algorithm

Angiography

Fluoroscopy

Interventional

Radiation

Phantom



ACKNOWLEDGEMENTS

I would like to use this opportunity to express my sincere and heartfelt appreciation to my supervisors: Professor Mary Boadu, Director, Radiological and Medical Sciences Research Institute (RAMSRI), Ghana Atomic Energy Commission, (GAEC) and Professor George Amoako of the Department of Physics, University of Cape Coast. Their excellent advice, thoughtful corrections, and encouragement had brought this study into fruitful end.

In addition, my sincere gratitude goes to Dr Philip Deatanyah and Associate Professor Stephen Inkoom both of Radiation Protection Institute, Ghana Atomic Energy Commission and School of Nuclear and Allied Sciences, University of Ghana, Atomic Campus, for their guidance and support.

Furthermore, my sincere thanks also, goes to the entire staff of the National Cardiothoracic Centre, Korle-Bu Teaching Hospital with a special mention of Dr Abdel Sameed Tanko and Senior Matron Miriam Sarfo, for their support and cooperation during the data collection process. Kudos to my colleagues and friends for their constructive criticism. Finally, I wish to thank my family for their encouragement and support.

DEDICATION

This study is to the Source of my Strength, and the Strength of my life.



TABLE OF CONTENTS

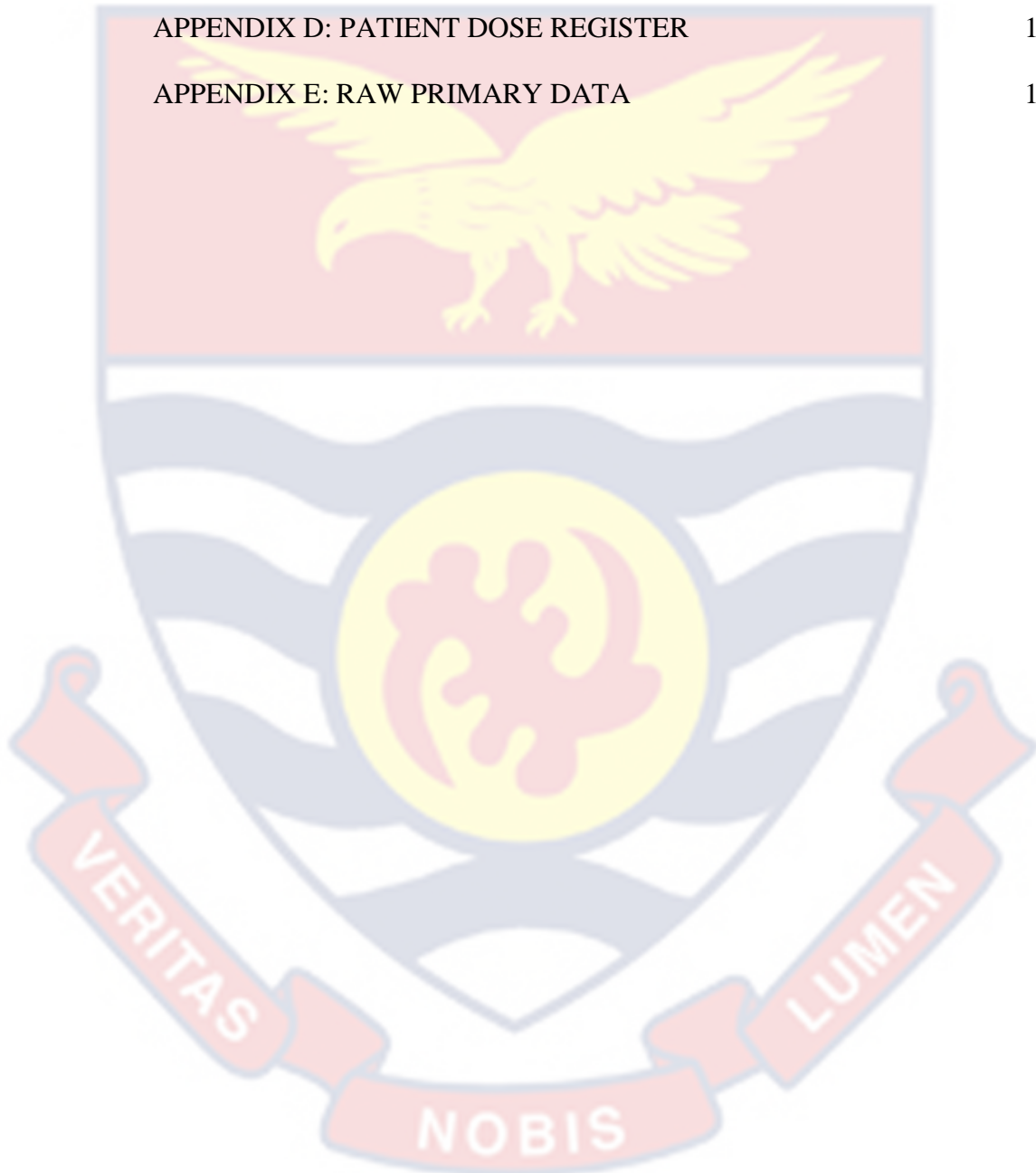
	Page
DECLARATION	ii
ABSTRACT	iii
KEY WORDS	iv
ACKNOWLEDGEMENTS	v
DEDICATION	vi
LIST OF TABLES	xi
LIST OF ABBREVIATIONS	xviii
CHAPTER ONE: INTRODUCTION	
Background to the Study	1
Problem Statement	3
Purpose of the Study	4
Research Objectives	4
Relevance / Justification of Work	5
Delimitations	6
Limitations	6
Organization of the Study	7
CHAPTER TWO: LITERATURE REVIEW	
Introduction	8
The Research Area KBTH	8
The Physics of Fluoroscopy: X-ray Production and Interaction	9
Fluoroscopy Machine (Technology and Mode of Operation)	21
Fluoroscopic Imaging Chain	21

Quality Control and Quality Assurance of the Angiography System	23
Review of Patient and Staff doses in Clinical Practice	24
Radiation Exposures to Patients in Diagnostic and Therapeutic Cardiac Catheterization	26
Staff Dosimetry	28
Cardiac Examinations	30
Basic Principles of Body Parameters and Radiation Exposures	33
General Model of Thermoluminescence Dosimetry	35
Chapter Summary	37
CHAPTER THREE: MATERIALS AND METHODS	
Introduction	38
Research Site	38
Equipment	38
Source: www.osti.gov/servlets/pur/1690410	41
Thermoluminescent Dosimeters	42
Sample Size	43
Methods	43
QC Measurements	47
Radiation Dose Measurement	49
Scatter Radiation Study in the Angiography Room	51
MCNP Simulations	56
Whole Body Dose Calculation	56
Risk from Radiation Exposure	57
Data Analysis	57
Chapter Summary	58

CHAPTER FOUR: RESULTS AND DISCUSSIONS

Introduction	59
Quality Assurance and Quality Control Procedure	59
Measured Body Parameters	62
Variation of Dose with BMI	63
Statistical Parameters Relating to Cardiology Procedures	67
Empirical Modelling	73
Modelled DAP and BMI Representations	75
Analysis of Dose Optimization	92
Converting Modelled Equations to Graphical User Interface (GUI)	92
Staff Effective Dose Using Double Dosimetry Algorithm	94
General Information on Radiation Protection and Safety in the Cath Lab	108
Scattered Radiation to Occupationally Exposed Workers in the Examination Room	111
Comparison of this Study with other Studies	111
Chapter Summary	113
CHAPTER FIVE: OVERVIEW, SUMMARY, CONCLUSION AND RECOMMENDATION	
Overview	114
Conclusions	115
Recommendations	116
REFERENCES	118
APPENDICES	126
APPENDIX A: MODELLING DAP AND BMI FOR MALE PATIENTS	126

APPENDIX B: MODELLING DAP AND BMI FOR FEMALE PATIENTS	130
APPENDIX C-1: ETHICAL CLEARANCE FROM UCC	133
APPENDIX C-2: ETHICAL CLEARANCE FROM KBTH	134
APPENDIX D: PATIENT DOSE REGISTER	136
APPENDIX E: RAW PRIMARY DATA	137



LIST OF TABLES

	Page
1 Radiological Specifications of the MagicMax QC kits	40
2 Characteristics of the dose rate meter (Radiagem 2000)	41
3 Radiological Specification of the Thermoluminescent Dosimeter	43
4 Algorithm proposed for effective dose calculation with a thyroid collar [adapted from (Järvinen et al., 2008a) and (Cousins et al., 2013a)]	47
5 kVp Accuracy and Reproducibility of the Angiography X-ray equipment	60
6 kVp, Timer, and Exposure Reproducibility of the X-ray equipment	60
7 Exposure Parameter Consistency and Linearity of X-ray equipment	61
8 Measured Height, Weight, Age, BMI for male	62
9 Measured Height, Weight, Age, BMI for female	62
10 Measured DAP, Fluoroscopy Time, kVp, mA for male	66
11 Measured DAP, Fluoroscopy Time, kVp, mA for female	67
12 Frequency of Patients and number of Procedures	67
13 Statistics of Parameters: Dose (DAP), Fluoroscopy time, Age and Body Parameters (BMI) of male	69
14 Statistics of Parameters: Dose (DAP), Body Parameters (BMI), Fluoroscopic time (FT) and Age of female patients during cardiology procedures	70
15 Staff effective dose (mSv) using three different algorithms for all four procedures	94
16 Number of Procedures for each Staff	95

17	Radiation Protection and Safety in the Cath Lab	109
18	Comparison of Patient DAP with other works	112



LIST OF FIGURES

	Page
1 The location of Korle-Bu Teaching Hospital on a map of Ghana indicated by the official logo	9
2 A typical X-ray tube containing evacuated envelope, filament cathode and target anode (Source: www.radiologymasterclass.co.uk)	11
3 The X-ray image intensifier showing its important components (Source: www. Radiology masterclass.co.uk)	13
4 Schematic diagram of the fluoroscopic imaging chain showing X-ray generator, collimator, monitor and other important components	22
5 Internal view of the Cath lab with Siemens (Artis Zee) biplane Angiography unit	39
6 Functional parts of the Thermoluminescent Dosimeter	42
7 CAD model of the Cath lab, showing the front and side views	52
8 Cath lab with showing the concrete walls, the back and with the roofed wall removed.	52
9 A typical head and body CT phantom, showing standard 16 cm head and 32 cm body	54
10 Modified MIRD phantom, representing a surgeon (male and female)	54
11 A PIMAL phantom with movable arms, representing a modified male and female surgeon	54
12 MCNP visual editor modelled of the Cath Lab.	55

13	Percentage distribution of female patients according to the BMI category	64
14	Percentage distribution of male patients according to BMI category	64
15	Variation in Patient DAP with BMI category	65
16	Percentage of males per various cardiac procedure during data collection	68
17	Percentage of females per procedure during data collection	68
18	Male BMI with the various cardiac procedure	71
19	Male DAP with their respective cardiac procedures, showing increasing uncertainty with increasing DAP	71
20	Female BMI with various cardiac procedure	72
21	Female DAP with their respective cardiac procedure, showing increasing uncertainty with increasing DAP.	73
22	Fitted Line Plot of DAP vs BMI for male CA Procedure	77
23	Predicted plot for DAP vs BMI for male CA. The blocked fitted red line shows the predicted DAP for any BMI value and the blue dashed lines show the 95 % prediction interval.	77
24	Fitted Line Plot for DAP vs BMI for male PCI Procedure	79
25	Predicted plot of DAP vs BMI for male PCI. The blocked fitted red line shows the predicted DAP for any BMI value and the blue dashed lines show the 95 % prediction interval	79
26	Fitted Line Plot for DAP vs BMI for male Combined CAPCI Procedure	81

27	Predicted plot of DAP vs BMI for male CAPCI. The blocked fitted red line shows the predicted DAP for any BMI value and the blue dashed lines show the 95 % prediction interval.	81
28	Fitted Line Plot for DAP vs BMI for male RHC Procedure	83
29	Predicted plot of DAP vs BMI for male RHC. The blocked fitted red line shows the predicted DAP for any BMI value and the blue dashed lines show the 95 % prediction interval.	83
30	Fitted Line Plot for DAP vs BMI for female CA Procedure	85
31	Predicted plot of DAP vs BMI for female CA. The blocked fitted red line shows the predicted DAP for any BMI value and the blue dashed lines show the 95 % prediction interval.	85
32	Fitted Line plot for DAP vs BMI for female PCI Procedure	87
33	Predicted plot of DAP vs BMI for female PCI with the blocked fitted red line showing the predicted DAP for any BMI value and the blue dashed lines showing the 95 % prediction interval	87
34	Fitted Line Plot for DAP vs BMI for female combined CAPCI Procedure	89
35	Predicted plot of DAP vs BMI for female combined CAPCI. The blocked fitted red line shows the predicted DAP for any BMI value and the blue dashed lines show the 95 % prediction interval	89
36	Fitted Line Plot for DAP vs BMI for female RHC Procedure	91
37	Predicted plot of DAP vs BMI for female RHC. The blocked fitted red line shows the predicted DAP for any BMI values and the blue dashed lines show the 95 % prediction interval	91
38	A flow diagram of the GUI modelling process.	93

39	A snapshot of the developed GUI	93
40	Staff Effective Dose by three different Algorithms	95
41	Staff effective Dose compared with ICRP Limit	96
42	Staff radiation dose using Chida et al, (2013), algorithm. The box represents first and third quartiles and the line in between indicate the median.	101
43	Staff radiation dose using NCRP 122, 1995 algorithm. The box shows the 25 th and 75 th percentiles with line between being the median	102
44	Staff radiation dose using Swiss et al. (2008), algorithm. The box represents the lower and upper quartiles whilst the line in between the median.	103
45	Staff radiation dose per CA Procedure. The box shows the first and third quartiles whilst the line in between the median.	104
46	Staff radiation dose per PCI Procedure with the box showing the lower and upper quartiles, whilst the line in between is the median	105
47	Staff radiation dose per combined CAPCI Procedure. The box represents the 25 th and 75 th percentiles with line in between being the median	106
48	Staff radiation dose per RHC Procedure with the box representing the 25 th and 75 th percentiles and the line in between is the 50 th percentile dose	107

49 Estimated Risk of Occupationally Exposed Workers considered
in the study, showing the staff with the low and high risk in
percentage 110

50 Result of Scattered Radiation in the Examination Room,
showing vantage positions for kVp of between 60 to 120 111



LIST OF ABBREVIATIONS

CCD	Charge Coupled Device
CAD	Coronary Artery Disease
ERA	Energy-Resolved Angiography

FPD	Flat Panel Detector
FT	Fluoroscopy Time
ISO	International Standards Organization
LCD	Liquid Crystal Detector
LED	Light Emitting Diode
NCRP	National Commission on Radiological Protection
NCTC	National Cardiothoracic Centre
PCI	Percutaneous Coronary Intervention
PMT	Photo Multiplier Tube
RHC	Right Heart Catheterization
TFT	Thin Film Transistor



CHAPTER ONE

INTRODUCTION

Background to the Study

The branch of medicine that deals specifically with the heart is known as cardiology. X-rays are used to perform life-saving procedures on the heart, for millions of people every year. The procedures often referred to as interventional cardiology procedures, include; Percutaneous Coronary Intervention (PCI), combined Coronary Angiography and Percutaneous Coronary Intervention (CAPCI), Transjugular Intrahepatic Portosystemic Shunt Creation (TIPS), head/neck endovascular therapeutic exams, and Right Heart Catheterization (RHC) (Kim et al., 2012).

In cardiology, a patient's radiation exposure is due primarily to interventional cardiac procedures which are increasing in number and account for an important share of patient radiation exposure in medicine. Some cardiac procedures such as electrophysiology, complex percutaneous coronary interventions are associated with high radiation doses and dose thresholds such as 2-6 Gy for erythema, 3 Gy for hair loss, and 18 Gy for necrosis have been established (Stratis et al., 2009a). As a result of these procedures, patient skin doses can be as high as 2-6 Gy to cause radiation injury and increase the risk of cancer (Stratis et al., 2009b).

Furthermore, occupational workers in catheterization and electrophysiology laboratories where cardiac examinations are performed, can receive high radiation doses when radiological protective tools are absent or improperly used. (Cousins et al., 2013a). Angiography is the process of imaging

cardiac arteries and the procedure is called angioplasty, most often referred to as Percutaneous Transluminal Coronary Angioplasty (PTCA) (WHO, 2011).

Procedures that require real-time radiological imaging of a patient's internal structures for diagnostic or therapeutic purposes are termed fluoroscopically guided (FG) procedures. These procedures are used to treat a growing range of diseases and injuries by a variety of physician specialists such as interventional radiologists, neuroradiologists, cardiologists, electrophysiologists, orthopedic surgeons, urologists, and gastroenterologists. Examples of some functional conditions or structures that can be treated using FG procedures include disorders of the heart, blood vessels, gastrointestinal system, biliary tract, bladder, ureters, and kidneys.

For minimally invasive examinations such as hip fracture plating, nailing, external fixation, and other orthopedic procedures, fluoroscopic imaging has been adopted and used (Kim et al., 2012). Ionizing radiation is used to guide small instruments through blood vessels or other body pathways to sites of clinical interest during interventional image-guided procedures. Interventional procedures, therefore, the alternative to invasive surgery is the use of ionizing radiation to provide image guidance for catheters and other small instruments through blood vessels and other body pathways to surgical areas of interest. By these techniques, the physician can map out the circulatory system of the heart and identify blockages.

The tremendous advantage of the techniques over invasive surgical procedures is that only a small incision is required, thereby reducing the risk of infection, and making patient recovery times shorter. Interventional procedures have been revolutionized because in all these procedures the patient is not “cut

open". However, there are now public health worries about radiation exposures due to the expanding use and complexity of interventional treatments, particularly for localized skin doses. For interventional procedures, where prolonged irradiation times are involved, multiple projections, beam geometry, dose rate, and repeat procedures can result in some of the largest doses encountered during cardiology procedures, hence tracking and documenting patient-specific skin and internal organ dose has been specifically identified (Balter et al., 2002).

Patient care has been significantly improved with diagnostic and interventional procedures. Invasive surgical procedures have been reduced to minimum with consequent reduction in the morbidity and mortality of numerous diseases through the application of diagnostic and interventional procedures. Monitoring radiation dose and assessment of radiation risk is therefore important for facilities and activities that use ionizing radiation to help prevent deterministic effect whilst minimizing stochastic effects from radiation exposure. Therefore, evaluation, assessment, and monitoring of doses for patients, workers, and for the sake of good work practices are needed for every radiation facility and activity.

Problem Statement

During cardiology operations, angiography equipment uses ionizing radiation (X-ray), which exposes patients and personnel to significant radiation doses. Ionizing radiation is used in medical diagnosis and treatment, necessitating effective, practical, and implementable radiation protection and safety guidelines for both the patient and the occupationally exposed worker(s) throughout the equipment's lifetime. Also, it is important to assess machine

exposure parameters such as kilovoltage, milliamperere current, time and filtration that are direct radiation dose determinants to both patients and staff to help prevent deterministic effects and minimize stochastic effects. Again, it is paramount to verify dosimetric quantities or values given by vendors through dose measurements for work efficiency. The motivation and the zeal to carry out this study are about the radiation protection and safety principles for the NCTC staff and the patients.

A preliminary study at the Centre as part of routine work indicates anxiety among the working staff in terms of their safety and protection from the use of ionizing radiation (Tsapaki, 2014). Risk for exposure to ionizing radiation is a major source of worry for all occupationally exposed persons because of the potential for deterministic and stochastic effects (Fallis, 2013; ICRP, 2012). The absence of studies and data on radiation exposure in cardiology procedures in Ghana could pose serious and complicated occupational and patient health hazard issues as well as legal issues in the event of incidents and accidents related to work safety, taking into account the fact that NCTC serves the whole West African subregion (Edwin et al., 2011).

Purpose of the Study

In the Cath lab of NCTC, KBTH, the research involved the collection of experimental data and statistical modelling of doses to patients and personnel during cardiology procedures.

Research Objectives

This study's main objective was to quantify the radiation dose and assess the radiation risk that interventional cardiology treatments pose to both staff and patients.

The following were the study's specific objective:

1. Assess functionality of the angiography machine at the catheterization laboratory (Cath lab).
2. Evaluate patients and staff radiation doses for compliance with internationally accepted reference levels and dose limits.
3. Establish correlation between body mass index (BMI) and delivered radiation dose to patients for interventional cardiology procedures.
4. Develop graphic user interface (GUI) platform as a quality assurance tool for prediction of effective radiation doses from body mass indices (BMI).
5. Analyze radiation risk levels from occupational exposure of interventional cardiology staff.

Relevance / Justification of Work

The knowledge of dose distribution and trends of radiation doses for personnel effective doses in any radiation facility or environment is important for the assessment of exposure during incidents and accidents. Little or no dosimetry records for occupational exposure of staff and patients coupled with a lack of diagnostic reference levels for patients at the NCTC in Ghana for future reference in the event of accidents, incidents, and medicolegal cases initiated the need for this study.

Essentially, it is prudent for any country to have a database of accurate knowledge of exposure levels with a graded approach. In order to create and monitor standards of best practice and to identify drawbacks for justification and risk assessment, it is fundamentally essential to assess the dose to patients

and employees during any medical X-ray imaging. Moreover, dose optimization is needed in cardiology to obtain the required diagnostic information.

In Ghana, there is an increasing number in the use of X-ray for diagnosis and treatment of cardiac interventional radiology procedures. Cardiology treatments such coronary angiography, right heart catheterization, and percutaneous coronary intervention are currently performed at the NCTC, and it involves high-risk radiation exposure.

A preliminary study at the Center recommended that further and effective work must be done to ascertain the radiation protection and radiation levels associated with the procedures (Njantang, 1987). Hence, adequate information on dose and image quality in radiology procedures would enable accurate assessment of risk to reduce the probability of tissue damage that might be caused by exposure to ionizing radiation.

Delimitations

The study covers patient and occupational staff radiation dose measurement during four major coronary angiography procedures performed at the National Cardiothoracic Centre, Korle-Bu Teaching Hospital. An exclusion and inclusion criteria used in the study was explained in the methodology.

Limitations

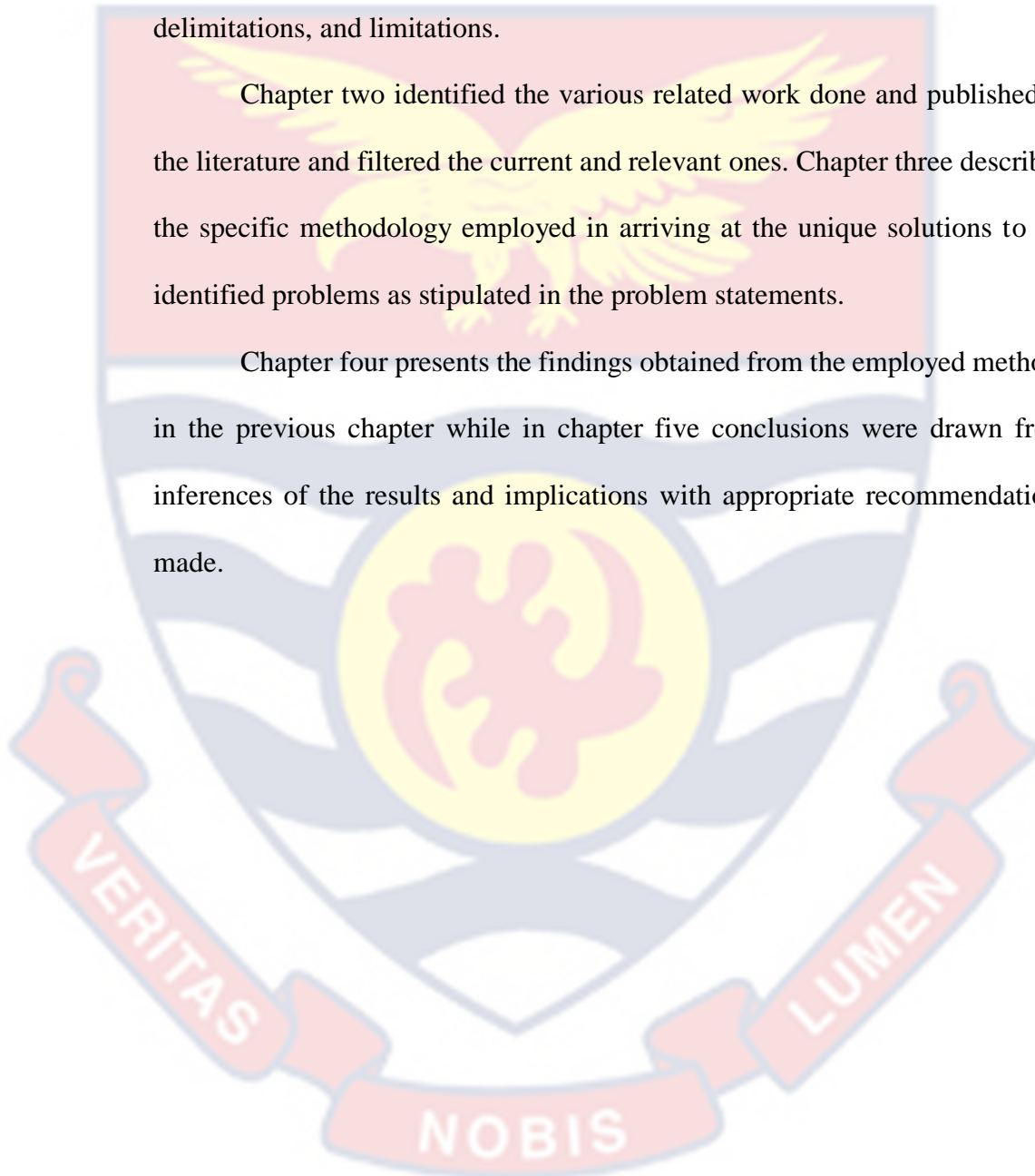
The limitation with this study is the fact that the image quality evaluation could not be carried out to relate radiation dose to the quality of the images obtained during the procedures due to technical challenges. Also, the quality control test carried out on the angiography unit at the Cath lab was not exhaustive due to unavailability of some quality control test kits.

Organization of the Study

The thesis is structured as follows: The first chapter provides an overview of the investigation topic as it is described above and includes the introduction, problem statement, research objectives, relevance/justification, delimitations, and limitations.

Chapter two identified the various related work done and published in the literature and filtered the current and relevant ones. Chapter three described the specific methodology employed in arriving at the unique solutions to the identified problems as stipulated in the problem statements.

Chapter four presents the findings obtained from the employed methods in the previous chapter while in chapter five conclusions were drawn from inferences of the results and implications with appropriate recommendations made.



CHAPTER TWO

LITERATURE REVIEW

Introduction

A brief history of the NCTC, KBTH is presented at the beginning of the chapter. It presents a review of literature on the general physics behind fluoroscopy: basic science, patient and occupational worker protection, the principle of radiation dose measurements and its associated risks. Furthermore, the review includes diagnostic and interventional cardiology procedures from recommended publications. BMI, BSI, and BSA are discussed in relation to radiation exposure factors including mA, kVp, and time with radiation doses. Patients' Dose area product (DAP) and worker effective dose measurements were reviewed from published articles.

The Research Area KBTH

Korle Bu means the valley of the Korle lagoon. It was founded on 9th October 1923 as a general hospital to address the health issues of the population. The NCTC, the National Plastic and Reconstructive Surgery Centre, and the National Centre for Radiotherapy and Nuclear Medicine are three centers of excellence at the KBTH, which is the country's top teaching hospital. Because of the sophisticated procedures provided in various fields, KBTH attracts patients from all over Ghana and the West Africa Sub-region and sometimes from other geographical regions of Africa.

The KBTH, the largest referral hospital in Ghana was the site of this research, situated at 5° 32' 16.2" north, 0° 13' 38.67" west, Guggisberg Avenue in the Greater Accra Metropolis of Ghana.

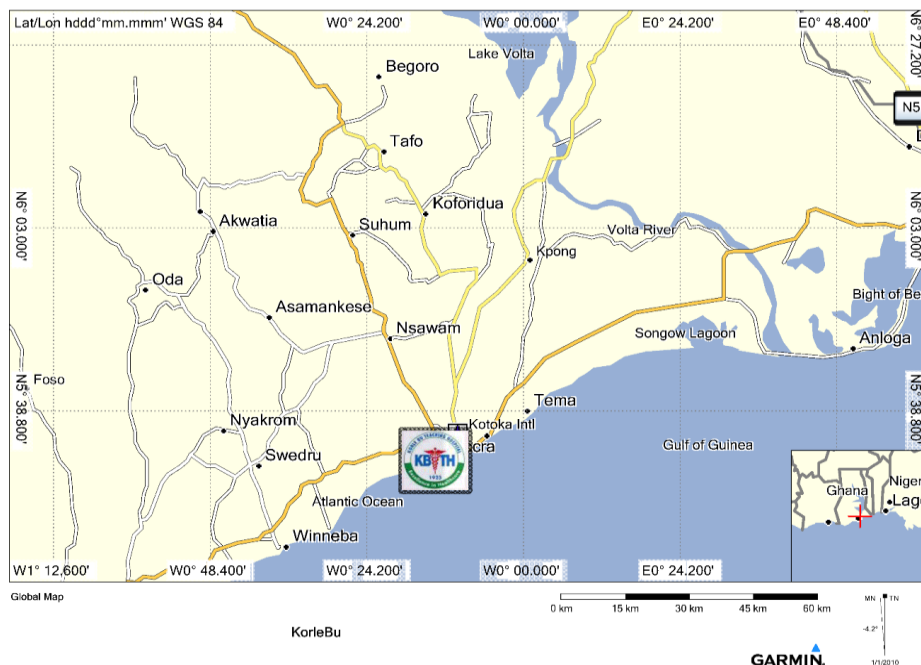


Figure 1: The location of Korle-Bu Teaching Hospital on a map of Ghana indicated by the official logo.

The NCTC of the KBTH (shown in Figure 1) is a very resolute cardiac catheterization unit. Cardiothoracic surgeons are joined by a team of cardiologists, anesthetists, cardiovascular perfusionists, nurses, technologists, and operators during procedures. The Cath lab, being a modern one is used for cardiac surgery diagnosis and treatment of many heart diseases without opening the heart of the patient.

The Physics of Fluoroscopy: X-ray Production and Interaction

Wilhelm Roentgen's observation that a screen coated with a barium compound shined when exposed to what was later termed X-rays in 1895, marked the beginning of fluoroscopy (Davros, 2007). X-ray is an electromagnetic wave which is ionizing radiation. After this observation, the first fluoroscopes were made. Following improvements made to the luminous coatings by Thomas Edison and others, fluoroscopy became widely used in the

early 1900s (Davros, 2007). An X-ray-based medical imaging technology called fluoroscopy is employed to monitor a process occurring inside the human body in real time. Due of its numerous uses, fluoroscopy can be found in many modern hospitals. Radiology, gastroenterology, surgery, pain management, cardiology, swallowing studies, upper and lower gastrointestinal imaging, and device placements such as stents, needles, lines, and tubes are among the fields where fluoroscopy is frequently utilized. Most of the current fluoroscopy equipment delivers X-rays in short pulses instead of continually, minimizing the radiation exposure to patients and staff. An X-ray tube serves as the source of X-rays in modern fluoroscopes. The ability to independently control the energy and quantity of X-rays generated is provided by the X-ray tube (Davros, 2007).

Production of X-rays

In an X-ray tube, X-rays are produced by accelerating electrons that have been liberated from a heated filament (cathode) and are directed onto a target anode. The electrons are normally accelerated by applying a high voltage potential of between 50-150 kVp between the electrodes, thereby making the electrons gather kinetic energy as they cross the gap.

The energy state of the electron changes when they cross the gap due to interactions with the target atoms or the positive charge field that surrounds each target nucleus. When the fast-moving electrons accelerate through the matrix of the positive target nuclei, an attractive positive force acts between them and the positive nucleus (Davros, 2007). The force first causes the electrons to be accelerated towards the positive nuclei, but since the electrons are moving very fast, they normally overrun the mark and move past the nucleus that attracts them. As a result, they decelerate past the nucleus giving up their kinetic energy

gained and are drawn towards the anode (Davros, 2007). The energy of the electron is given up in the form of photonic radiation, which is a spectrum, from low energy infra-red (heat) photons up to X-ray photon energies. In other words, the accelerated electron creates an electric field that interacts with other atomic particles of the anode material resulting in the release of energy in the form of X-ray as shown in Figure 2.

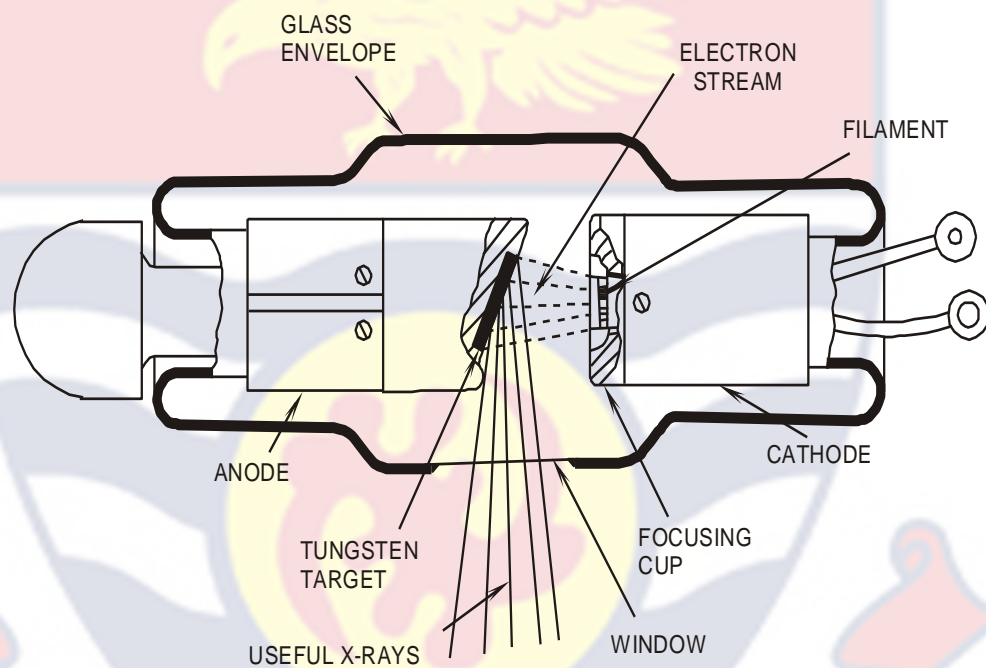


Figure 2: A typical X-ray tube containing evacuated envelope, filament cathode and target anode (Davros, 2007).

The quantity, intensity, and duration of X-rays that exit an X-ray tube can all be separately adjusted (Cusma et al., 1999). The energy of X-rays that emerge from an X-ray tube can be altered by varying the voltage, as measured from the electron source, the filament or cathode, to the anode and the voltage is mostly given as the peak kilovolts (kVp).

For clinical purposes, the kVp value ranges between 50 and 150 kVp and the number of X-rays produced depends on the variation of the flow of

electron across the gap between the cathode and the anode, and is mostly stated as milliamperes (mA) (Davros, 2007). For current fluoroscopy units, the mA settings can be between 1 and 1000 mA in value and the range helps to support short-duration pulsed radiation modes (Stratis et al., 2009a). Timing circuit is often used to regulate X-ray exposure and it is expressed in seconds or minutes (Cusma et al., 1999).

Recent innovations

Fluoroscopy has seen improvements as a result of technological advancement, such as the change from large image enhancing screens to more portable flat panel array detectors (Nett, 2022). Additionally, charge-coupled device camera (CCD camera) has replaced the older television tubes in many fluoroscopes. Fluoroscopy has undergone significant improvements in radiation delivery and recent units deliver X-rays as short pulses rather than continuous, thereby lowering patients and staff radiation exposures (Ogden et al., 2014).

Image Enhancer Technology

Chamberlain was the first to identify the requirement for image intensification to get beyond the limits of the human visual system in low-light conditions that are typical of early fluoroscopy in terms of lack of sharpness and dark adaption (Cusma et al., 1999). Coltman invented the image intensifier (II), a technique that satisfies these demands of image intensification (Valentin, 2000). The radiologist needed to be dark adapted for optimal information transfer prior to performing a study because the technology, that is the single Patterson scintillator screen which was frequently used for real-time imaging did not have enough light output. Instead of depending on one conversion and

amplification step (X-rays to light), as with the simple scintillator, the image intensifier was built with a three-stage conversion and amplification procedure to create a light image of much larger intensity. The use of fluoroscopy in clinical diagnosis was therefore revolutionized with this technology. A cross-sectional diagram illustrating the functions of a modern X-ray image intensifier is shown in Figure 3.

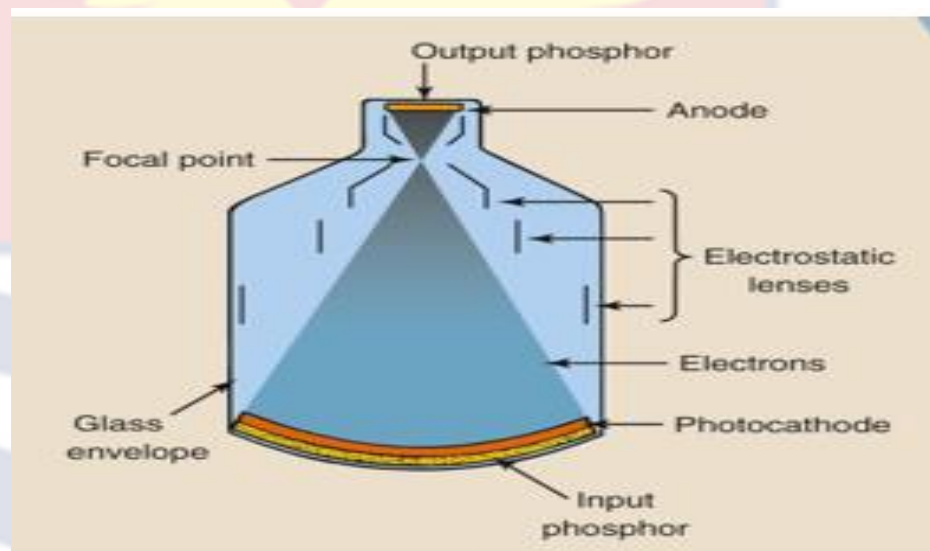


Figure 3: The X-ray image intensifier showing its important components (Risti, n.d.)(Valentin, 2007)

The input phosphor scintillator converts X-rays into light photons, the photocathode releases a proportional number of electrons that are accelerated and focused using cylindrical electrical focusing gradients to an output phosphor, and light photons are produced. In a closed-circuit setup, optical lenses couple the light from the output phosphor to the TV camera, producing a video signal that is later re-rendered on a video monitor for viewing the X-ray fluoroscopy sequence (Valentin, 2000).

Over a huge range of incident exposures, the intensifier's light intensity response is linear. The television camera does not, however, react in the same

way when the incident light is converted to the matching video signal amplitude or digital value (nor does the video display monitor, for that matter). The image intensifier or television system now offers excellent image quality for both low dose fluoroscopy and higher dose tests like Digital Subtraction Angiography (DSA) and electronic spot imaging, especially when equipped with low noise and wider dynamic range CCD cameras.

Flat Panel Detectors (FPD):

The solid-state X-ray digital radiography device known as a flat panel detector shares some fundamental principles with the image sensors used in digital photography and video. A flat panel detector works on the idea that after X-ray passes through the object being imaged, X-rays strike the detector thereby creating a light image (Jones & Goel, 2013). For signal acquisition and digitization, two main FPD technologies have been developed.

These technologies are based on the indirect conversion of X-rays to light (using an X-ray scintillator) and then to proportional charge (using a photodiode), or the direct conversion of X-rays into charge (using a semiconductor material). The image quality of the image intensifier or television system is superior at the lowest exposure levels typically used in fluoroscopy, even though these detectors have demonstrated remarkable performance for high-exposure interventional procedures.

The scintillator substance, either gadolinium oxysulfide or caesium iodide in the indirect flat panel detectors transforms X-rays into light. The sensors are the exact same size as the image they record because concentrating X-rays is not a practical option. Amorphous silicon on a glass detector array, created using a method akin to that used to create Liquid Crystal Detector (LCD)

televisions and computer monitors, is right behind the scintillator layer, just like a Thin Film Transistor (TFT) LCD where millions of 0.2 mm pixels each containing a thin film transistor that form a grid-patterned like amorphous silicon on the glass substrate.

Each pixel also includes a photodiode that produces an electrical signal in proportion to the light emitted by the area of the scintillator layer in front of the pixel, unlike an LCD but like the image sensor chip in a digital camera. To create an accurate and sensitive digital representation of the X-ray image, additional electronics are placed at the edges or behind the sensor array and are used to amplify and encode the signals from the photodiodes. Direct FPDs are amorphous Selenium-based semiconductor detectors (aSe). Because X-ray photons are transformed directly into charge, FPDs are referred to as "direct" detectors. In most designs, the flat panel's outer layer is a high-voltage bias electrode (Jones & Goel, 2013).

In aSe, electron-hole pairs are produced by X-ray photons, and the passage of these electrons and holes is influenced by the biasing voltage potential. A TFT array can be used to read the charge pattern the same way images produced by indirect detectors are read (Jones & Goel, 2013). Flat panel detectors are more sensitive and faster than film and their sensitivity allows for a lower dose of radiation for given picture quality than does a film. Flat panel detectors can be produced in larger sizes, they are lighter, durable, less in volume, accurate, and have few image distortions compared to image intensification detectors (Jones & Goel, 2013).

Geometric distortion, veiling glare, consistent response across the field of view, and improved ergonomics with greater patient access are all advantages

of FPD image quality. Improved detection quantum efficiency suggests that the patient dose could be decreased while adhering to As Low As Reasonably Achievable (ALARA) guidelines. First-generation FPD devices have, however, been implemented with acquisition flexibility that is less than ideal and the presence of residual signals from prior exposures, an additional equipment cost, and long-term maintenance are significant barriers to purchase and implementation (Jones & Goel, 2013).

Many present problems should be resolved by the second generation and upcoming hybrid FPD systems, making FPD substantially superior for fluoroscopy imaging suites (López et al., 2018).

The Physics behind X-ray Interactions with Matter

The interactions of X-rays with matter can be photoelectric, coherent, and Compton where coherent scattering has no impact on the majority of diagnostic X-ray operations, but Photoelectric and Compton effects both contribute to image, and dose (Nett, 2022). Photoelectric and Compton effects are therefore, the two dominant interaction types in diagnostic X-ray and the interaction can result in image formation depending on the interaction, energy and X-ray types (Nett, 2022).

The influence of Compton scatter and the photoelectric effect, as well as how they behave in relation to energy, can considerably enhance the capacity to choose the optimal technical parameters for a certain clinical condition (Nett, 2022). When X-ray photons interact with a medium's particles and travel through it, they disperse or absorb energy and some of the photons can pass through the material entirely without interacting to form an image.

Total Absorption or Photoelectric Effect

For photoelectric effect the X-ray that enters the medium, becomes halted, and its energy is deposited locally. Photoelectric effect is the primary interaction responsible for the formation of a signal in an X-ray image. Photoelectric interaction occurs when X-ray interacts with an electron in the matter thereby making the photon to be completely absorbed, and its energy transferred to an electron that is removed from the electron cloud (B. Nett, 2022). The electrons in the inner shells are in a more stable configuration, hence the electrons in the outer shells' transit to an inner shell and a characteristic X-ray will be emitted.

The probability of such interactions occurring within the inner shells depends strongly on atomic number Z (Z^3) which is the number of protons in the nucleus (Nett, 2022). Image contrast in diagnostic and therapeutic radiology is much better for materials with high X-ray absorbing characteristics (high atomic number elements).

The interaction is such that electrons move to the inner shell, preserving energy leading to the emission of secondary X-ray photons. Predominantly, in photoelectric interaction, an X-ray photon interacts and deposits most of its energy locally in an energetic electron. Photoelectric effect occurs when low energy or low kVp photon gives all of its energy to the inner shell electron of atom making the electron to be ejected from the atom creating a vacancy on the shell (Nett, 2022). Photoelectric effect represents anatomic structures with high X-ray absorption characteristics, such as radiopaque structures, tissue with high atomic numbers, or with high mass density (bone) strives well with photoelectric interaction (Kim et al., 2012). Generally, maximizing the

contribution of photoelectric interactions will lead to the highest image contrast and it can be achieved by using high Z materials as contrast agents and/or using lower energy X-rays where the photoelectric effect becomes more likely (Kim et al., 2012).

Compton Scattering

Another important X-ray imaging interaction is Compton scattering where X-ray photon interacts with an electron in the outer shell (Serman et al., 2000). In Compton scattering, an X-ray photon knocks off an electron and, to maintain momentum, scatters in the opposite direction as the electron. All the energy is not deposited locally in Compton interaction hence the scattered photon can have a significant fraction of the energy of the incoming photon and can travel through the patient thereby, potentially creating secondary scatter effect.

In Compton scattering, an X-ray photon knocks off an electron and scatters in the opposite direction of the electron to conserve its momentum (Serman et al., 2000). As a result, some of the energy is scattered and some absorbed by the tissue. Soft tissue and high energy photons are likely to experience Compton effect, which increases with photon energy. Scattered radiation normally degrades the quality of the image and is the main source of radiation exposure to staff (Serman et al., 2000).

Coherent (Classical) Scattering

Coherent or Elastic (Rayleigh) scattering is a type of interaction that can also occur between X-rays and the human body.

Coherent Scattering occurs when an X-ray photon interacts with electron cloud, thereby scattering the electrons, and leaves with the same energy. Coherent scattering occurs at energies below 10 keV for diagnostic imaging. For most of the energy spectra used in diagnostic imaging, not many photons below 10 keV pass through pre-patient attenuators, hence this effect is less relevant compared to Compton and the photoelectric effects (Jones & Goel, 2013).

Coherent scattering is dependent on the number of protons, hence more protons mean high probability of having coherent scattering and it is inversely proportional to the square of the energy. This effect is less likely to occur as the energy of the X-ray increases, resulting in no effect for most diagnostic X-ray procedures. This type of interaction is only an additional interaction to Compton and Photoelectric effects, occurring only at exceptionally low energies, hence, is not important as the other two types of effects (Nett, 2022).

Energy Dependence of Interactions

Different contributions result from photoelectric and Compton scattering in various body areas and at various energy levels. Photoelectric and Compton effects behave similarly as a function of energy when the human body is regarded as a phantom with water acting as soft tissue and some bone dispersed throughout (Serman et al., 2000). However, energy at which transition from photoelectric to Compton dominance occurs is higher in the case of bones. At low energies, photoelectric effect predominates, and for high atomic numbered materials, the transition energy at which Compton effect predominates is considerably higher (Serman et al., 2000). Coherent scattering occurs for energies below 10 keV, and at about 30 keV the switch between

photoelectric and Compton dominance occurs, depending on the kind of material. Photoelectric effect is dominant at lower energies and Compton is dominant at higher energies depending upon the spectrum of energy. Photoelectric effect dominates if the spectral has many photons with low energy and its occurrence is dependent on the cube of the atomic number whilst the occurrence of Compton effect does not depend on the atomic number. Bones are significantly higher atomic number materials; hence, X-ray images of bones are excellent (Nett, 2022).

Impact on Image Contrast

For standard diagnostic energy spectrum, X-ray image is not affected by coherent scattering. The primary source of image contrast is photoelectric effect whilst background haze in an X-ray image is due to Compton effect.

Impact on Dose

In interventional radiology, the patient's dose is not greatly due to coherent scattering. Local energy deposition by the electrons causes both photoelectric and Compton effects to significantly contribute to patient dose. In diagnostic radiology, coherent scattering and the photoelectric effect do not considerably increase staff dose. Compton effect is the primary source of ambient radiation, which increases the occupational dose. Staff members who remain in the beam during interventional radiology receive dose due to the photoelectric and Compton effects (Serman et al., 2000).

X-ray Attenuation

The number of photons transmitted through the material depends on the tissue thickness, tissue electron density and the photon's energy (kVp). Photon

attenuation passing through the matter can be described by Beer–Lambert’s law as defined by equation 1.

$$I_x = I_0 e^{-\mu x} \quad (1)$$

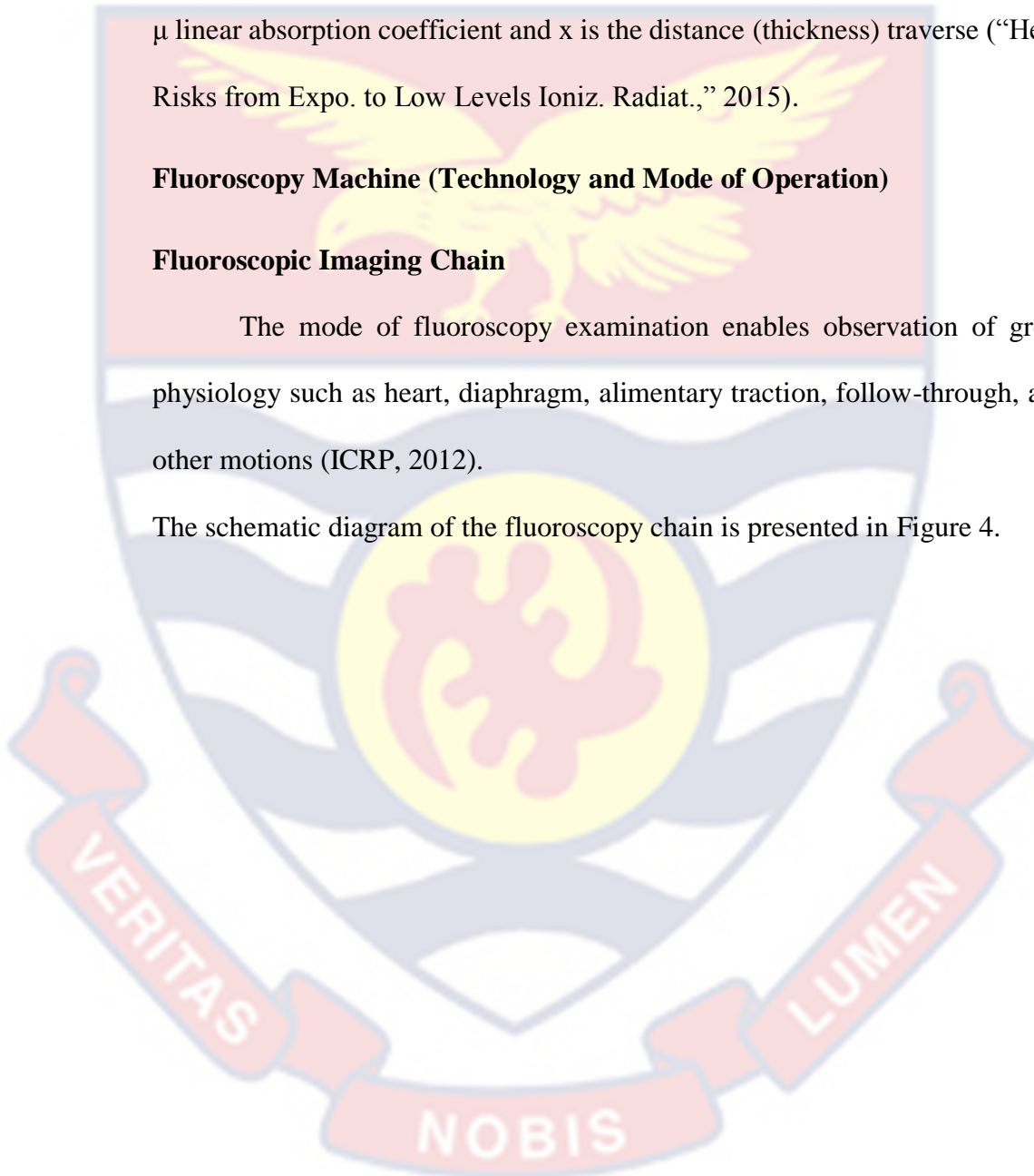
where I_0 is the initial intensity of the photon, I_x represents transmitted intensity, μ linear absorption coefficient and x is the distance (thickness) traverse (“Heal. Risks from Expo. to Low Levels Ioniz. Radiat.,” 2015).

Fluoroscopy Machine (Technology and Mode of Operation)

Fluoroscopic Imaging Chain

The mode of fluoroscopy examination enables observation of gross physiology such as heart, diaphragm, alimentary traction, follow-through, and other motions (ICRP, 2012).

The schematic diagram of the fluoroscopy chain is presented in Figure 4.



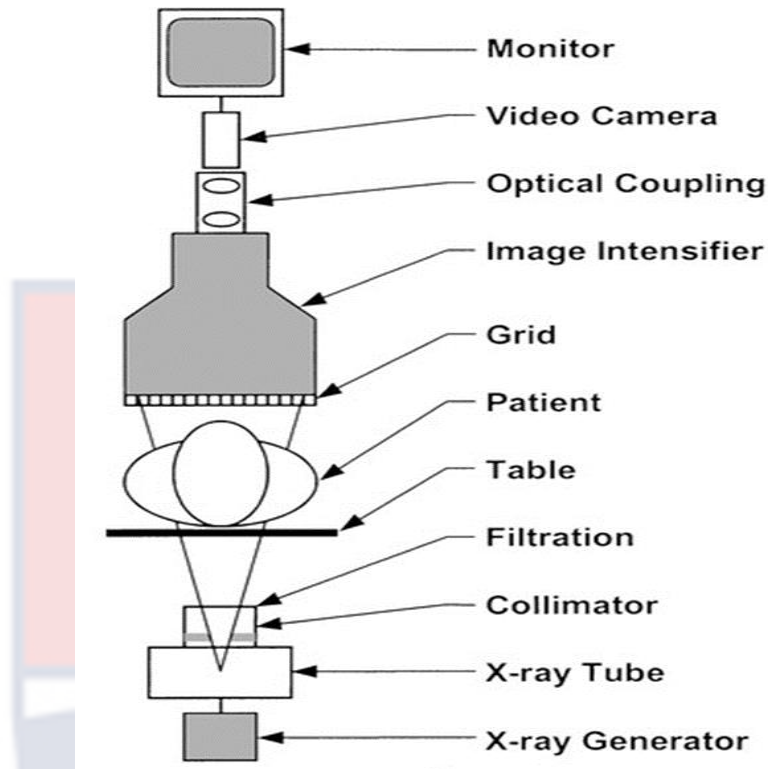


Figure 4: Schematic diagram of the fluoroscopic imaging chain showing X-ray generator, collimator, monitor and other important components.

The following constitutes the main elements required for the production and management of fluoroscopic images. An X-ray generator that generates electrical energy for the X-ray tube is under and above the patient table for under and over couch fluoroscopy units, respectively (Valentin, 2000).

Electrical energy from the X-ray generator is converted into X-rays by the mounted fluoroscopic tower (Cusma et al., 1999). To precisely specify the area that will be exposed to radiation, a collimator device consisting of multiple shutters is used. The fundamental purpose of collimator is to prevent unwanted regions of the body from being irradiated by coning down to the region of interest so that the dose to patient and workers can be reduced (Jones & Goel, 2013). During the duration of examination, patient table and pad carefully

supports the patient, and an optimum image quality is obtained with the appropriate collimation.

Quality Control and Quality Assurance of the Angiography System

Quality Assurance Program

In radiology practice the objective of quality assurance (QA) program is to guarantee that patients are consistently given timely and correct diagnoses. QA program with three secondary goals namely, keeping to optimum diagnostic image quality, reduce radiation exposure to patients and workers with least possible cost will enable the target goal to be achieved.

A good QA program should contain a detailed action plan that outlines policies and procedures with the aims and goals that would help attain the best results. Administrative procedures and quality control (QC) tests should form the content of the QA program with effective verification of QC testing (the respective tests carried out should be at the stated interval, done correctly, results evaluated promptly and accurately, with all corrective actions taken promptly (*X-RAY IMAGING IN AFRICA “ Enhancing Capacity Building of Medical Physicists to Improve Safety and Effectiveness of Medical Imaging ,”* 2020).

Quality Control Program

Equipment must be continuously inspected after successful installation and acceptance test to guarantee sustained, dependable functioning with procedure being evaluated periodically, for the purpose of detecting changes that could bring about clinically significant degradation in the quality of the image and increased radiation exposure (IAEA, 2010). Series of standardized tests must be developed to detect variations in the function of the angiography

equipment from its original level of performance. The tests must be carried out routinely to allow for prompt corrective actions that would help maintain X-ray image quality and optimize dose. The objective, therefore, is to ensure diagnostic or therapeutic accuracy by improving results while limiting radiation exposure (Ramos et al., 2010).

Review of Patient and Staff doses in Clinical Practice

Interventional cardiology procedures are frequent diagnostic and therapeutic interventions that are guided by fluoroscopy. Patient sometimes undergo repeat complex therapeutic interventional procedures thereby being exposed to high radiation doses (Dragusin et al., 2011). A number of case studies describing deterministic impacts that are more concerning than stochastic long-term dangers are presented in the specialized literature (Dragusin et al., 2011). Skin dose issues of challenging radiological procedures have attracted the attention of the World Health Organization (WHO) and International Commission on Radiological Protection (ICRP), thereby making patient dosimetry approaches a principal issue. Many published dose data are presented as vaguely defined dose values and lack clear justification for the measurements that were made (Dragusin et al., 2011). Currently, patient dosimetry techniques in interventional cardiology can be categorized into three, based on their objectives as; dosimetry for quality assurance; dosimetry for stochastic risk evaluation; and dosimetry for deterministic effects evaluation (Dragusin et al., 2011).

Quality Assurance Dosimetry

This is done to evaluate the optimization process, establish diagnostic reference levels (DRL) for routine examinations, and compare the performance

of equipment, operator skills, and radiological practice across different teams or facilities using dose area product, DAP as dose quantity. Usually, the total DAP for the whole procedure is documented during cardiac interventions. Sometimes a procedure may require both a DAP for the fluoroscopy part (DAP fluoro) and a DAP for the cine angiography portion (DAP cine).

The total fluoroscopy time, total number of images obtained, total number of series of acquired images, and the average number of images per series are among the extra technical metrics that some writers have suggested in the dosimetry for quality assurance (Dragusin et al., 2011).

Dosimetry Values for Stochastic Risk Assessment

The organ equivalent doses, and effective doses are the dose quantities used for stochastic risk. In the assessment of the stochastic radiation exposure effects to the population, the organ equivalent dose and effective dose are the radiation quantities used, since these radiation parameters allow comparisons of exposures from diverse types of procedures, radiation type, radiation quality, and irradiation geometry. With the effective dose, and the appropriate risk coefficients from ICRP Report 103, it is possible to evaluate the detriment of individuals or populations from medical exposure (Dragusin et al., 2011).

Dosimetry for Deterministic Effects

Skin dose assessment is important in complex interventional cardiology procedures with the knowledge of irradiated skin area for the potential of deterministic effects of radiation exposure (Octeville & Sanitaria, 2019). Several methodologies are used to estimate and express the maximal skin dose (MSD). These are; by calculations, direct measurements on the patient with point detectors which could be array of TLDs, solid-state detectors, portal

detectors and films (Dragusin et al., 2011). However, all the methods are not feasible for routine work. Alternatively, threshold exposure quantities like fluoroscopy time and measurable dose area product values when reached are able to alert catheterization laboratory staff about the occurrence of deterministic effects (Dragusin et al., 2011).

Procedures involving electrophysiology with the use of stationary fields, electronic point detectors or computational methods are used to assess the distribution of skin dose and possible deterministic effect occurrence. However, comparison of patients' published doses data in interventional cardiology should be done with circumspection, since there is lack of standardization in acquisition of data and there are various uncontrolled variables such as equipment differences, radiographic technique, the complexity of the procedure, and patient characteristics (size, age, sex).

Radiation Exposures to Patients in Diagnostic and Therapeutic Cardiac Catheterization

Most adults frequently have CA for diagnostic purposes and PCI for therapeutic evaluations of coronary artery diseases and many articles have reviewed patient radiation doses in this respect (Dragusin et al., 2011). Authors report data for CA procedures on subcategories basis, like CA with left ventricular angiography, or and cardiac catheterization (Octeville & Sanitaria, 2019). PCIs are also subcategorized due to complication in a considerable number of technical factors, such as the number of lesions treated, the wire technique, simple ostial or bifurcation stenting, flow and pressure wire and any other special devices used (Dragusin et al., 2011). The most common quantities used were dose area product, fluoroscopy time, cine frames, cine time

(dosimetry for quality assurance), effective dose (dosimetry for stochastic risks), and skin dose (dosimetry for deterministic risks). These quantities are mostly presented as median values, sometimes as a range of values. Due to procedural complexity, examination technique, use of radiation-reducing techniques, operator experience, workload, in catheterization laboratory examination; values for interventional procedures vary as revealed in literature (Dragusin et al., 2011). DAP for CA of 47.7 vs. 23.4 Gy cm^2 and for PCI, 72.2 vs. 51.6 Gy cm^2 were the values stated by (Dragusin et al., 2011) when he compared patient dosimetry for biplane versus single intensifier system respectively, thus revealing that biplane system provides greater imaging capability but with an increased dose (Dragusin et al., 2011).

Again, when the effect of complexity of PCI interventions were investigated by (Cousins et al., 2013a) and (López et al., 2018) by grouping the procedures into simple, medium and complex procedures, with emphasis on a set of technical and clinical factors, they reported median DAP values of 66.7, 96.4 and 132.7 Gy cm^2 for simple, medium and complex procedures respectively (Dragusin et al., 2011). (Siiskonen et al., 2018) compared the radial arterial approach to the femoral approach in terms of radiation dose. (Siiskonen et al., 2018) in comparing radial arterial to the femoral approaches found that the radial approach yielded significant higher doses of 51 and 75 Gy cm^2 for CA and PCI respectively whilst the femoral approach yielded 38 and 47 Gy cm^2 for CA and PCI respectively (Dragusin et al., 2011). Patient doses of flat-panel systems was also, compared with image intensifier systems by (Tsapaki, 2014) and (Foti et al., 2008) and their study shows that despite the potential of FPD to produce

optimum images with lower dose, clinical practice and other factors associated with the examinations reveal opposite results of patient doses.

Similarly, (Foti et al., 2008) reported 33.4 Gy cm^2 for flat panel detectors and 31.1 Gy cm^2 for image intensifier respectively during CA examinations and 66.9 Gy cm^2 for flat panel detectors and 52.0 Gy cm^2 for image intensifier during PCI procedures (Kim et al., 2012). Patient dosimetry as presented by some publications is in terms of fluoroscopy contribution and image acquisition in relation to the total dose area product (DAP) as reported by (Efsthathopoulos et al., 2006) and (Kuon et al., 2003). Fluoroscopy and image acquisition mean DAP values calculated and reported in literature are 18% DAP fluoroscopy and 81% DAP image acquisition for CA procedures whilst PCIs had DAP values of 41% fluoroscopy and 59% image acquisition. There is wide variation in patient radiation doses as reported in published articles. Physician expertise, X-ray equipment, patient parameters and procedure type are responsible for the difference in these values (Dragusin et al., 2011).

Staff Dosimetry

The highest X-ray doses currently reported among medical workers who use X-rays are occupational doses during interventional procedures guided by fluoroscopy. Due to their proximity to the radiological source, interventional cardiologists are exposed to radiation at the same level as the patient. Working in high-volume cardiac catheterization labs exposes interventional cardiologists to significant occupational radiation risks of developing certain illnesses, such as upper respiratory illness, hematological malignancies, thyroid diseases, skin diseases, or cataracts (Dragusin et al., 2011).

Consequently, it is essential and mandatory for workers to monitor their personal doses. It is prohibited to exceed the occupational exposure limits, which are 20 mSv/year, averaged over five years. The equivalent dose should not be more than 500 mSv for the skin (average dose across 1 cm² of the skin's most heavily irradiated area) and 150 mSv for the eye's lens, 500 mSv for the hands and feet (Valentin, 2007). Important personnel shields such as thyroid shields, eye goggles, wraparound two-piece aprons are prescribed for use by occupational staff during procedures whilst the Personnel doses are monitored with X-ray film badges or thermoluminescent dosimeters (TLDs). These detectors are placed in holders and the monitors can be worn for one month before they are submitted to the laboratory to be read for effective dose to be evaluated.

It is recommended that the interventional cardiologists wear two badges, whilst first one is worn on top of the lead protective apron at the neck region, the second one should be worn at the waist region under the lead protective apron to monitor the effectiveness of the lead apron. Single badges worn at the collar level on top of the apron by occupational workers in the catheterization laboratory gave a mean collar level dose per case for a cardiologist who performs CA and PCI as range of values from 0.04 to 0.16 mSv as reported in literature (Dragusin et al., 2011) and (Access, 2019). Publications focus on personnel dose estimation for different anatomical locations by placing TLD for every procedure (Kim et al., 2012).

According to study conducted by (Efstathopoulos et al., 2006) by measuring doses with five TLDs placed on the left part of eyeglasses, on the chest, above and below the lead apron, the left-hand and knee; the results of

dose per procedure for cardiologists were 6 μGy (eyes), 0 μGy (Chest below apron), 5.75 μGy (chest above apron), 22.5 μGy (left hand), and 16.75 μGy (left knee) respectively (Clerinx et al., 2008). The workers that assisted received fewer dose per procedure as 5.5 μGy (eyes), 0 μGy (chest below apron), 4 μGy (chest above apron), 17.5 μGy (left hand), 3.5 μGy (left knee).

A survey carried out for a period of 15 years by (Heidbuchel et al., 2014) and (Greffier et al., 2017) to evaluate the occupational doses of cardiologist reported that the mean values in mSv per year decreased from 11.6 (1989-1992) to 1.6 (1993-1998) and 1.2 (1999-2004) respectively (Järvinen et al., 2008a). The results show a reduction in effective dose by a factor of 10 which was explained by the training in radiation protection, optimization of procedures and improved performance of X-ray systems. Risk of stochastic effect to interventional cardiologist increases with increase in radiation dose. To prevent radiation-associated diseases, radiation exposure to workers must be reduced by using modern generation cardiac X-ray systems, in performing diagnostic and interventional procedures with less fluoroscopic duration and the use of effective shields to protect from radiation.

Cardiac Examinations

Angiography and Angioplasty

There are two distinct medical treatments that deal with the blood vessels: angiography and angioplasty. Angioplasty includes enlarging the restricted arteries to treat the condition, whereas angiography is used to evaluate or examine the blood vessels for a probable heart condition. Like an angiography, angioplasty starts with local anesthetic being administered to the patient and the vascular surgeon then creates an incision in the femoral artery

and threads a catheter tube into the artery, threading it to the location of the blockage or narrowing.

The words angiography, angiogram, and arteriogram all refer to a process used to detect artery blockages or narrowing in the body. Whatever part of the body is being examined, the process is the same with Coronary angiography (CA) being the umbrella term for the process of using X-rays to identify a damaged artery (Cousins et al., 2013b).

Percutaneous Coronary Intervention

A non-surgical procedure called percutaneous coronary intervention is performed to widen arteries that feed the heart muscle with blood (coronary arteries). 'Percutaneous' simply means 'through intact skin. A catheter is inserted into an artery through the skin of the arm or groin to perform percutaneous coronary intervention.

Typically, a balloon, stent, or cutting tool (atherectomy tool) can be put at the leading tip of this catheter along with other devices. The coronary artery constriction or blockage is reached by threading the catheter and its devices back into the artery's interior. The term "percutaneous coronary intervention," which is still used in the literature, originally referred to percutaneous transluminal coronary angioplasty (PTCA). Today, the term includes balloons, stents, and other modifications to the catheter tip, such as tools that can remove plaque and open a narrowed artery.

One of the most important uses of percutaneous coronary intervention is the treatment of acute heart attacks, but it also has other uses. With the help of percutaneous coronary intervention, angina can be treated or reduced, heart attacks can be prevented, congestive heart failure can be treated, and some

patients can avoid surgical treatment Coronary Artery Bypass Graft (CABG), which requires extensive surgery and frequently requires a lengthy recovery period (López et al., 2018).

Balloon Angioplasty

During cardiology procedure known as balloon angioplasty a thin catheter with a deflated balloon tip is introduced into an artery through the skin of the groin or arm. The coronary artery, which is narrowed or blocked, is reached after the catheter has been threaded through the artery by placing its tip through the constricted space. When the balloon is placed inside the constricted space, it is inflated, pressing the plaque against the vessel walls to lessen the constriction. The catheter is then taken out when the balloon has been deflated. A dye is injected to allow the cardiologist see the process and watch the blood flow through the arteries. (Cousins et al., 2013b).

Stent

A stent is an extensible metal scaffold that can be used to maintain the opening of previously restricted coronary artery after angioplasty. Like balloon angioplasty, a coronary artery stent is implanted using the same technique.

The distinction is that the balloon is encircled by the stent when it is not expanded or compressed. When the balloon is filled, the stent that surrounds it expands. The balloon's encircling stent latches into place against the plaque or arterial artery wall when it has extended. After the balloon is inflated, the stent remains inside the artery. When the balloon is released, stents keep the coronary artery open, which prevents most arteries from narrowing once more (a process known as elastic recoil). Due to the development of scar tissue, recurrent

constriction (restenosis) can occasionally still happen after the stent has been implanted (Cousins et al., 2013b).

Basic Principles of Body Parameters and Radiation Exposures

Height, weight, Body Mass Index (BMI), Body Surface Index (BSI), and Body Surface Area (BSA) are significant body parameters to take into consideration when estimating the body's exposure to radiation.

Body Height and Weight

Several terminologies have been used to characterize the link between body weight and height. The BMI, BSA, and BSI stand out among them. Research proves that there is a positive relationship between body height and weight and formulae that describe the relationship between height and weight have been published (Tsapaki, 2008).

For Men weight-to-height relationship is:

$$W = 12.1e^{0.01H} \quad (2)$$

For Women weight-to-height relationship is:

$$W = 9.5e^{0.0108H} \quad (3)$$

where W is weight in kg and H is height in cm.

With the help of a BMI calculator, one can determine whether a person's weight is appropriate for the height. Adolphe Quetelet, a polymath from Belgium developed a method for calculating the body index while working on social physics (Eknoyan, 2008). Until, Ancel Keys coined the name BMI in 1972, it was known as the Quetelet Index ("Body Surface Area," 2020). The

standard unit for BMI is the kg/m^2 and it represents human body fat between the ages of 18 and 65 years (Eknoyan, 2008). Available literature indicates that the average adult BMI in Ghana is $25.7 \text{ kg}/\text{m}^2$ for males and $21.65 \text{ kg}/\text{m}^2$ for females (Tsapaki, 2008).

Body Surface Area and Body Surface Index

Two additional body characteristics namely, BSA and BSI have been developed since the BMI was established to evaluate the correlation that existed between body height and weight. In order to further compare the surface area of the human body to height and weight, the term BSA was created and it gives specific estimated value that shows that the average body size and height normally increases with increasing age (Eknoyan, 2008). A broad framework that states the relationship between the parameters of the body and the relation with the organ dimensions has contributed significantly to the understanding, as well as brought solution to; human health as was reported in literature as:

$$BSA = \alpha_0 H^{\alpha_1} + M^{\alpha_2} \quad (4)$$

where M is mass (kg), and H is the height (cm) (Shirazu et al., 2017).

The average body surface area was found to vary with gender and age and the reported values from literature compared appropriately. The estimated average BSA of an adult was found to be 1.9 m^2 , whilst that of female was 1.6 m^2 . For younger children the average BSA was found to vary according to age and was reported as a range of 1.07 m^2 to 1.14 m^2 for ages of between 10 to 16 years (Vano et al., 2011).

A precise indicator than BMI and BSA is the BSI which relates the body surface area to the body weight and is calculated by dividing the body weight

with the calculated square root of its body surface area and expressed mathematically as:

$$BSI = \frac{weight}{\sqrt{(BSA)}} \quad (5)$$

The application of BSA and BSI in clinical services is important, since it can be used in predicting renal clearance (RC), which is typically reduced by either BSA or BSI to get the true glomerular filtration rate (GFR).

Additionally, the cardiac index that provides a more accurate representation of the effective heart rate can be obtained by dividing the cardiac output by the body surface area. The link between average body size and height is defined and represented by BMI, BSA, and BSI and how that relationship changes with aging (Tsapaki, 2008). According to research, BMI and radiation dose during cardiology procedures have a significant relationship since obese patients need more radiation during radiation diagnosis and treatment procedures than patients with normal BMI. (Memon et al., 2018).

General Model of Thermoluminescence Dosimetry

When a substance is exposed to radiation, the process known as luminescence occurs. During this process, energy is absorbed and subsequently released as a photon in the visible spectrum. A type of luminescence called thermoluminescence occurs when heat is applied to a semiconductor crystal, and it causes it to emit light. In the semiconductor crystal, the valence band is where electrons are located. Electrons can migrate freely from the valence to the conduction band when the material is exposed to radiation. As a result, holes can be created within the semiconductor crystal due to the absence of an electron. Electrons and holes traps that are defects therefore develop in the band gap between the valence and conduction bands due to doping and impurities in

the semiconductor crystal. The electrons and holes will not have enough energy to escape if the traps are deep. However, by heating the semiconductor crystal their energy would be increased and they can leave the traps, recombine at centers of luminescence, and can be emitted as light photons.

Mechanism of Thermoluminescence Dosimetry

A TLD is an integrating detector in which the quantity of trapped electrons and holes equals the quantity of electron-hole pairs formed during exposure. Every trapped electron hole pair ideally emits one photon. As a result, the number of charge electron hole pairs, which are proportional to the dose that the semiconductor crystal absorbed, is equal to the number of photons that are released.

TLD Reader

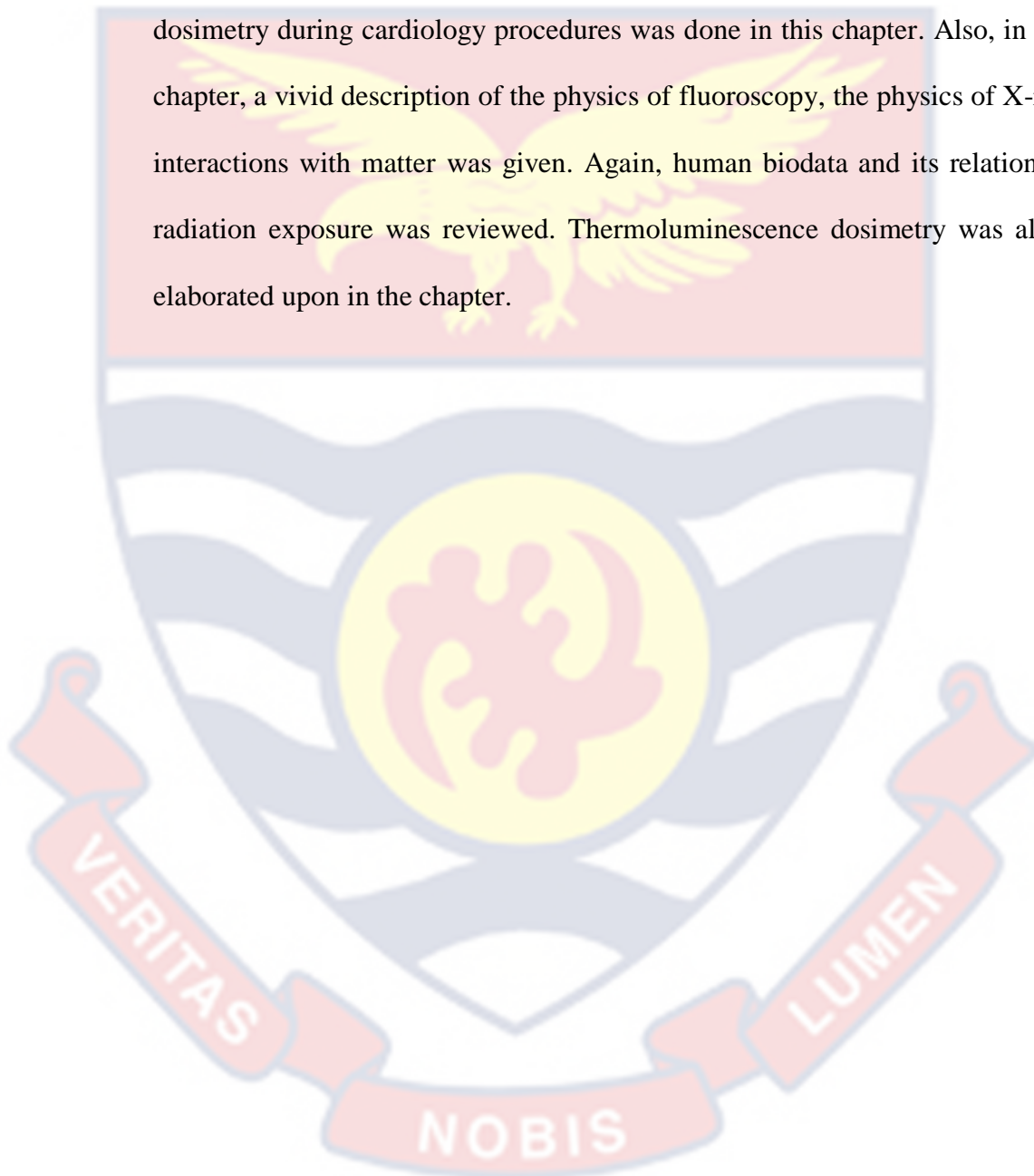
Usually, the dosimeters are mounted on a metal tray inside the chamber of the reader and are heated by a heating coil in good contact with the tray and dosimeter. The temperature of the heating cycle in the chamber is normally measured with the aid of a thermocouple and the signal generated by air contaminants is reduced using nitrogen gas. Light emitted because of the thermoluminescence effect is measured after passing through optical filters and entering the photomultiplier tube (PMT) through the light guide. When the output of the PMT is integrated, the number of photons produced is proportional to the absorbed dose.

Pulse counting can be used in place of integration, converting the output into pulses that can be counted. The reader device is connected to a computer,

and the measured data are either printed out or stored on the computer's hard drive (Savva, 2010) .

Chapter Summary

A comprehensive review of the literature on patient as well as staff dosimetry during cardiology procedures was done in this chapter. Also, in the chapter, a vivid description of the physics of fluoroscopy, the physics of X-ray interactions with matter was given. Again, human biodata and its relation to radiation exposure was reviewed. Thermoluminescence dosimetry was also, elaborated upon in the chapter.



CHAPTER THREE

MATERIALS AND METHODS

Introduction

This chapter, contain relevant information on the study area, the materials as well as the methods used in the study to evaluate and simulate patient and staff radiation dose, and as well measure patient biostatistics. The process for calculating body mass index, body surface area, body surface index, and the link between staff and patient radiation dose have been described.

The study identified various items and measuring techniques that were applied to evaluate staff as well as patient radiation doses. Additionally, methods and guidelines for determining staff and patient effective doses for dose optimization were covered. Detailed modelling done with Minitab as an analytical tool and MATLAB for validation of results was presented. The study was limited to the National Cardiothoracic Centre where procedures are performed on patients with heart-related conditions.

Research Site

Korle-Bu Teaching Hospital (KBTH), Ghana's largest referral hospital, was the site of this research, situated at 5° 32' 16.2" north, 0° 13' 38.67" west, in the Greater Accra Metropolis of Ghana at Guggisberg Avenue as shown in Figure 1 in the previous chapter.

Equipment

The Angiography Unit at the Cath lab is a Siemens type (Artis Zee/ZeeGo) Megalix catplus 125/40/90 – 121 GW, model No. 10144181 and serial number 640041673. The maximum tube voltage is 125 kV IEC 60613

with 0.8 mm Al/80 kV as total filtration. The machine was manufactured in February 2016 in Germany.

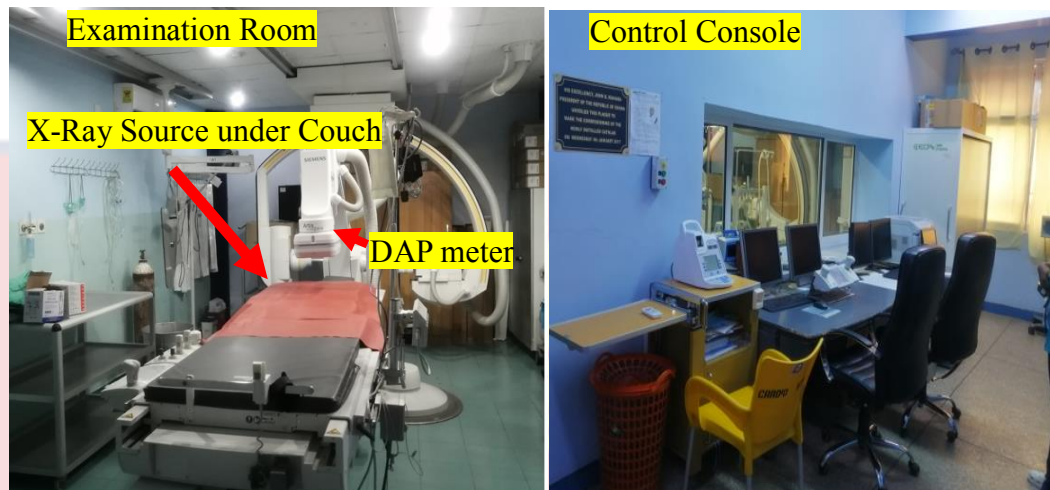


Figure 5: Internal view of the Cath lab with Siemens (Artis Zee) biplane Angiography unit.

The MagicMax quality control (QC) kit is an IBA Dosimetry GmbH X-ray quality control product. The Universal Multimeter: a unit of the MagicMax is a PC-based, USB-powered automatic precision instrument that measures and displays multiple X-ray exposure parameters concurrently. In built is a software that control and display the measured values of the instrument as readout on a screen. The MagicMax QC kits was used in this study to carry out the various quality control tests on the Siemens biplane Artis Zee angiographic system.

Table 1 shows the characteristics of the MagicMax QC kits used for this study (MPD Model XR Detector ver. 01, Serial number R17-0471; and Universal Multimeter of Model number XR Detector ver. 02 and Serial number G17-0391).

Table 1: Radiological Specifications of the MagicMax QC kits

Item	Characteristics	
Type of Detector	Silicon photodiode	
Measurement principle	Ionization current in silicon semiconductor	
Measurable Parameters	Peak voltage, Peak Practical Voltage, Half value layer, Dose and Dose Rate, Dose per pulse, Time for Exposure, and Wave shape	
Length of detector cable	80 cm (31.5")	
Radiation quality	<ul style="list-style-type: none"> • Range • Accuracy 	<ul style="list-style-type: none"> • 40-150 kV • $\leq \pm 2\%$ or 0.7 kV
Radiography and Fluoroscopy	<ul style="list-style-type: none"> • Total filtration • Sensitivity 	<ul style="list-style-type: none"> • 2-22 mm (0.08"-0.87") • 3 mm (0.11") Al, 50 kV, 1 mA @50 cm (19.7")
Specification of Detector for radiography and fluoroscopy		
Dose	Accuracy	$\leq \pm 5\%$
	Range	50 nGy-50 Gy
Dose Rate	Accuracy	$\leq \pm 5\%$
	Range	160 nGy/s-160 mGy/s
Dose per pulse	Accuracy	$\leq \pm 5\%$
	Range	50 nGy/pulse-50 mGy/pulse
	Pulse Rate	5.67 μ R/pulse-5683.37 R/pulse
	Pulse Length	1-1000 pulses/s (at the highest sampling rate)
		1 ms-300 s
		1-0.3X10 ⁶ pulse

Source: www.iba-dosimetry.com

Dose Area Product Meter

The Kerma X-plus is made of a transparent ion chamber, model 120-131HS and serial number 01A04042, (50 – 150 kVp, Class II – type B), < 0.5 mm Al, 15-20V, 80 mA with a reader “10–digit LCD “Single Line Display”, model 120-210 with serial number 01E004774. The device which was

manufactured by the IBA dosimetry service can estimate from the angiography system the dose area product (DAP) of the patient during interventional procedure.

Dose rate meter

The Radiagem 2000 was used to measure ambient Dose Equivalent Rate (DER), $H_p(10)$ * of X-ray exposure during a surgical procedure. The Radiagem has an alerting system, and audio-visual and vibration alarms. Table 2 shows the characteristics of the dose rate meter used for this study. Area radiation monitoring during the procedures was conducted using the calibrated dose rate meter.

Table 2: Characteristics of the dose rate meter (Radiagem 2000)

Specifications	Detail Description
Model number	76687
Serial number	4354
Detector	GM tube halogen-quenched, with detection area equal to 15.5cm ²
Sensitivity	0.83 c/s per $\mu\text{Sv/h}$ or about 3,000 counts per μSv (¹³⁷ Cs)
Measurement Range	0.01 $\mu\text{Sv/h}$ -100 mSv/h
Display Ranges	0.01 $\mu\text{Sv/h}$ -99.9 mSv/h
Accuracy	For the display is $\pm 15\%$ and for point of least significant digit is ± 1
Energy Range	40 keV to 1.50 MeV regarding IEC 60846. The measurement goes further than 1.5 MeV
Operating temperature	-10 °C to +50 °C
Storage temperature	-25 °C to +60 °C
Alarm type	Visual, audio, vibration

Source: www.osti.gov/servlets/pur/1690410

Thermoluminescent Dosimeters

The thermoluminescent dosimeters (TLDs) used for this study were passive reading dosimeters that are suitable for occupational radiation dosimetry as well as patient absorbed dose measurement. Staff absorbed radiation dose comprising of personal deep Hp (10) dose equivalent, Hp (0.07) personal surface dose equivalent and Hp (0.03) personal dose equivalent from X-rays were measured with series of thermoluminescent dosimeters from the same batch.

The TLDs were calibrated at the Lumina Consult Dosimetry laboratory. The design and characteristics of the TLD used for the study are shown in Figure 6 and Table 3, respectively.

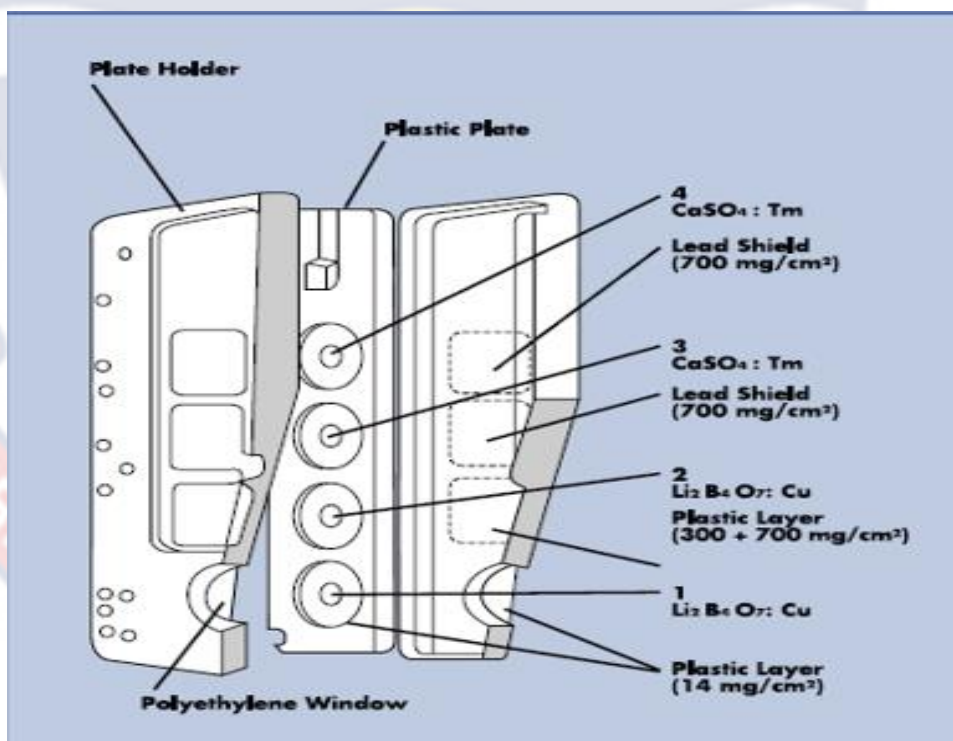


Figure 6: Functional parts of the Thermoluminescent Dosimeter

Table 3: Radiological Specification of the Thermoluminescent Dosimeter

Element Number	Purpose	Thermoluminescent Material	Radiation Shield	Measurement Range
1 st Element	Skin dose	Li ₂ B ₄ O ₇ : Cu	Thin window	100 μSv~10 Sv
2 nd Element	10 keV ~ 10 MeV	Li ₂ B ₄ O ₇ : Cu	Plastic	100 μSv~10 Sv
3 rd Element	25 keV ~ 10 MeV	CaSO ₄ : Tm	Plastic	10 μSv~500 mSv
4 th Element	25 keV ~ 10 MeV	CaSO ₄ : Tm	Lead + Plastic	10 μSv~500 mSv

Sample Size

The sample for the study comprised a team of cardiothoracic surgeons assisted by cardiologists, anesthetists, nurses, and technologists who conduct and take part in fluoroscopically guided procedure at the NCTC and 498 of those with coronary artery disease (CAD) as set by the inclusive criteria, form the sample size of this study. In the study, 189 females and 309 males who underwent coronary angiography and various angioplasty procedures were considered. The data for the study was collected for a period of three years (from 2019 to 2022).

Methods

The method employed in the sampling was field measurement and survey. Application for ethical clearance was sought from the Institutional Review Boards of the University of Cape Coast and Korle-Bu Teaching Hospital, since the study examined information about actual patients. Approval was obtained from both Institutional Review Boards with reference numbers

UCCIRB/CANS/2020/04 and KBTH-IRB/00084/2020), respectively (Appendix C-1 and C-2).

Study Design

This is a cross-sectional study. In medical research, a cross-sectional study (also known as a cross-sectional analysis, transverse study, prevalence study) is a type of observational study that analyzes data from a population, or a representative subset, at a specific point in time—that is, cross-sectional data.

That is a type of observational research that analyzes data of variables collected at one given point in time across a sample population or a pre-defined subset. A cross-sectional study is used to determine if exposure to specific risk factors might correlate with a particular outcome. For instance, if diagnosis and treatment of patients with ionizing radiation could correlate with incidence of cancer. The participants in a cross-sectional study are just selected based on the inclusion and exclusion criteria set for the study. Cross-sectional designs are used for population-based surveys and to assess the prevalence of diseases in clinic-based samples.

This study is usually conducted relatively faster and are inexpensive. The study enables the estimation of the odd ratios to the study and hence the association between exposure (incidence) and the outcomes in the design. These study designs are useful for public health planning, monitoring, and evaluation. The study would enable measurement of effective radiation dose as outcome to both patients and staff as a function of x-ray exposure factors as the exposures (incidence) in the study of participants undergoing cardiology procedures at the same time.

Sampling Procedure

The study would employ purposive sampling, since the study is interested in all adult outpatients who come to the Centre for cardiac disease diagnosis and treatment, and whose initial vital signs such as respiratory rate, blood pressure, pulse rate and temperature reveals cardiac diseases. In purposive sampling the researcher adhering to the objective of the study selects a sample that would be useful to the study with a tangible reason and justification.

The study does not involve interview but data collection. All the data for the study would be collected within a period of one year. Basic patients' biostatistics (weight, age, height, sex), would be collected, with no other patient information, in exception of machine exposure parameters (kVp, mA, time, filtration) and images which are generated automatically by the software of the x-ray machine.

Instruments

Research Instruments are measurement tools designed to obtain data on a topic of interest from research subjects. The instrument for this study includes observational guide, and patient dose register (X-ray exposure parameters) to be filled in by the in-charge nurse (matron) at the study center.

An observational guide is an important outline of items for the research. It is an important tool regardless of the observer's role. In this study detached observation with no participation on the part of the researcher (complete observer) is employed. It involves participants as observers and as complete participants in the data collection with the assistance of the in-charge nurse. The

study employs the use of observational check list, which is a list of items comprising patients' vital signs and biostatistics data to be collected.

Inclusion and Exclusion Criteria

Adult outpatients who came to the center for cardiac disease diagnosis and treatment, and whose initial vital signs such as respiratory rate, blood pressure, pulse rate and temperature reveal cardiac diseases participated in the study. Adult outpatients whose initial vital signs did not reveal any possible cardiac disease were excluded from the study.

Additionally, a survey was carried out to gather data on the basic characteristics of the equipment as well as radiation protection and safety for both staff and patients.

Imaging Procedure

The first step in the basic data collection protocol was the pre-imaging procedure which involves gathering patient data such as gender, age, height, and weight in accordance with the center's standard protocol for inclusion criteria.

Also, DAP, fluoroscopy time, mA and kVp were the post image data collected in addition to the BMI which was calculated using equation 6. The relationship between DAP and BMI was established by the regression analysis of the Minitab application software.

$$BMI = \frac{W}{H^2} \quad (6)$$

where W = weight in kg and H = height in m.

Effective dose for each staff was obtained using the measured Hp (10) * values and the algorithms marked * in Table 4. Risk (total detriment) was estimated

using ICRP Publication 103 (2007) risk coefficients for the whole body and adult worker.

Table 4: Algorithm proposed for effective dose calculation with a thyroid collar [adapted from (Järvinen et al., 2008a) and (Cousins et al., 2013a)]

Source	Dosimetry Type	Effective Dose Estimation
NCRP Report 122 (NCRP, 1995) (Moladoust et al., 2015)	Single	$E = H_p(10)_{over} * \frac{1}{21}$
Martin and Magee (2013) (López et al., 2018)	Single	$E = 0.1 * H_p(10)_{over}$
*NCRP Report 122 (NCRP, 1995)	Double	$E = 0.5H_p(10)_{under} + 0.025H_p(10)_{over}$
*Swiss Ordinance (2008) (Järvinen et al., 2008b)	Double	$E = H_p(10)_{under} + 0.05H_p(10)_{over}$
Clerinx et al, 2008 (Clerinx et al., 2008)	Double	$E = 1.64H_p(10)_{under} + 0.075H_p(10)_{over}$
*Chida et al, 2013 (Kato et al., 2011)	Double	$E = 0.89H_p(10)_{under} + 0.075H_p(10)_{over}$

QC Measurements

Standard QC tests were carried out on the angiographic machine in accordance with American Association of Physicists in Medicine Basic Quality Control in Diagnostic Radiology Protocol (AAPM Protocol) and IAEA Human Health Series Number 47, Handbook of Basic Quality Control Tests for Diagnostic Radiology Protocol (IAEA Protocol); to ascertain its consistent performance prior to all cardiology procedures.

The following parameters were checked: kVp accuracy and reproducibility, mA(s) linearity and exposure reproducibility and compared with the standard limits provided and documented by the AAPM and the IAEA Protocols (*X-RAY IMAGING IN AFRICA “ Enhancing Capacity Building of Medical Physicists to Improve Safety and Effectiveness of Medical Imaging ,”* 2020); (VIENNA, 2021). The room size was measured using a survey tape measure. All the quality control tests were conducted with the X-ray source at 1 m from the patients' couch.

The radiation dose measurement for the patient was obtained from the DAP meter, while the radiation dose measurement for the personnel was obtained from the TLD readings. Patient dose and scattered radiation are dependent on any variation; in kVp, fluoroscopy time and milliamperere (mA) value of the angiographic system. An accurate kV calibration was done with a non-invasive tube voltage check at a 10 kVp interval for five kilovoltage settings of the angiographic X-ray machine. This was done by keeping the mAs constant and measuring the kVp. From the measurements, the kilovoltage accuracy was determined. The kVp accuracy was determined by finding the uncertainty using equation (7).

$$Uncertainty (Error) = \frac{Measured\ kVp - Norminal\ kVp}{Norminal\ kVp} \times 100\ \% \quad (7)$$

The uncertainty should be within $\pm 5\ %$ per the AAPM and the IAEA protocols to indicate that the kVp is accurate.

Also, the kilo voltage was set at (70, 80, 90, 100, and 110) kVps whilst the mAs was varied. The measured results were used to assess the kilo voltage reproducibility. The kilo voltage reproducibility was assessed by computing the coefficient of variation (COV) using equation (8). The COV should be less than

or equal to 0.05 (5 %), per the AAPM and the IAEA Protocols; to indicate that the kVp is reproducible.

$$COV = \frac{\text{Standard deviation}}{\text{Mean}} \quad (8)$$

where,

$$\text{Standard Deviation } (\mu) = \sqrt{\frac{\sum(X_i - \bar{X})^2}{(N-1)}} \quad (9)$$

and

$$\text{Mean value } (\bar{X}) = \frac{\sum X_i}{N} \quad (10)$$

Where X_i = observations (samples); N = total number of observations (samples).

The kilo voltage and the mAs were varied to verify output variation with mAs. The measured results obtained were used to determine the consistency and linearity of the tube output. The kVp consistency was determined by computing the ratio mGy/mAs. The ratio mGy/mAs between adjacent nominal kVp should be constant to show or indicate consistency. The kVp linearity was determined by finding the output linearity value (OLV) using equation (11)

$$OLV = \left[\frac{(\text{max} - \text{min})}{(\text{max} + \text{min})} \right] < 0.1 \text{ (10 \%)} \quad (11)$$

The OLV should be less than 0.1 (10 %) per the AAPM and IAEA protocols to indicate the linearity of the kVp.

All the consistency and linearity measurements were done using the MagicMax QC kits.

Radiation Dose Measurement

All the TLDs used were calibrated at the X-ray energy (70-100) kVp which is the range of energy at which cardiac procedures were performed and

was done at the Lumina Consult Dosimetry Laboratory with a unique ID assigned to the TLD of each staff in the team.

All the measurements were conducted in a thirty-six-calendar month at the Cath lab. For each type of procedure, the dose for each worker in a team was measured. Two TLDs were issued to each member of a team conducting a surgical procedure.

The patient's dose was measured from the DAP meter fixed on the collimator of the angiographic equipment. The following parameters were recorded: the type and the number of procedures performed by each worker, patient dose (DAP) per procedure, and the screening time of each procedure. Furthermore, $H_p(10)$ personal deep dose equivalent, $H_p(0.07)$ personal surface dose equivalent and $H_p(0.03)$ personal eye dose equivalent, from each TLD were recorded monthly for each TLD worn over and under the lead apron. Each worker's dose per procedure was calculated using the total time for all the procedures and the specific time for the specific procedure. The X-ray machine parameters, including tube voltage, tube current and filtration were recorded.

Patient Biodata

The patient pre-imaging or biodata recorded includes the gender, weight, height, and age with the corresponding cardiac procedure type whilst fluoroscopy time (FT), kilovoltage (kVp), milliampere current (mA), dose area product (DAP) that were exposure parameters constitute the post-imaging data recorded. Patient body weight was measured with the weighing scale and patient height with a measuring meter. BMI was computed using equation 6 and correlation between patient DAP and BMI was modeled using Minitab software as a statistical tool.

Scatter Radiation Study in the Angiography Room

Model Geometries

In order to assess scatter radiation in the Cath lab, the Monte Carlo method, which is a statistical approach that mimics a mathematical or physical experiment on a computer, was used. The method can simulate complex problems that comprise of different random processes with known or assumed probability density functions. The physical geometry and factors that made up the Cath lab and surgical processes during radiation exposure were modeled using the Monte Carlo approach.

Cath Lab Room

A Three Dimension (3D) Computer-Aided Design (CAD) tool called SimpleGeo version 4.3 was used to make a model of the Cath lab that is currently in use at KBTH. The dimensions of the facility were used in the model. The room area of the facility was made up of $(830*445)$ cm² from the outside. In the surgical procedure room, it was $(470*400)$ cm² with an $80*200$ cm² couch about 1 m above the ground. A control room of $(140*220)$ cm² was partitioned with a 0.5 mm lead thickness. The lead screen shields the operators and workers from scattering radiation.

The facility had two entrances in front: the main entrance and a staff entrance. The third door connects the surgical theatre to a storeroom of dimensions $(400*105)$ cm². The walls and the roof are made up of 45 cm thickness of ordinary concrete with a density of 2.3 gcm⁻³. The main and the staff entrance doors are 0.5 mm lead-lined and that of the store is made of wood. Figures 7 and 8 show the descriptions of the Cath lab suite.

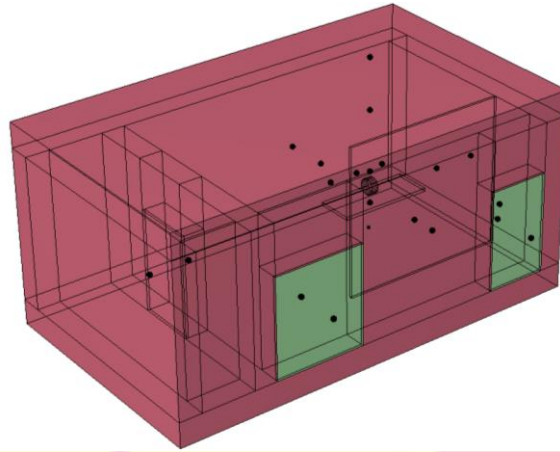


Figure 7: CAD model of the Cath lab, showing the front and side views.

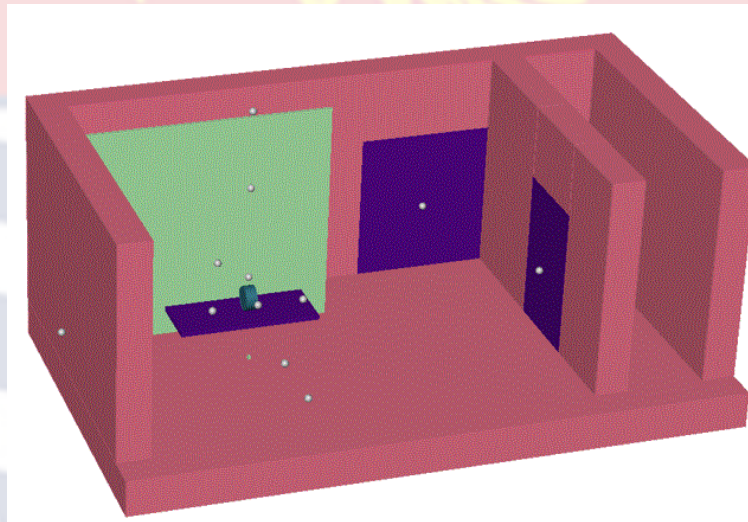


Figure 8: Cath lab showing the concrete walls, the back and with the roofed wall removed.

X-ray source

Important component of X-ray was considered to accurately model the X-ray tube. The angiographic unit at the Cath lab as shown in Figure 5 was Siemen's type (Artis Zee/Zeege) Megalix catplus 125/40/90–121 GW, model number 10144181 and serial number 640041673. The maximum voltage of the tube is 125 kV-IEC 60613 with a filtration of 0.5 mm Al/80 kV was manufactured in February 2016 in Germany.

A spectrum processor was utilized to generate the X-ray spectrum required for simulations rather than modeling the machine parts and an electron source. The X-ray spectrum was calculated in steps of 0.5 keV using data on the properties of the X-ray tube, namely target material, tube voltage, anode angle, filter material, and thickness. Instead of an electron source, a photon source approximation was used. The accuracy of MCNP 6.1 beam model was checked by comparing its main dosimetric properties to the values measured at an output of 125 kVp and it was used to calibrate the Monte Carlo beam output.

Phantom

Three different mathematical phantoms were used to mimic the human tissue since it was unethical to use humans for radiation exposure experiments. The first one was an adult Computer Tomography (CT) phantom made of Perspex material. The CT phantom was made up of 32 cm diameter and 1 cm detector diameter. The second was a MIRD phantom modified as male and female to predict the realistic exposure to the various organs for male and female patients during surgical procedures. The third was a Phantom with Moving Arms and Legs (PIMAL) representing the surgeon (male and female). The CT phantom was used for the calibration of the output X-ray beam. MIRD phantom was used as a patient undergoing a surgical procedure and the PIMAL phantom was used in place of the surgeon performing surgery. Figures 9, 10 and 11 show the CT, MIRD and PIMAL phantoms, respectively.

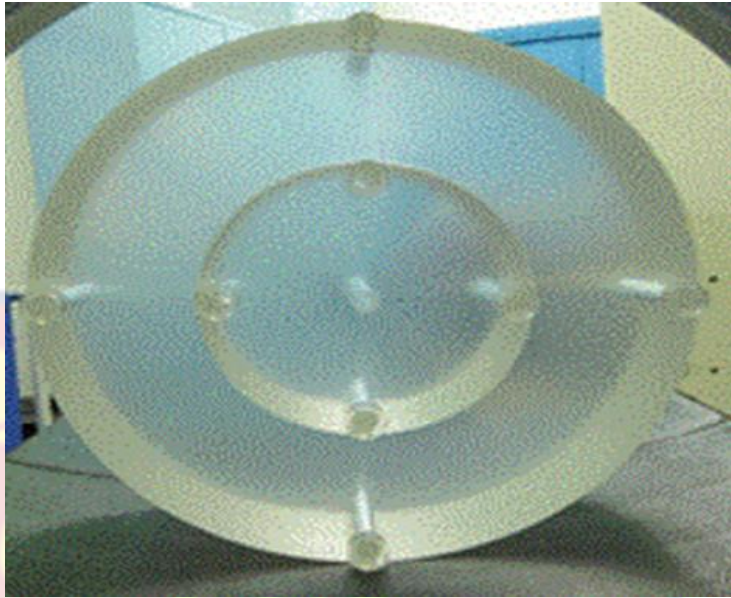


Figure 9: A typical head and body CT phantom, (standard 16 cm head and 32 cm body) phantom.

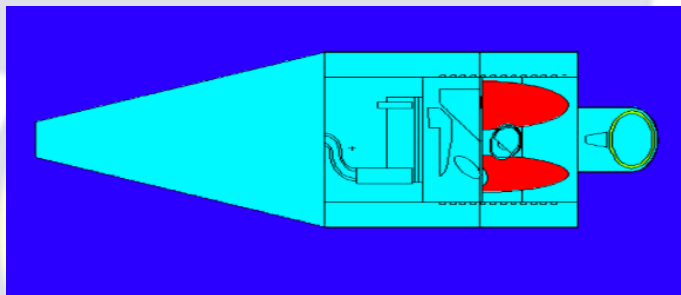


Figure 10: Modified MIRD phantom, representing a surgeon (male and female)

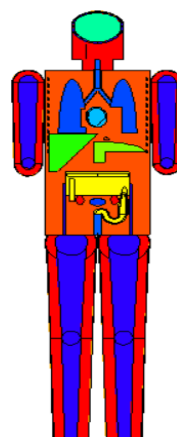


Figure 11: A PIMAL phantom with movable arms, representing a modified male and female surgeon.

Detection System

The TLD detector used by staff and surgeons during procedures is made up of a piece of semiconductor crystalline material placed in a transparent package. The semiconductor crystalline material absorbs and trap energy of the radiation during exposures in its lattice. In Monte Carlo modelling, the TLD detector was modelled as a 1 cm³ sphere of TLD materials.

MCNP Visual Editor

The CAD models were transformed into the general-purpose Monte Carlo for Neutral Particle Transport (MCNP 6.1) input format using the Monte Carlo Neutral Particle Transport Visual Editor (MCNPVISED). Figure 12 shows the output in a visual editor.

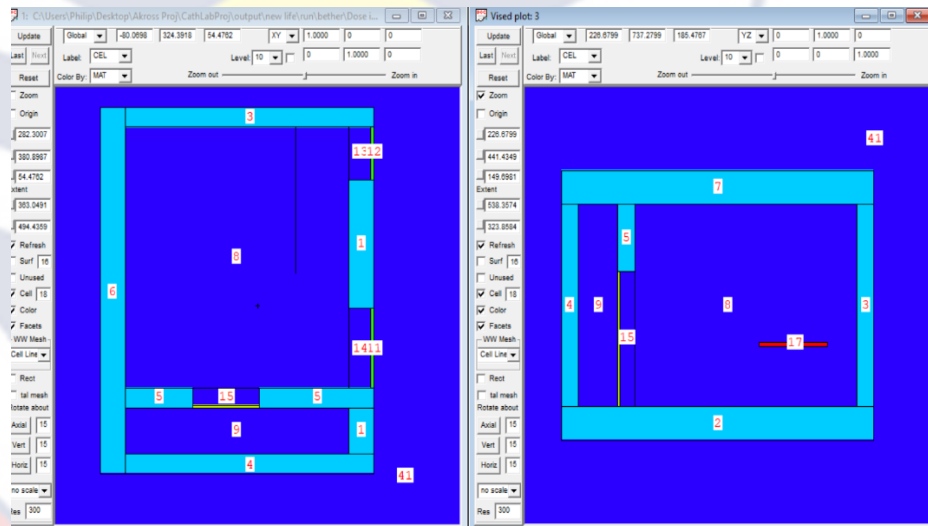


Figure 12: MCNP visual editor modelled of the Cath Lab.

Minor corrections were made to the input file. Using the visual editor of MCNP 6.1, the materials constituting the facility were modelled from their elemental and percentage abundances.

MCNP Simulations

The first step in the simulation process was to calibrate the X-ray beam using the actual measured patient dose at the isocenter to the simulated patient dose at the same spot. After calibration, the simulation process involved three main scenarios; these were: Simulation of the dose at locations where TLD was placed, simulation of patient dose and simulation of a surgeon during surgery.

In each case, enough X-ray photons were simulated for a good statistical output. MCNP has an in-built statistical test that is required for a good result. The results from the simulations were all subjected to inbuilt statistical checks until they passed all the tests. The results were processed into effective doses and compared to actual measurements in the various surgical procedures.

Whole Body Dose Calculation

Effective dose to workers were estimated with the results from the TLD measurements, as stated in (NCRP, 1995) and (ICRP, 2013). The dosimeter values for H_p below the apron and H_p above the protective apron was used to calculate the effective dose, E . various algorithms have been developed which combine dose recorded from the two dosimeters, even though there is yet to be accepted international consensus about which algorithm to use. Table 4 presents several of the algorithms proposed by different authors for effective dose calculation for both single dosimeters and double dosimeters.

The algorithms marked * in Table 4 were used in this study based on recommendations of ICRP publication 120 (ICRP, 2013) for single and double dosimetry. These algorithms were used because they are the most recently and commonly used since they incorporated protective collars where $H_p(10)_{over}$

the deep dose from the dosimeter is placed around waist level over the lead apron and $H_p(10)_{under}$ is the dose from the dosimeter worn around the neck region below the protective apron.

Also, lead apron thickness was considered in developing them (important radiation protection measurer). The value of the equivalent dose used in this calculation was obtained by using equation 12.

$$H_p(10)_{real} = k * H_p(10) \quad (12)$$

where k is the calibration factor $H_p(10)_{read}$ is the value read from TLD. The same procedure was applied to $H_p(0.07)$ information on the personnel radiation protection (Järvinen et al., 2008b).

Risk from Radiation Exposure

Radiation risk assessment was done using the risk coefficient values recommended by ICRP 2007 recommendations. Cancer, heritable effect, total detriment, and lifetime risk have been estimated for each surgeon working with radiation. Equation 13 used for cancer and heritable effect risk.

$$Annual Risk(AR) = E_{annual}(Sv) * Nominal Risk Coefficient \quad (13)$$

with the annual effective dose being E in Sievert (Sv) and the nominal risk coefficient in Sv^{-1} . The total detrimental effect was estimated by summing the annual cancer risk and annual heritable effect risk (Järvinen et al., 2008b).

Data Analysis

The data was analyzed using Minitab and GraphPad Prism software, which are statistical tools that provide functions to solve statistical problems and analyze the results. The mean value for patient dose, patient measured and

calculated body parameters as well as exposure factors were compared using independent t-test.

Evaluation of relationship between parameters was performed using Pearson's correlation coefficient and prediction of patient dose based on patient BMI and exposure factors by multiple linear regression analysis. Results were considered significant at 95 % confidence level with an alpha value of 0.05 when p-value is below 0.05.

Chapter Summary

In summary, the chapter explained the relevant methodology and materials used to achieve stated objectives of the study. The chapter gave comprehensive information on the numerous measuring techniques used to gauge, gather, and process the primary data in order to properly complete the study's objective. Additionally, in the chapter the limitations encountered during the study as well as the statistical models and software used to analyze the data was described.

CHAPTER FOUR

RESULTS AND DISCUSSIONS

Introduction

Findings from the research is presented in this chapter. The results consist of performance or QC test of the angiography equipment and compliance with the regulatory standard in Ghana. Furthermore, patient biodata measurement, occupational dose measurement, patient dose measurement, and staff risk assessment are presented.

Tabular representations, graphical representations, and model equations were used to indicate the relationship between the various parameters. The mean, maximum, and minimum values of the parameters and the distribution of the datasets were presented. Based on the scope and the study objectives the relationship between measured and estimated parameters were presented, discussed and the findings were also compared with other studies and recommendations.

Quality Assurance and Quality Control Procedure

The Performance or Quality Control Tests

Tables 5 to 7 show performance tests results or the results of quality control tests carried out on the angiography machine used for the research.

Kilovoltage accuracy

The performance of experimental equipment was expected to be consistent and accurate. This was particularly important since this equipment was used in diagnoses and the results were required to be reproducible. Reproducibility is the extent to which consistent results are obtained when the

experiment is repeated several times. Table 5 shows the kVp accuracy and reproducibility of the angiography equipment.

Table 5: kVp accuracy and reproducibility of the angiography X-ray equipment

Nominal kVp	Measured (Mean) kVp	kVp Accuracy %
70	69.12 ± 0.01	1.26
80	79.44 ± 0.02	0.70
90	89.99 ± 0.05	1.00
100	102.00 ± 0.12	2.00
110	113.28 ± 0.05	2.98

Source: Field Data 2019-2022

The kVp accuracy was determined by finding the uncertainty using equation (7).

The uncertainty should be within ± 5 % to indicate that the kVp is accurate according to regulatory requirements per AAPM and IAEA diagnostic radiology protocols (VIENNA, 2021);(X-RAY IMAGING IN AFRICA “*Enhancing Capacity Building of Medical Physicists to Improve Safety and Effectiveness of Medical Imaging*,” 2020)

Reproducibility of Exposure Parameter

Table 6 shows the kVp, timer, and exposure reproducibility of the X-ray equipment.

Table 6: kVp, timer, and exposure reproducibility of the X-ray equipment

Reproducibility @ 80 kVp and 20mAs		
Measured Mean kVp	Measured Mean Time/s	Measured Mean Exposure/mGy
80.17 ± 0.01	0.9308 ± 0.00	19.54 ± 0.00
80.19 ± 0.01	0.9311 ± 0.00	19.54 ± 0.00
80.17 ± 0.01	0.9314 ± 0.00	19.54 ± 0.00
COV = 0.00014402	COV = 0.0003222	COV = 0

Acceptable Standard, COV ≤ 0.05 (5 %).

Source: Field Data 2019-2022

The mean values obtained were used to assess the kilovoltage, current, timer and exposure reproducibility. The reproducibility was assessed by computing the COV according to equation (8). The acceptable COV should be less or equal to 0.05 (5 %) of the mean value to indicate the kVp, mAs, timer, and exposure were reproducible.

Linearity and Consistency of Exposure Parameters

To ascertain the linearity and consistency of the exposure parameters, the kilovoltage of the angiography X-ray equipment was varied between (70 and 110 kVp) and (10 and 25 mAs) to verify the output variation with mAs.

Table 7 shows the Linearity and Consistency of exposure parameters.

Table 7: Exposure parameter consistency and linearity of X-ray equipment

Exposure (mGy)	mA s	mGy/mA s	mAs Linearity (OLV)	Acceptable Criteria
4.968	10	0.4968	0.001608	≤ 0.1
7.965	16	0.4978		
9.961	20	0.4981		
12.460	25	0.4984		

Source: Field Data 2019-2022

The mean value obtained was used to determine the consistency and linearity of the tube output. The kVp consistency was determined by computing the ratio of dose to the current in mGy/mAs. The ratio of dose to the current between the adjacent nominal kVp should be constant to indicate consistency.

The kVp linearity on the other hand was determined by finding the output linearity value (OLV) using equation (11) and the resulting value should be less than or equal to 10 % of the actual value (i.e., $OLV \leq 0.1$ (10 %)).

IMAGING IN AFRICA “ Enhancing Capacity Building of Medical Physicists to

Improve Safety and Effectiveness of Medical Imaging ,” 2020);(VIENNA, 2021).

All the performance tests or the QC tests were assessed using MagicMax QC kits and were found to be consistent.

Measured Body Parameters

The measured body parameters required in achieving the objectives of the studies were height, weight, and age. Patient’s height and weight were used to estimate the body mass index. Tables 8 and 9 give the mean, maximum, and minimum values of the three body parameters and the body mass index depending on gender variation.

Table 8: Measured Height, Weight, Age, BMI for male

Sex/BMI	Measure	Age (yrs.)	Male Weight (kg)	Height (cm)	BMI (kg/m ²)
Less than 20	Mean	56.00±17.45	58.28±15.94	178.66±11.28	17.57±4.06
	Max	76.00	79.00	198.90	19.97
	Min	19.00	17.30	160.00	5.43
20-24.9	Mean	58.90±12.60	67.01±6.30	170.77±6.96	23.10±1.38
	Max	78.00	79.00	183.00	24.81
	Min	29.00	47.00	151.00	20.01
25-29.9	Mean	61.26±9.54	80.16±7.89	171.27±7.66	27.29±1.39
	Max	85.00	105.00	192.00	29.80
	Min	36.00	60.00	150.00	25.00
30-34.9	Mean	56.95±6.57	91.35±7.98	168.95±7.12	31.73±1.32
	Max	69.00	103.00	178.00	33.95
	Min	42.00	60.00	136.00	30.04
35-39.9	Mean	57.76±12.25	102.77±11.84	167.15±10.38	36.69±1.34
	Max	75.00	120.70	185.00	39.76
	Min	36.00	69.00	136.00	35.01
More than 40	Mean	56.60±11.57	117.47±17.63	162.31±14.10	45.97±7.00
	Max	77.00	159.20	188.00	58.00
	Min	36.00	81.00	130.00	40.17

Source: Field Data 2019-2022

Table 9: Measured Height, Weight, Age, BMI for female

Sex/BMI	Measure	Female			
		Age (yrs.)	Weight (kg)	Height (cm)	BMI (kg/m ²)
Less than 20	Mean	43.09±11.70	50.09±5.80	166.36±7.39	18.01±1.27
	Max	56.00	56.00	179.00	18.96
	Min	19.00	35.00	155.00	14.57
20-24.9	Mean	51.77±14.85	61.64±4.93	164.61±6.92	22.43±1.47
	Max	68.00	70.00	175.30	24.44
	Min	16.00	49.00	150.00	20.08
25-29.9	Mean	58.65±13.10	73.43±6.63	163.10±6.18	27.44±1.25
	Max	80.00	85.00	175.00	29.41
	Min	26.00	58.00	150.00	25.00
30-34.9	Mean	56.71±11.08	83.09±6.28	160.99±5.39	31.74±1.15
	Max	72.00	99.00	172.00	34.22
	Min	32.00	70.00	147.00	30.01
35-39.9	Mean	60.59±12.34	95.37±10.50	159.94±8.69	37.20±1.64
	Max	79.00	110.00	175.00	39.84
	Min	37.00	72.00	142.00	35.06
More than 40	Mean	54.67±10.59	118.33±9.98	163.37±7.40	45.83±5.93
	Max	73.00	134.00	175.00	57.99
	Min	36.00	102.00	150.00	40.12

Source: Field Data 2019-2022

Variation of Dose with BMI

Patient DAP was measured and the BMI of both males and females calculated. The BMI of patients were categorized into six as follows; category one, those with BMI < 20 kg/m², category two with BMI 20-24.9 kg/m², category three BMI 25-29.9 kg/m², category four are patients with BMI 30-34.9 kg/m², category five BMI 35-39.9 kg/m² and category six for BMI > 40 kg/m². Identification of prevalence of underweight, normal weight, overweight, and obesity in relation to cardiovascular diseases and radiation dose formed the bases for the categorization.

For the male patients, the subjects in each group were 16, 70, 129, 62, 17, and 15; whilst for the female patients, the subjects in each group were 11, 30, 63, 59, 17 and 9, respectively. From Figure 13, the data showed that out of 189 female patients, 6 % are underweight, 16% have normal weight, 33% are

overweight, whilst 45% are obese patients. From Figure 14, out of 309 male patients, 5% were underweight, 23% have normal weight, 42% are overweight, whilst 30% are obese as shown (Owusu-Banahene et al., 2018; Salah et al., 2018).

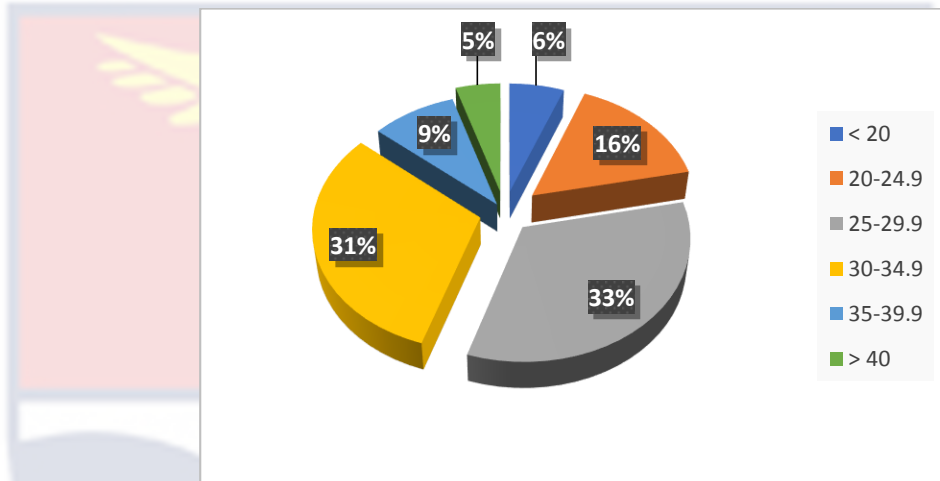


Figure 13: Percentage distribution of female patients according to the BMI category

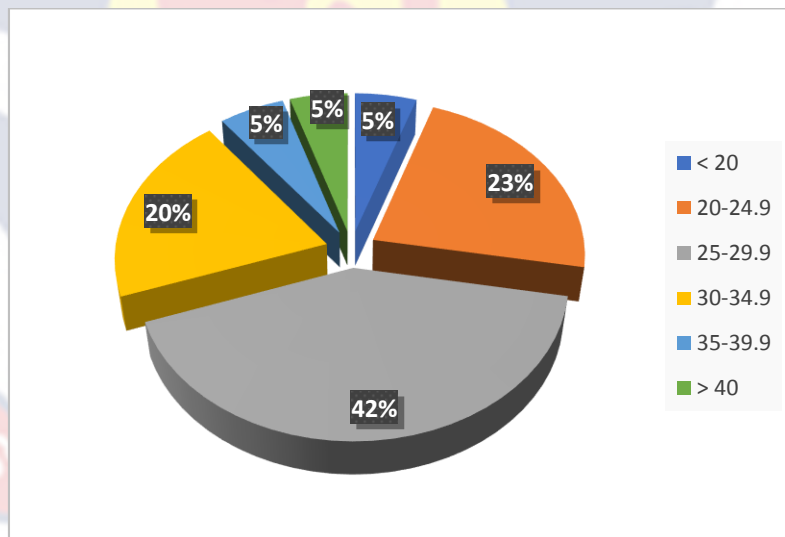


Figure 14: Percentage distribution of male patients according to BMI category

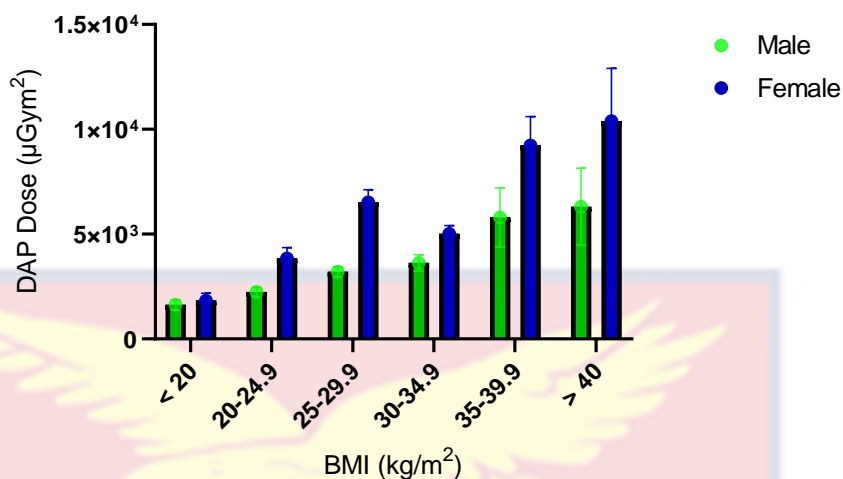


Figure 15: Variation in Patient DAP with BMI

It was observed that there was more obese female than male patients which is depicted in Figure 15. The radiation dose (DAP values) indicates that 6% of female and 5% of male require a lower amount of radiation (BMI<20), whilst 16%, 33%, (BMI between 20-29.9) and 45% (BMI of 30 and above) of female and 23%, 42% (BMI between 20-29.9) and 30% (BMI of 30 and above), of male, respectively require a high amount of radiation to effectively diagnose due to the high body mass index.

The data showed that the 45% and 30% BMI group needs four to five times the radiation required by the 6% and 5% BMI group whilst the 16% and 23% need three times the radiation exposure of the 6% and 5% group for female and male, respectively.

Measured Patient Dose, Fluoroscopy Time, kilovoltage and current.

The mean, maximum and minimum values of measured patient dose (DAP), fluoroscopy time, kilovoltage (kVp) and milliamperere current (mA) based on gender variation is presented in Tables 10 and 11. Figures 16 and 17

represents the males and females that participated in various cardiac examinations, namely CA, PCI, CAPCI, and RHC.

Table 10: Measured DAP, Fluoroscopy Time, kVp, mA for male

Sex/BMI	Category	DAP (μGym^2)	Fluoroscopy Time (mins)	kVp	mA
Male					
Less than 20	Mean	1634±943	10.18±6.05	82.87±3.82	538.80±200.40
	Max	2828	20.00	88.00	892.00
	Min	177	0.17	77.30	281.80
20-24.9	Mean	2243±1751	13.05±13.79	79.99±5.69	591.20±579.10
	Max	7256	65.30	102.50	5129.00
	Min	70	0.17	73.00	82.00
25-29.9	Mean	3206±2664	14.21±16.32	79.24±4.69	577.30±595.30
	Max	12868	90.30	101.70	5129.00
	Min	34	0.17	77.30	82.00
30-34.9	Mean	3628±3040	8.64±6.82	77.62±1.79	459.50±166.00
	Max	13738	25.60	84.70	781.60
	Min	145	0.17	73.00	82.00
35-39.9	Mean	5796±5460	18.42±14.02	78.89±8.75	476.60±180.70
	Max	14125	114.80	88.00	799.80
	Min	72	0.17	77.30	10.00
More than 40	Mean	6308±7567	15.81±27.15	82.45±3.66	453.50±222.00
	Max	23809	38.00	98.00	782.80
	Min	345	0.17	73.00	100.00

Source: Field Data 2019-2022

Table 11: Measured DAP, Fluoroscopy Time, kVp, mA for female

Sex/BMI	Category	DAP (μGym^2)	Fluoroscopy Time (mins)	kVp	mA
Female					
Less than 20	Mean	1833 \pm 1133	6.33 \pm 3.79	79.17 \pm 3.51	407.5 \pm 171.80
	Max	4112	14.00	85.30	799.8
	Min	437	2.70	73.00	106.9
20-24.9	Mean	3846 \pm 2814	8.93 \pm 6.21	77.86 \pm 2.13	479.2 \pm 153.20
	Max	11754	22.00	84.70	799.8
	Min	409	0.17	73.00	105.9
25-29.9	Mean	6514 \pm 4828	9.12 \pm 6.98	79.11 \pm 3.41	548.8 \pm 169.10
	Max	19767	30.60	87.60	799.8
	Min	1470	0.17	73.00	100.0
30-34.9	Mean	5015 \pm 2965	6.94 \pm 4.85	78.54 \pm 4.60	481.9 \pm 169.20
	Max	14440	19.20	96.00	799.8
	Min	13	0.17	73.00	82.0
35-39.9	Mean	9526 \pm 5670	11.39 \pm 8.38	79.21 \pm 4.82	547.6 \pm 182.90
	Max	20961	30.40	96.00	799.8
	Min	2443	1.70	77.30	196.3
More than 40	Mean	8466 \pm 4928	14.74 \pm 11.94	81.36 \pm 6.64	489.7 \pm 148.90
	Max	18243	36.80	95.80	782.8
	Min	1508	2.20	76.90	82.0

Source: Field Data 2019-2022

Statistical Parameters Relating to Cardiology Procedures**Number of Procedures Performed.**

Table 12 shows the statistics of patients and coronary angiography procedures during the period of data collection.

Table 12: Frequency of Patients and number of Procedures

Procedure	Male	Female	Total
CA	154	159	313
PCI	46	21	67
Combined CAPCI	53	31	84
RHC	26	31	57
Total	279	242	521

Source: Field Data 2019-2022

The data was then transformed into a pie chart for further clarity, and this was revealed by Figures 16 and 17 for males and females respectively.

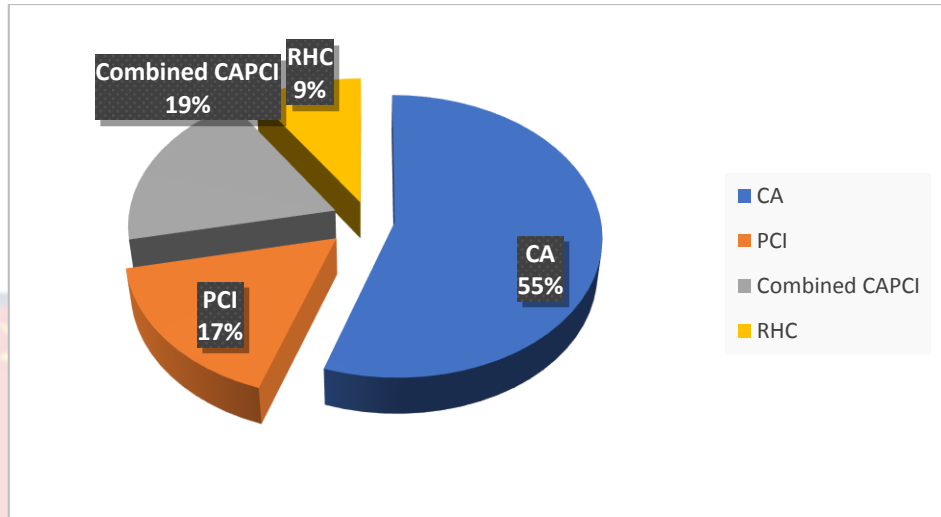


Figure 16: Percentage of males per various cardiac procedure during data collection

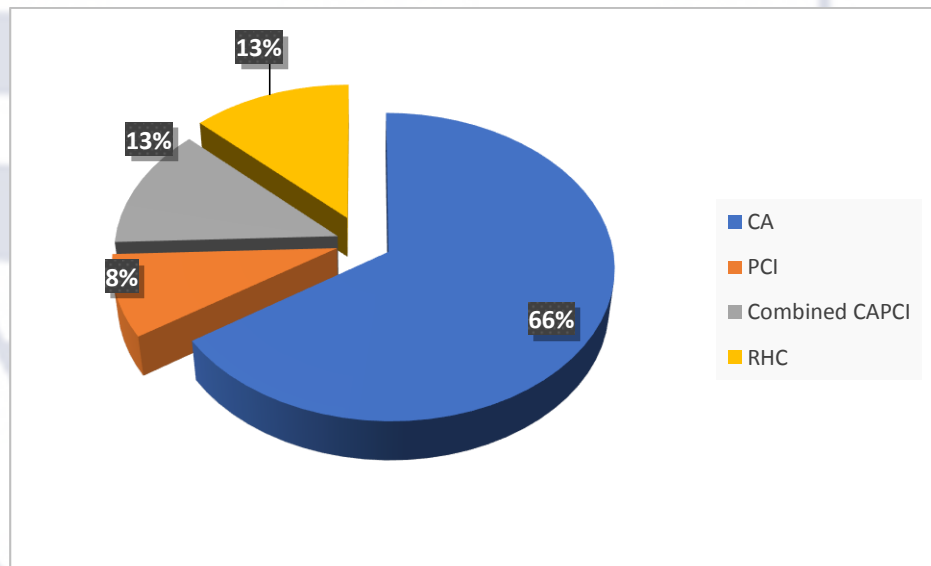


Figure 17: Percentage of females per procedure during data collection

Figures 16 and 17 shows that coronary angiography was the commonest procedure performed by the cardiologist at the center, for both males (55%) and females (66%). This was expected since CA is a diagnostic procedure. Angioplasty procedures comprising, PCI, CAPCI and RHC which are treatment

procedures for males are 17%, 19%, 9% and for females the values were 13%, 13%, and 8 % respectively.

Statistics of Parameters during Cardiology Procedures

Tables 13 and 14 show the various measured statistical data relating to dose, BMI, time, and age.

Table 13: Statistics of Parameters: Dose (DAP), Fluoroscopy time, Age and Body Parameters (BMI) of male

Procedure/Parameter	Min	Max	Mean	Standard Error of Mean	Standard Deviation
CA					
DAP (μGym^2)	34.00	4511	1734	102	1262
BMI (kg/m^2)	18.59	35.93	27.14	0.33	4.03
Fluoroscopy time (mins)	0.17	90.30	10.57	1.06	13.13
Age (years)	29.00	84.00	59.96	0.894	11.09
PCI					
DAP(μGym^2)	249	53299	7477	1651	11199
BMI (kg/m^2)	20.61	40.56	28.50	0.69	4.66
Fluoroscopy time (mins)	0.17	114.8	30.19	3.14	21.27
Age (years)	42.00	87.00	62.17	1.53	10.34
Combine CAPCI					
DAP (μGym^2)	345	45547	8717	1475	10739
BMI (kg/m^2)	13.580	40.17	28.142	0.673	4.903
Fluoroscopy time (mins)	0.17	45.50	18.60	1.59	11.57
Age (years)	26.00	82.00	58.79	1.57	11.46
RHC					
DAP (μGym^2)	437	12286	3487	735	3748
BMI (kg/m^2)	11.94	31.22	22.08	0.98	4.99
Fluoroscopy time (mins)	2.90	43.10	11.25	1.85	9.42
Age (years)	19.00	77.00	43.73	2.76	14.08

Patients during cardiology procedures

Source: Field Data 2019-2022

Table 14: Statistics of Parameters: Dose (DAP), Body Parameters (BMI), Fluoroscopic time (FT) and Age of female patients during cardiology procedures

Procedure/Parameter	Min	Max	Mean	Standard Error of Mean	Standard Deviation
CA					
DAP (μGym^2)	13.00	70491	6944.0	604.0	7615
BMI (kg/m^2)	18.03	52.34	29.92	0.437	5.506
Fluoroscopic time (mins)	0.167	46.20	9.074	0.664	8.369
Age (years)	26.00	87.00	60.30	1.00	12.65
PCI					
DAP(μGym^2)	1551	34762	13349	2059	9437
BMI (kg/m^2)	18.82	49.45	29.33	1.39	6.35
Fluoroscopic time (mins)	2.70	73.00	23.41	4.43	20.32
Age (years)	34.00	79.00	58.10	2.56	11.74
Combine CAPCI					
DAP (μGym^2)	345	45988	8090	1936	10779
BMI (kg/m^2)	20.81	46.31	28.88	1.05	5.84
Fluoroscopic time (mins)	3.30	45.30	20.40	1.94	10.81
Age (years)	41.00	80.00	57.97	1.77	9.86
RHC					
DAP (μGym^2)	409	13349	3427	629	3502
BMI (kg/m^2)	11.94	34.02	22.99	0.933	5.196
Fluoroscopic time (mins)	1.80	60.00	12.52	1.95	10.88
Age (years)	16.00	79.00	42.71	2.74	15.25

Source: Field Data 2019-2022

The mean BMI of male patients who were diagnosed with CA is (27.14 ± 4.03) kg/m^2 with a mean age of (59.96 ± 11.09) years. The mean BMI and age of male patients who underwent PCI were (28.50 ± 4.66) kg/m^2 and (62.17 ± 10.34) years, respectively.

For the male combined procedure, CAPCI, the mean BMI and age were (28.14 ± 4.90) kg/m^2 and (58.79 ± 11.46) years, whilst for the male RHC mean BMI and age values were (22.08 ± 4.99) kg/m^2 and (43.73 ± 14.08) years. Figure

18 shows the relationship between males BMI and procedures whilst Figure 19 shows relation between males DAP and procedures.

From Figure 18 it can be deduced that male patients who underwent RHC procedure have average BMI more than 20 kg/m², whilst most of the male patients who underwent CA, PCI, and combined CAPCI have BMI below 30 kg/m².

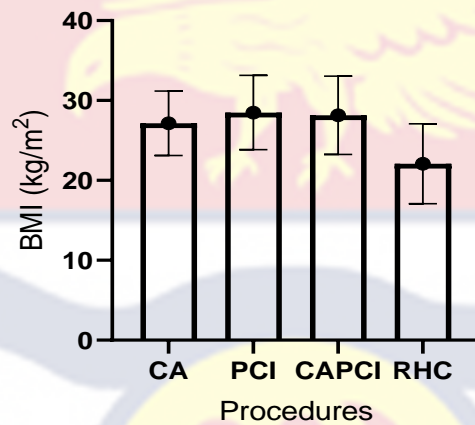


Figure 18: Male BMI with the various cardiac procedure

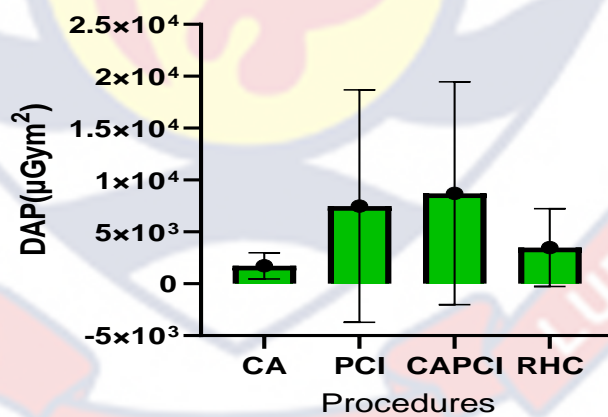


Figure 19: Male DAP with their respective cardiac procedures, showing increasing uncertainty with increasing DAP.

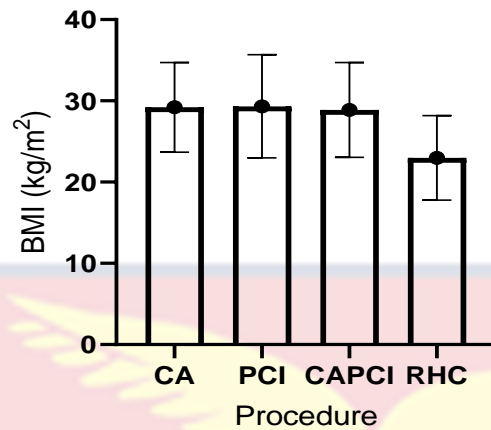


Figure 20: Female BMI with various cardiac procedure

For the female patients who were diagnosed with CA, the mean BMI was (29.92 ± 5.51) kg/m² with mean age of (60.30 ± 12.65) years. The mean BMI and age of female patients who underwent PCI were (29.33 ± 6.35) kg/m² and (58.10 ± 11.74) years, respectively.

For the female combined procedure of CAPCI, the mean BMI and age were (28.88 ± 5.84) kg/m² and (57.97 ± 9.86) years, whilst for the female RHC mean BMI and age values were (23.00 ± 5.20) kg/m² and (42.71 ± 15.25) years.

Figure 20 shows the relationship between females BMI and procedures whilst Figure 21 shows relation between females DAP and procedures.

From Figure 20, female patients who underwent RHC cardiac examination had average BMI a little above 20 kg/m², whilst majority of female patients who underwent CA, PCI and combined CAPCI, coronary artery disease diagnosis and treatment had mean BMI close to 30 kg/m².

An average BMI of 26.47 kg/m² and 27.60 kg/m² across the four main procedures have been found for both males and females respectively indicating the prevalence of overweight in the population used for the study. (BMI > 25 kg/m²). Figures 19 and 21 show the mean dose distribution and SD whilst

Figures 18 and 20 show the mean BMI distribution and SD for the various cardiology procedures for both male and female, respectively. From Tables 13 and 14, the variation between the mean DAP, mean BMI and their respective SD values gave an indication of PCI and CAPCI procedures being relatively high dose procedures for both male and females.

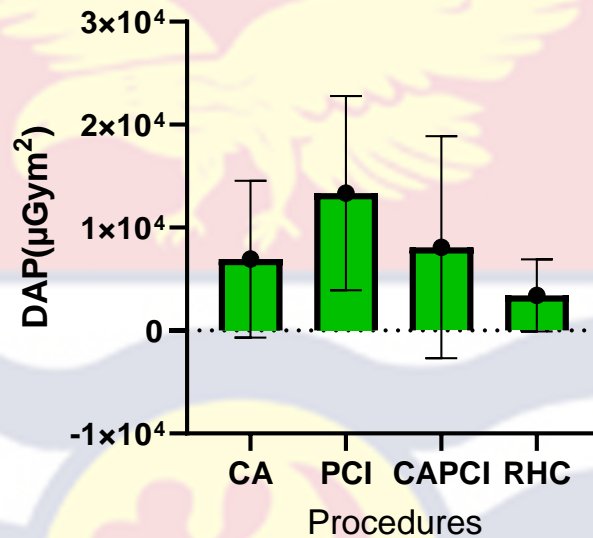


Figure 21: Female DAP with their respective cardiac procedure, showing increasing uncertainty with increasing DAP.

Empirical Modelling

Using the observed data and parameters, the statistical modeling process was based on a linear technique of modeling the relationship between scalar dependent variables and independent variables. Linear predictor functions whose unknown model parameters were determined from the data were used to model the relationships between the parameters. The focus of the linear regression was the conditional probability distribution of the Normal Probability Plot (NPP) of the variables. To determine if the data set is approximately normally distributed and to determine the descriptive parameters

of the modelled equations, four graphical techniques namely normal histogram, normal probability plot, Versus Fits, and Versus Order were used (Siiskonen et al., 2018).

In addition, a theoretical normal distribution density function was plotted against the equations modeled so that the points formed an approximated straight line. However, for some of the procedures for both males and females, a non-linear model representing the best fit was used. The graphs were used to analyze the goodness-of-fit and the linear regression analysis were generated by the residual plots, on which the plots were based to determine if the ordinary least squares assumptions were being met (Jones & Daly, 1995). The unbiased coefficient estimates were satisfactorily provided with the least variance (≤ 0.05) based on the assumptions. Four main techniques were employed as follows:

The histogram of residuals was used to check for outliers and determine whether the data was skewed. The assumption that the residuals are normally distributed was verified using the normal probability plot of the residuals. The assumption that the residuals have a constant disagreement was further checked using residuals verses fits, and the assumption that the residuals are uncorrelated with one another was examined using residuals versus order of data. (Jones & Daly, 1995).

The Appendices A-1 to A-4 for male cardiology procedures and B-1 to B-4 for female cardiology procedures provide the results of these model verification diagrams. The model equation, standard deviation, predictor, and p-value are the four components that make up the particular model equation. The model is better if the standard deviation is smaller, the R-Squares are closer

to 100%, and a small p-value (usually ≤ 0.05) indicates strong evidence against the null hypothesis, which leads to the rejection of the null hypothesis (i.e., no evidence for correlation).

To make decisions about how to analyze the data for the various models, the decision rule and conclusion hypothesis were used. The null hypothesis to accept a model was based on the condition that the p-value must be less than the 5% significance level ($p < 0.05$) or fail to reject if otherwise.

Additionally, the rule to accept the model was also based on the model predictor, a model of 80 % or better was considered significant for clinical application. With these rules for decision, a comparative study on DAP and BMI for the various cardiology procedures was carried out. The results of the multiple comparative tests performed for various procedures and gender variations of the underlying dependent variables of the models were presented. The models were designed as Graphical User Interface (GUI) to facilitate its acceptance and use for clinical applications.

Modelled DAP and BMI Representations

The graphic relationship between patient dose DAP and BMI for both males and females for the various angiography and angioplasty procedures are presented in this section. It also shows the model equations with the graphs for the various cardiology procedures and the regression model for the prediction of the relation that exists between scaler-dependent variable DAP and independent variable BMI for both males and females.

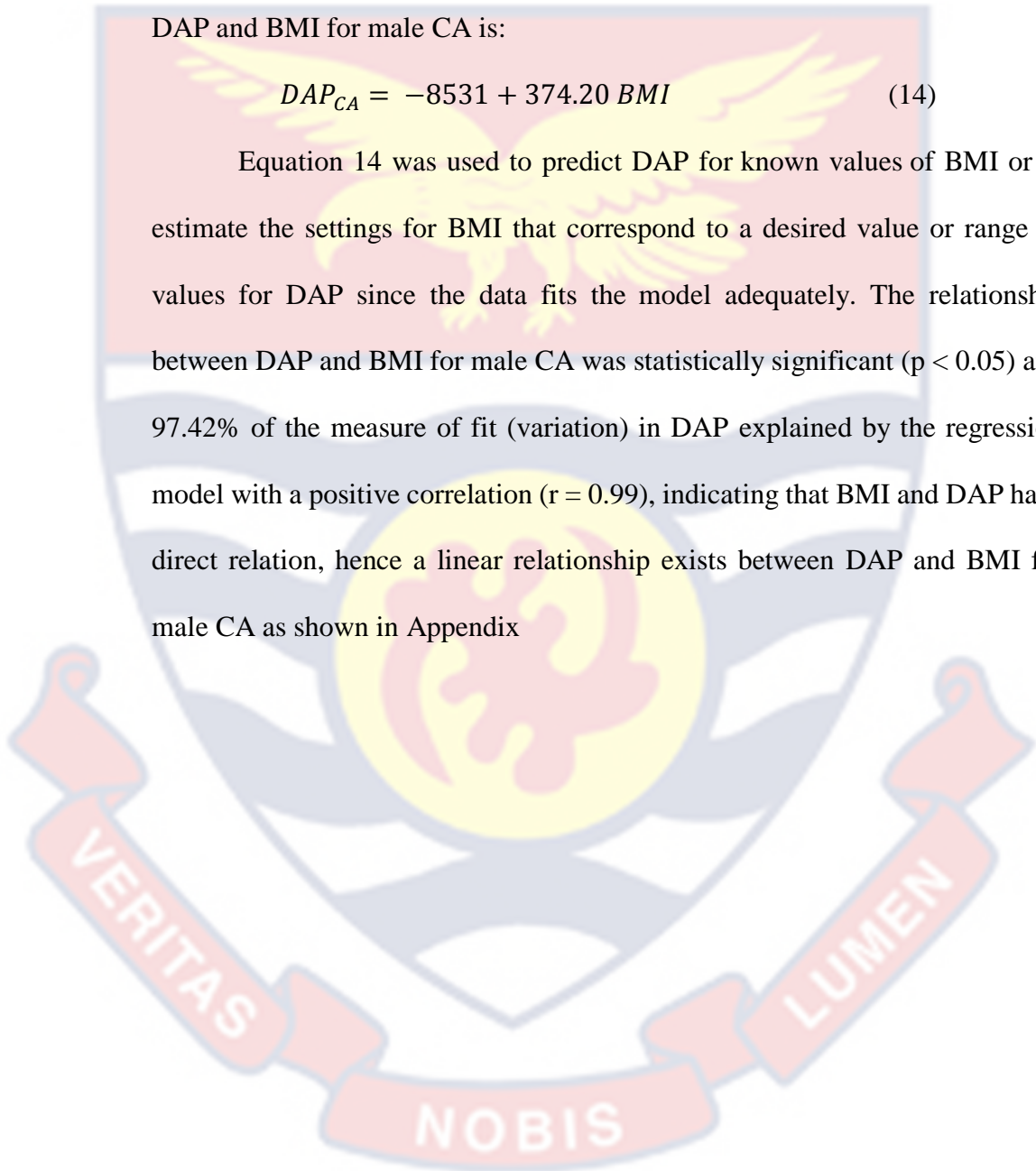
Modelled DAP and BMI for Male CA.

Figures 22 and 23 present a linear relationship between patient DAP and BMI for male CA procedures. The modelling shows the relation that exists

between a scalar dependent variable DAP and independent variable BMI. Figure 22 shows the regression plot for DAP vs BMI with SD 178.165 and predictor R-SQ of 97.42%, whilst Figure 23 shows the predicted plot of DAP verses BMI for male CA. The equation that fits the model and describes the relation between DAP and BMI for male CA is:

$$DAP_{CA} = -8531 + 374.20 BMI \quad (14)$$

Equation 14 was used to predict DAP for known values of BMI or to estimate the settings for BMI that correspond to a desired value or range of values for DAP since the data fits the model adequately. The relationship between DAP and BMI for male CA was statistically significant ($p < 0.05$) and 97.42% of the measure of fit (variation) in DAP explained by the regression model with a positive correlation ($r = 0.99$), indicating that BMI and DAP have direct relation, hence a linear relationship exists between DAP and BMI for male CA as shown in Appendix



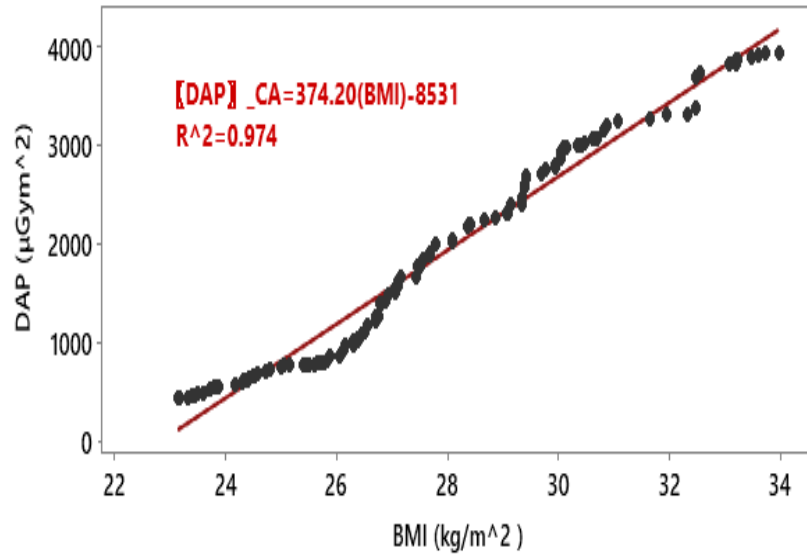


Figure 22: Fitted Line Plot of DAP vs BMI for male CA Procedure

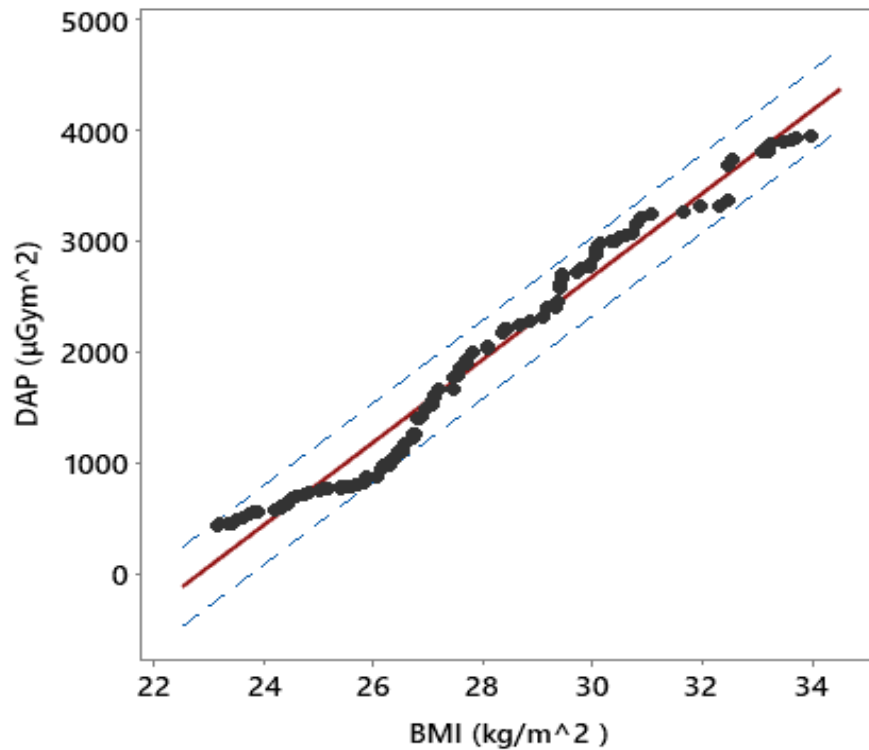


Figure 23: Predicted plot for DAP vs BMI for male CA. The blocked fitted red line shows the predicted DAP for any BMI value and the blue dashed lines show the 95% prediction interval.

Modelled DAP and BMI for Male PCI

Figures 24 and 25 represents a linear relation that exist between patient DAP and BMI for male PCI. Figure 24 shows the regression plot whilst Figure 25 is the predicted plot for DAP and BMI. The modelling indicates the relation between a scalar dependent variable DAP and independent variable BMI with SD of 149.624 and the predictor R-SQ of 97.47%. The equation that fits the model and describes the relation existing between DAP and BMI for male PCI is:

$$DAP_{PCI} = -11132 + 532.3BMI \quad (15)$$

Equation 15 is used to estimate DAP for values of BMI or to calculate the settings for BMI that corresponds to the desired values of DAP for male PCI, since the data fits the model well. The relationship between DAP and BMI for male PCI is statistically significant ($p < 0.05$). The model indicates that 97.58% of the measure of fit (variation) in DAP can be explained with the model. There is a positive correlation ($r = 0.99$), an indication that when the independent variable (BMI) increases the dependent variable DAP also tends to increase showing a linear relation exists between DAP and BMI for male PCI as shown in Appendix A-2

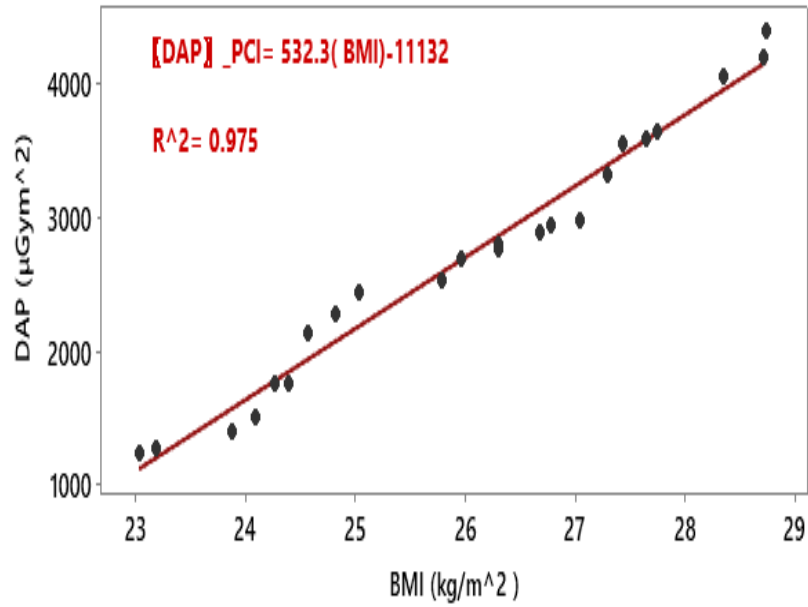


Figure 24: Fitted Line Plot for DAP vs BMI for male PCI Procedure

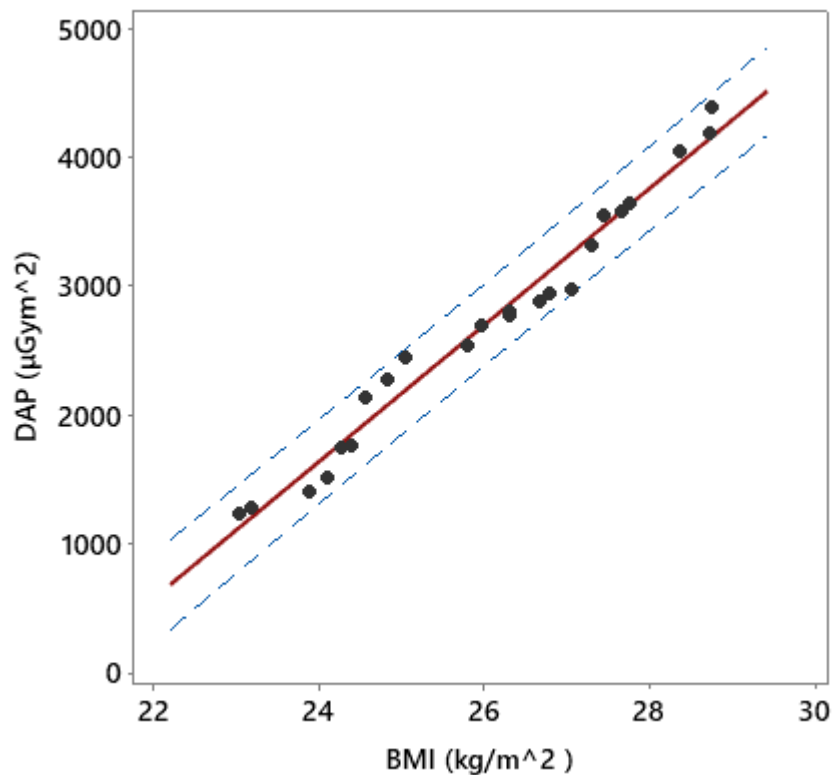


Figure 25: Predicted plot of DAP vs BMI for male PCI. The blocked fitted red line shows the predicted DAP for any BMI value and the blue dashed lines show the 95% prediction interval.

Modelled DAP and BMI for Combined Male CAPCI.

Figures 26 and 27 present the relationship between patient DAP and BMI for combined male CAPCI. Figure 26 illustrates regression model between scalar dependent variable DAP and independent variable BMI with SD of 163.758 and the predictor R-SQ of 95.36%. Figure 27 is the predicted plot between DAP and BMI for the combined CAPCI procedure. The equation that fits and describes the relationship between DAP and BMI for males combined CAPCI is a quadratic model given as:

$$DAP_{CAPCI} = 11286 - 1205BMI + 33.06(BMI)^2 \quad (16)$$

Equation 16 was used to predict DAP for values of BMI or to determine the settings for BMI that correspond to desired values or range of values for DAP because the data fits the quadratic model satisfactorily. A non-linear relationship exists between DAP and BMI for the combined procedures as indicated in Appendix A-3. However, the relation between DAP and BMI is statistically significant ($p < 0.05$) with 95.80% of the variation in DAP been explained by the regression model.

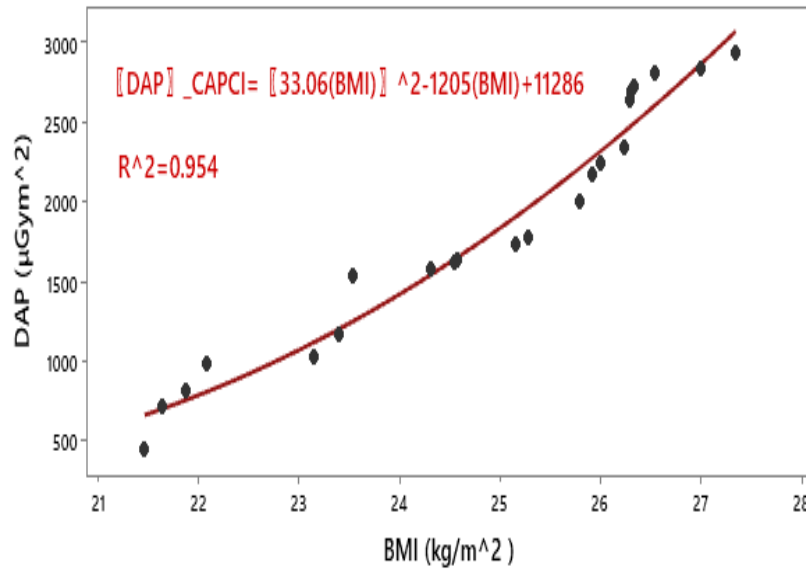


Figure 26: Fitted Line Plot for DAP vs BMI for male Combined CAPCI Procedure

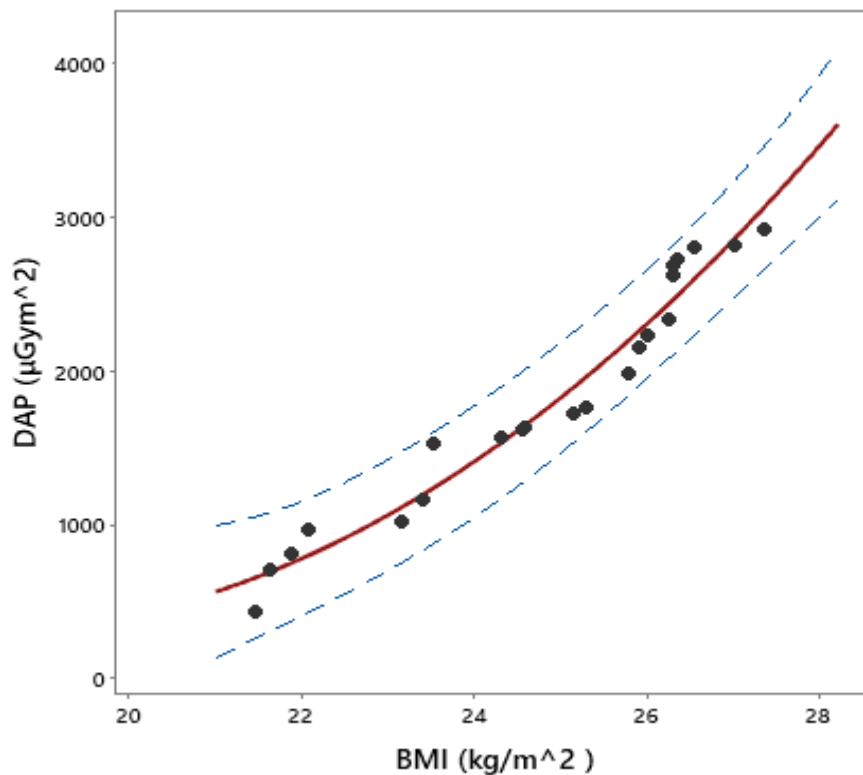


Figure 27: Predicted plot of DAP vs BMI for male CAPCI. The blocked fitted red line shows the predicted DAP for any BMI value and the blue dashed lines show the 95% prediction interval.

Modelled DAP and BMI for Male RHC

Figure 28 and 29 present linear regression model and predicted model between patient DAP and BMI for male coronary angioplasty RHC respectively. The linear method was used to model the relationship between a scalar dependent variable DAP and independent variable BMI with SD of 180.029 and predictor R-SQ of 96.66%. The equation that fits and describes the relation existing between DAP and BMI for male RHC is a linear model given as:

$$DAP_{RHC} = -5238 + 331.3 BMI \quad (17)$$

Equation 17 was used to predict DAP for values of BMI or find the settings for BMI that correspond to a desired values or range of values for DAP since the data fits the model well. There is significant statistical relationship between BMI and DAP ($p < 0.05$) with 96.66% of the variation in DAP being explained by the regression model. A positive correlation ($r = 0.98$) indicates the existence of direct relation between BMI and DAP; hence a linear relationship exists between DAP and BMI for male RHC procedure as shown in Appendix A-4.

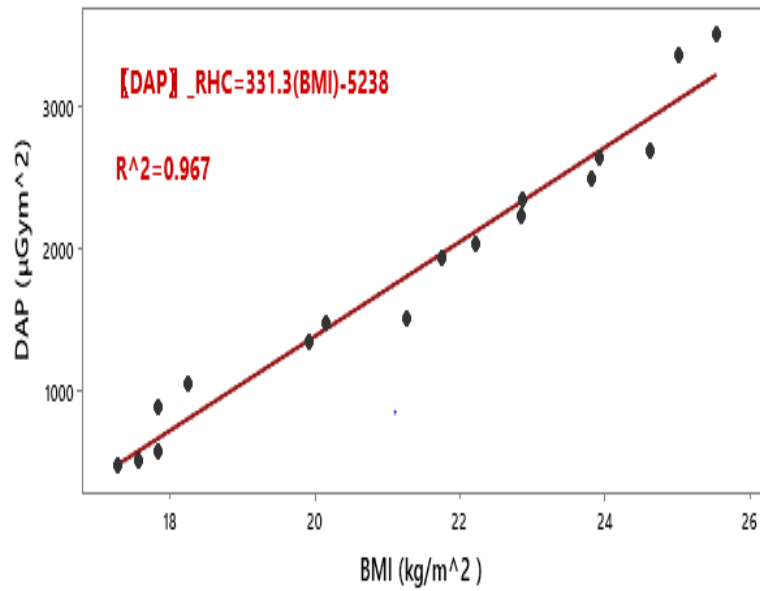


Figure 28: Fitted Line Plot for DAP vs BMI for male RHC Procedure

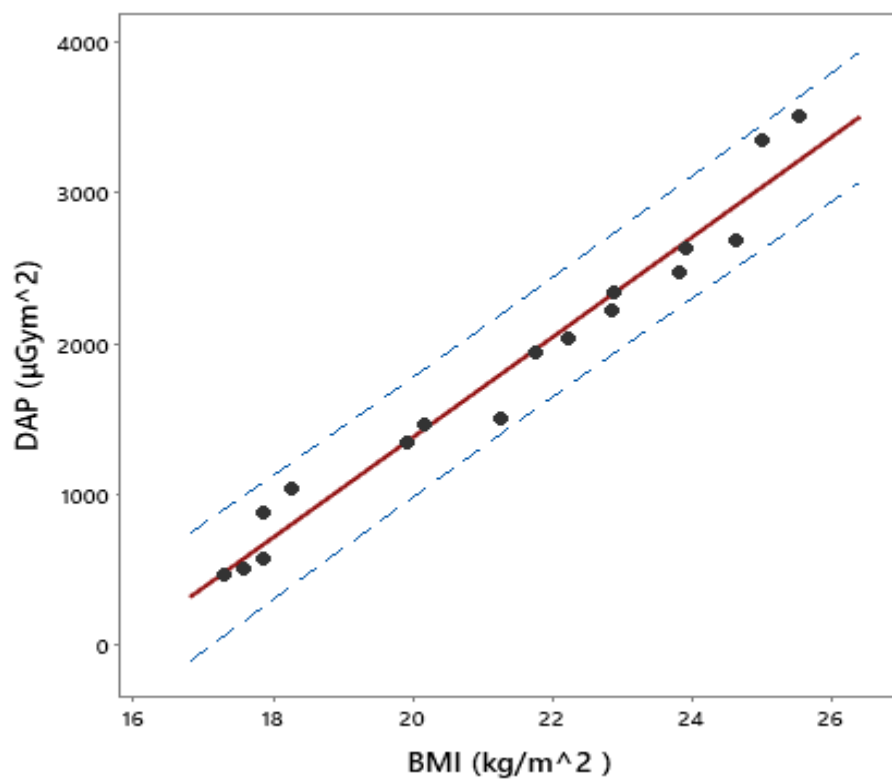


Figure 29: Predicted plot of DAP vs BMI for male RHC. The blocked fitted red line shows the predicted DAP for any BMI value and the blue dashed lines show the 95% prediction interval.

Modelled DAP and BMI for Female CA

Figures 30 and 31 present linear regression relationship and predicted relation between patient DAP and BMI for female CA procedures. It is a way of modelling the relation that exist between scalar dependent variable DAP and independent variable BMI. The SD of the regression plot is 87.145 and the predictor R-SQ that gives the statistical measure of fit (variation) of the dependent variable, DAP and the independent variable BMI being 99.03%. The equation that fits and describes the relation between DAP and BMI for female CA is a linear model given as:

$$DAP_{CA} = -10653 + 519.33 BMI \quad (18)$$

The data fits the model well; hence, Equation 18 was used to predict DAP for values of BMI or find the settings for BMI that correspond to desired values or range of values for DAP. The relation between DAP and BMI for female CA was found to be statistically significant with $p < 0.05$, whilst 99.05% of the measure of fit (variation) in DAP being explained by the regression model with a positive correlation ($r = 1.00$), indicating there is a direct linear relation between BMI and DAP for female CA as shown in Appendix B-1

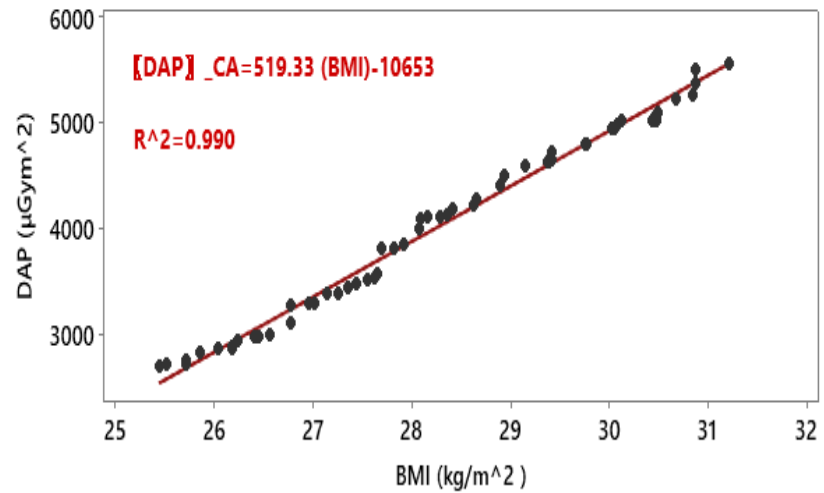


Figure 30: Fitted Line Plot for DAP vs BMI for female CA Procedure

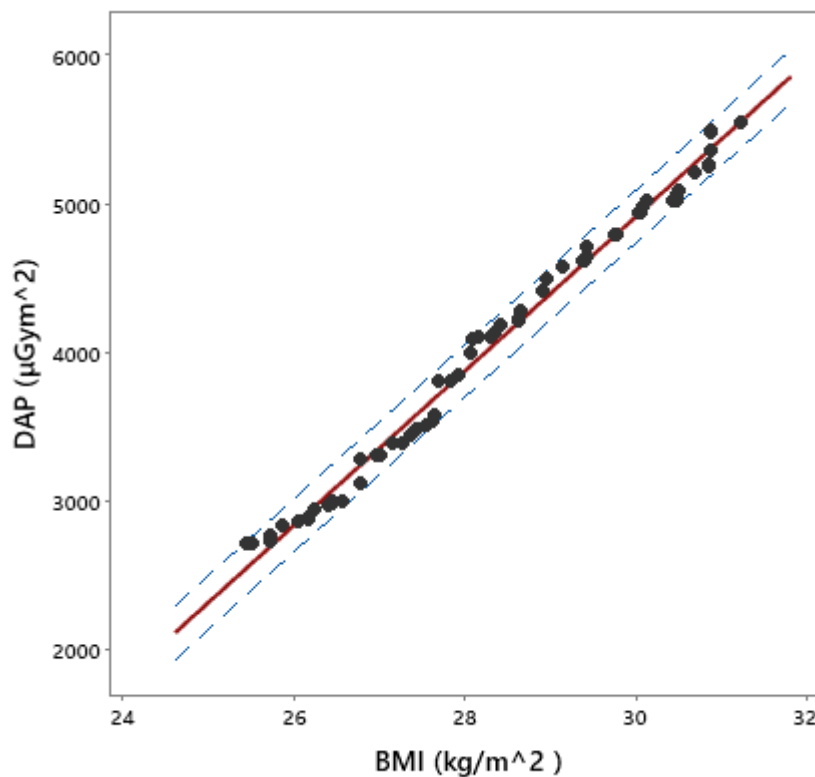


Figure 31: Predicted plot of DAP vs BMI for female CA. The blocked fitted red line shows the predicted DAP for any BMI value and the blue dashed lines show the 95% prediction interval.

Modelled DAP and BMI for Female PCI.

Figures 32 and 33 represent the linear regression between patient DAP versus BMI whilst figure 33 is the predicted plot between DAP and BMI for female PCI. The SD for the model is 348.729 and the predictor R-SQ which explains the statistical measure of fit (variation) of the dependent variable, DAP and the independent variable BMI being 99.65%. The equation that fits and describes the relationship between DAP and BMI for female PCI is a linear model given as:

$$DAP_{PCI} = -77654 + 3121BMI \quad (19)$$

Equation 19 was used to predict DAP values for BMI or find the settings for BMI that correspond to desired values or range of values for DAP for female PCI since the data fits the model well. The relation that exists between DAP and BMI is statistically significant with $p < 0.05$ and 99.65% of the measure of fit (variation) in DAP being explained by the regression model and a positive correlation ($r = 1.00$) indicating that BMI increases with increasing DAP hence a linear relation exists between DAP and BMI for female PCI as shown in Appendix B-2.

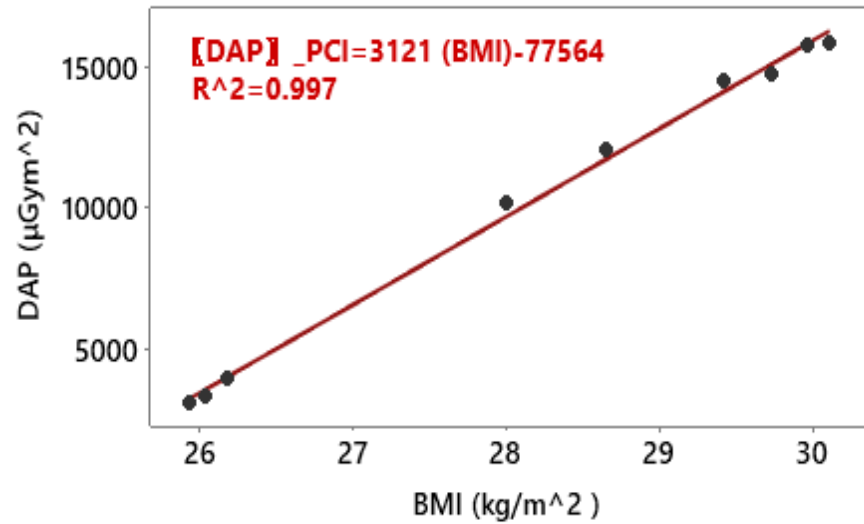


Figure 32: Fitted Line plot for DAP vs BMI for female PCI Procedure

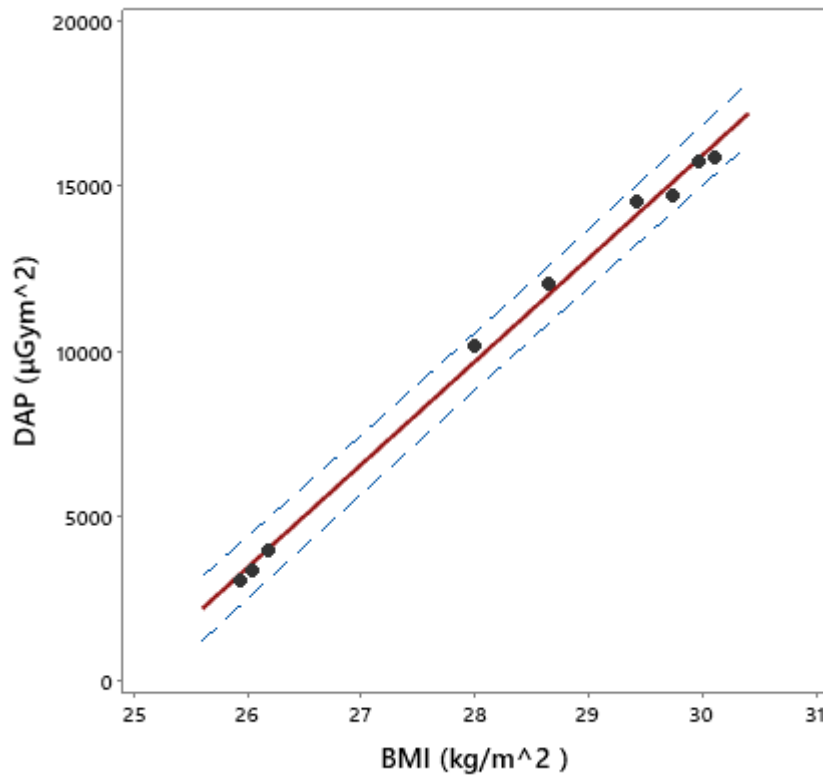


Figure 33: Predicted plot of DAP vs BMI for female PCI with the blocked fitted red line showing the predicted DAP for any BMI value and the blue dashed lines showing the 95% prediction interval.

Modelled DAP and BMI for Combine Female CAPCI.

Figure 34 expresses the regression relationship between DAP and BMI whilst Figure 35 is the predicted plot between patient DAP and BMI for the female combined CAPCI. Figure 34 is the modelling relation between DAP, a scalar dependent variable and BMI, independent variable with SD of 113.048 and predictor R-SQ which estimates the statistical measure of fit (variation) of the dependent variable, DAP and the independent variable BMI being 98.46%. The equation that fits and describes the relation between DAP and BMI for female combined CAPCI is a quadratic model given as:

$$DAP_{CAPCI} = 1137 - 1111BMI + 28.8 (BMI)^2 \quad (20)$$

Equation 20 was used to predict DAP for values of BMI or find the settings for BMI that correspond to desired values or range of values for DAP for female combined CAPCI since the data fits the quadratic model well. The relation that exists between DAP and BMI for female combined CAPCI was found to be statistically significant ($p < 0.05$) and 98.65 % of the variation in DAP being explained by the regression model. Thus, a non-linear relationship exists between DAP and BMI for female combined CAPCI procedures as shown in Appendix B-3.

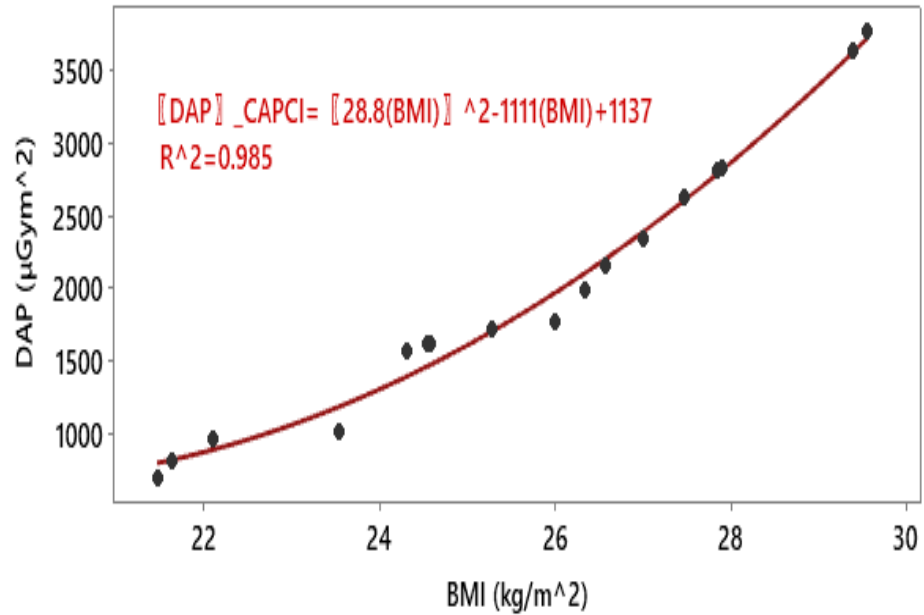


Figure 34: Fitted Line Plot for DAP vs BMI for female combined CAPCI Procedure

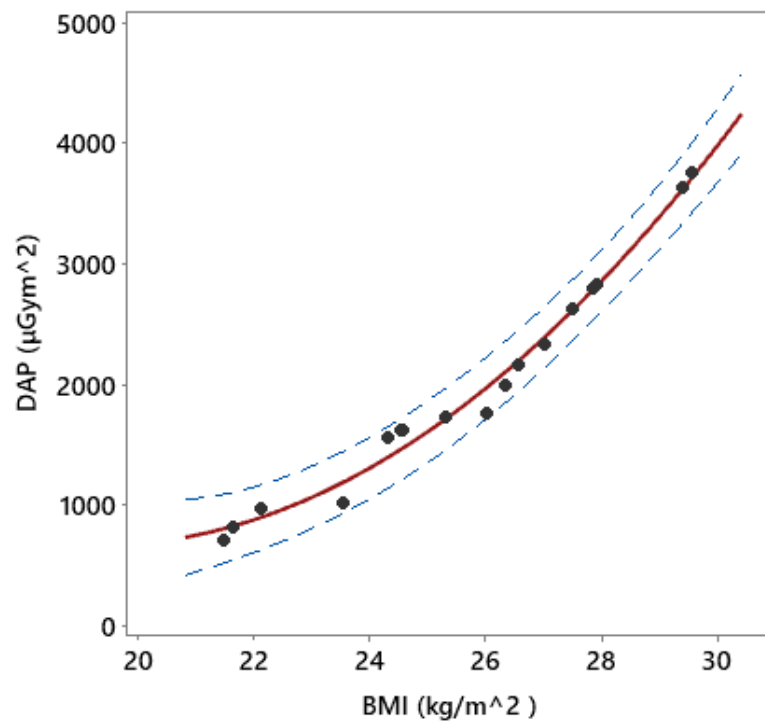


Figure 35: Predicted plot of DAP vs BMI for female combined CAPCI. The blocked fitted red line shows the predicted DAP for any BMI value and the blue dashed lines show the 95% prediction interval.

Modelled DAP and BMI for Female RHC

Figure 36 presents linear relationship between patient DAP and BMI, whilst Figure 37 is the predicted plot of DAP versus BMI for female RHC procedure. The model shows the relation that exists between DAP, a scalar dependent variable and BMI independent variable with SD of 83.788 and the predictor R-SQ of 98.62%, which indicates the statistical measure of fit (variation) of the dependent variable, DAP, and the independent variable BMI. The equation that fits the linear model describing the relationship between DAP and BMI for female RHC is:

$$DAP_{RHC} = -3617 + 257.1BMI \quad (21)$$

Equation 21 was used to predict DAP for values of BMI or find the settings for BMI that correspond to desired values or range of values for DAP since the data fits the model correctly. There is significantly statistical relationship between BMI and DAP ($p < 0.05$) with 98.62% of the variation in DAP being explained by the regression model. A positive correlation ($r = 0.99$) shows that BMI and DAP are directly related, hence linear relationship exist between DAP and BMI for female RHC procedure as shown in Appendix B-4

It has been observed that patient dose (DAP) increases with increasing BMI; an indication that an increased BMI is an increase in tissue density, hence an increase or higher radiation dose.

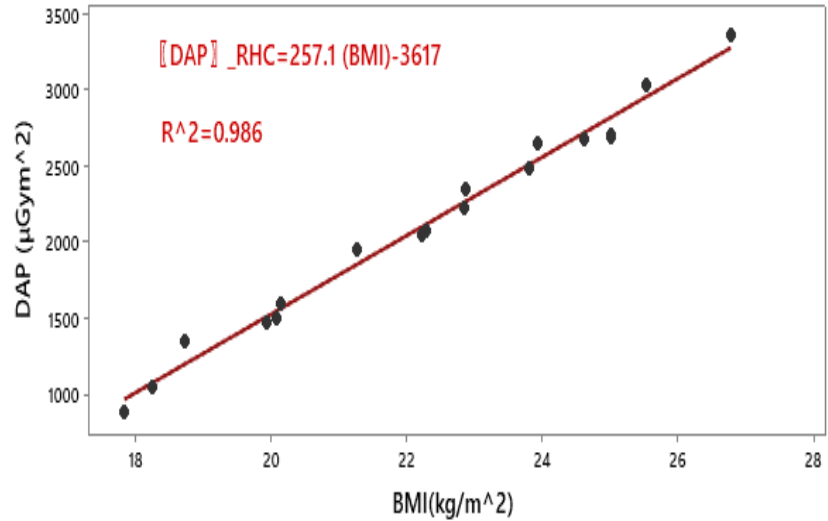


Figure 36: Fitted Line Plot for DAP vs BMI for female RHC Procedure

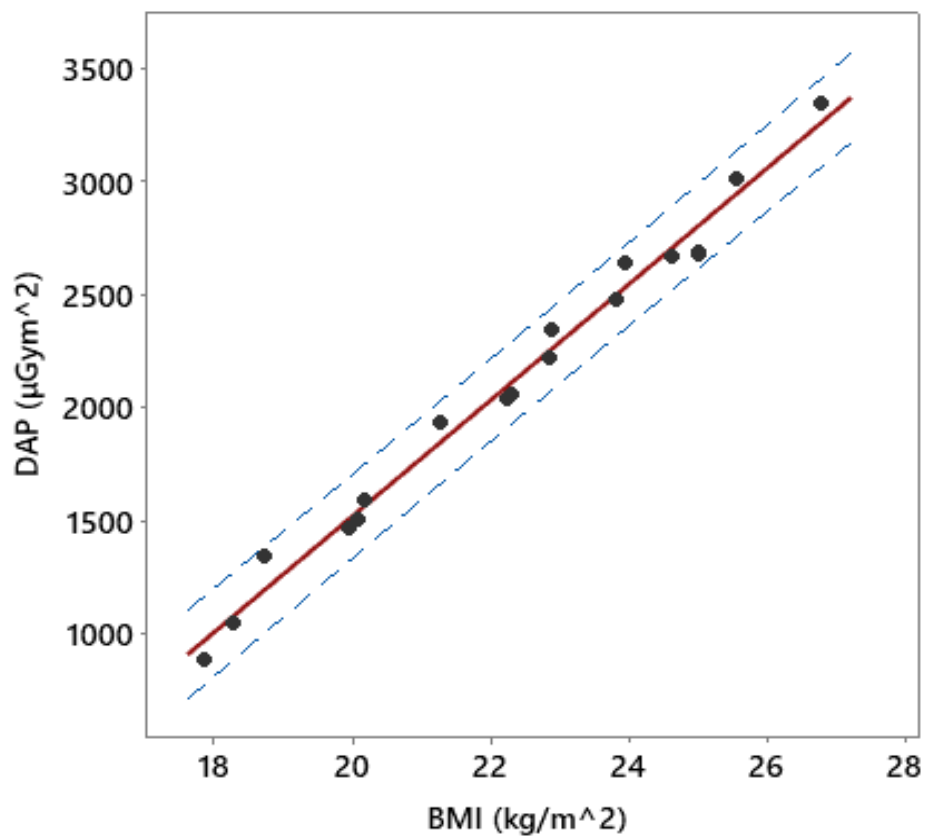


Figure 37: Predicted plot of DAP vs BMI for female RHC. The blocked fitted red line shows the predicted DAP for any BMI values and the blue dashed lines show the 95% prediction interval.

Analysis of Dose Optimization

With the help of equations derived from experimental data as well as equations from statistical software, the dose for the associated BMI was calculated using a simple and direct numerical procedure. The results were compared for the minimum dose in order to establish a trade-off between dose and BMI for the patient's dose optimization procedure (ALARA principle) and the results were test run ensuring that expected output is obtained.

Converting Modelled Equations to Graphical User Interface (GUI)

The developed model was processed into GUI in two phases: seventy (70) per cent of the data was used in the development of the model and the remaining thirty (30) per cent was used to evaluate the model. The developed model agrees very well with the experimental data.

The GUI was processed based on the model parameters. Figure 38 illustrates the Modelling process leading to the development of GUI. The process starts by prompting the user to enter the height and weight of the patient. The app uses information to calculate the BMI and stores it. In the next step, the user is prompted to enter the sex and depending on the sex, the process continues by prompting the user to enter the medical procedure. After deciding on the surgical procedure, the app calculates and outputs the dose, confidence level, BMI, and distribution (graphical plot of BMI and dose) as indicated in Figure 39.

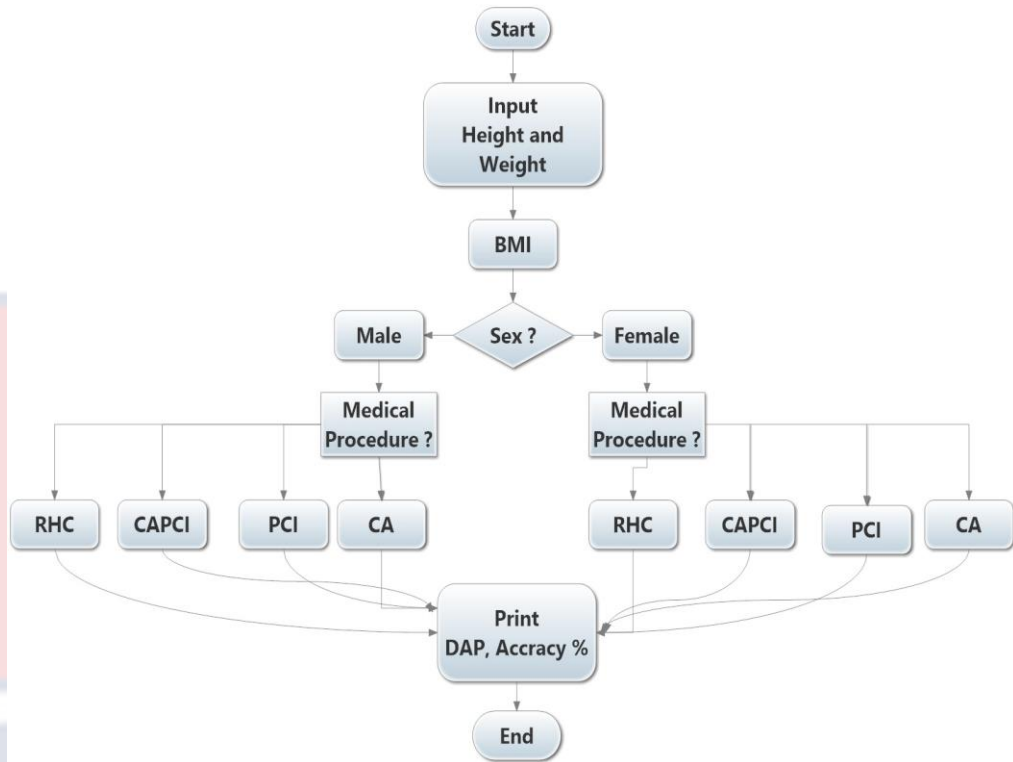


Figure 38: A flow diagram of the GUI modelling process.

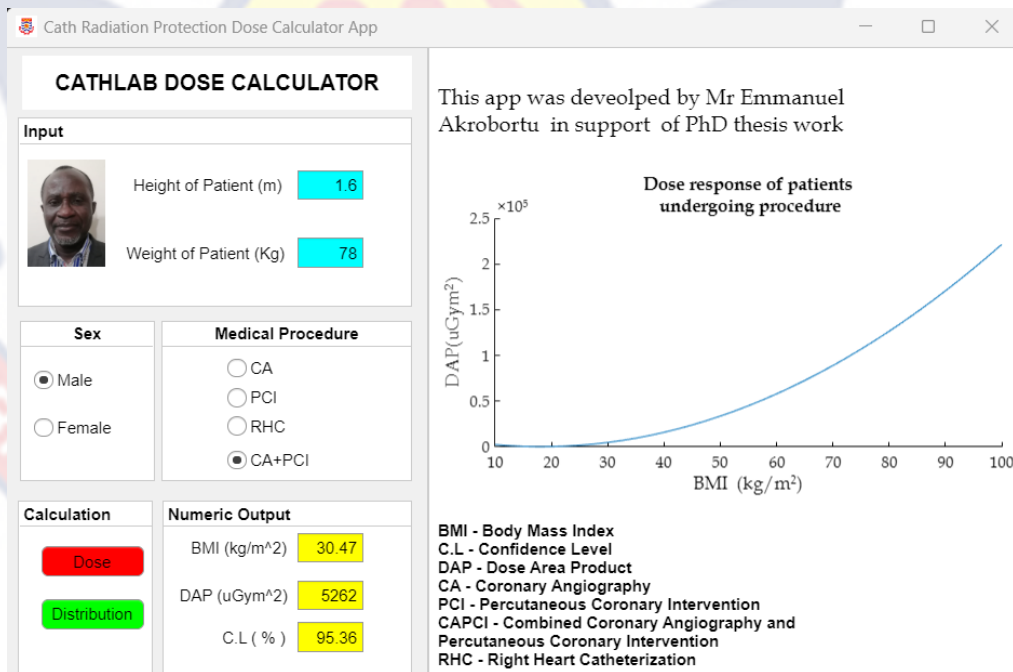


Figure 39: A snapshot of the developed GUI

Staff Effective Dose Using Double Dosimetry Algorithm

The three-algorithm marked * in Table 4 is used to estimate the staff radiation dose incurred while performing surgical procedures. Figures 40 show the data (effective dose) in the form of a histogram and Figure 41 show staff effective dose compared with ICRP 103 (2007) limit of 20 mSv. Figures 42 to 44 show the data in the form of boxplot with emphasis on type of algorithm whilst Figures 45 to 48 present the data (effective dose) in the form of boxplot with particular interest on total and type of procedure performed.

Table 15: Staff effective dose (mSv) using three different algorithms for all four procedures.

Algorithm	NCRP	Swiss	Chida
Type/Staff	(Algorithm)	(Algorithm)	(Algorithm)
Identity	Dose (mSv)	Dose (mSv)	Dose (mSv)
ADA	0.542675	1.08535	1.000945
AGY	0.756525	1.51305	1.396665
FOL	1.088250	2.17650	1.986190
DOK	0.584625	1.16925	1.079825
AKA	1.098825	2.19765	1.996565
MIR	0.470525	0.94105	0.868675
IIH	0.805325	1.61065	1.464985
ASH	0.492900	0.98580	0.908960
ABL	0.449650	0.89930	0.829840
SAP	0.522068	1.04414	0.961694
ANG	0.484825	0.96965	0.892055
FOK	0.209650	0.41930	0.386780

Source: Field Data 2019-2022

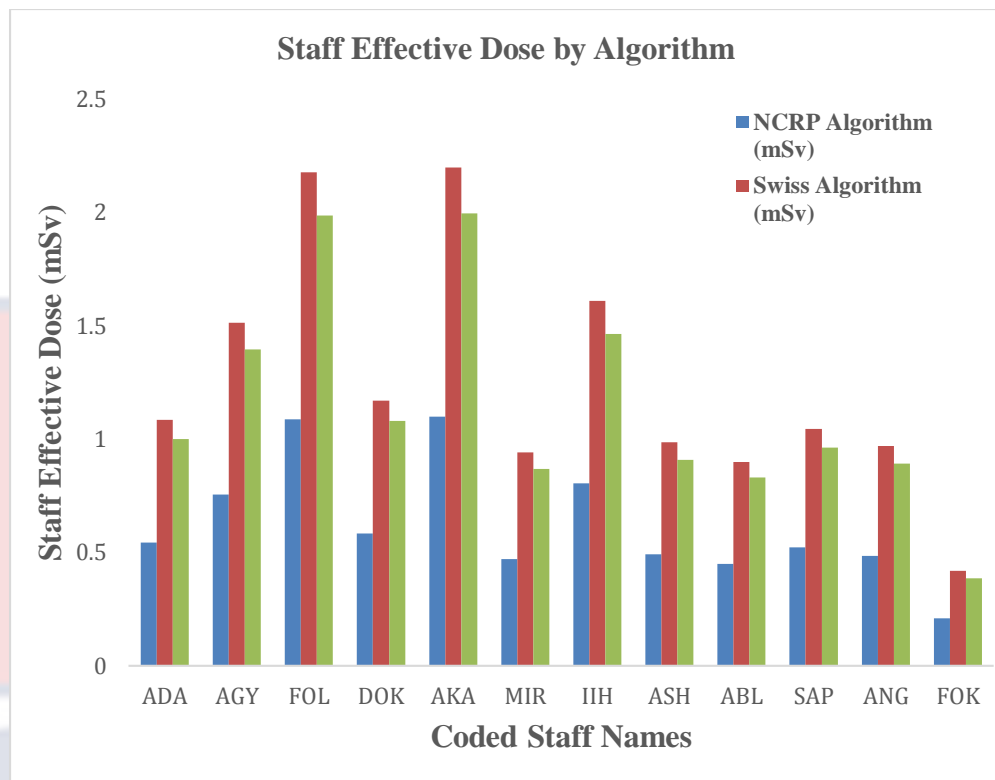


Figure 40: Staff effective dose by three different Algorithms

Table 16: Number of Procedures for each Staff

Staff ID	Number of procedures				Total
	CA	PCI	CAPCI	RHC	
ADA	102	13	12	6	133
AGY	72	13	10	4	99
FOL	37	8	3	2	50
DOK	44	7	8	1	60
AKA	60	18	10	5	93
FOK	18	4	2	2	26
MIR	130	21	20	8	179
IIH	111	19	12	8	150
ASH	90	19	15	3	127
ABL	105	17	14	5	141
ANG	75	15	10	4	104
SAP	108	13	7	7	135

Source: Field Data 2019-2022

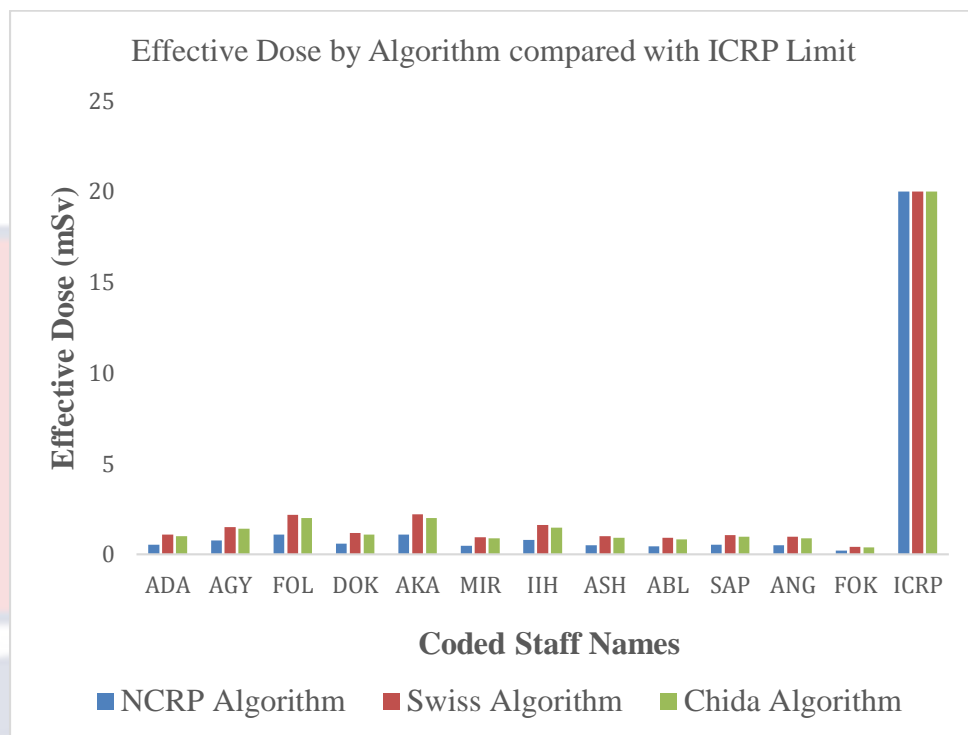


Figure 41: Staff effective dose compared with ICRP Limit

Staff Effective Dose Using Different Algorithms as Explained by Histogram.

The SWISS algorithm predicted a higher effective dose, followed by that of CHIDA. The least effective dose was predicted by the NCRP algorithm. The dose predicted by the NCRP algorithm is about two times less the dose predicted by SWISS and CHIDA algorithms (Järvinen et al., 2008b).

By the three algorithms, the range of dose for the cardiologists is (0.54-2.20) mSv; for the nurses, the range of dose is (0.45-1.61) mSv, whilst the dose received by the operator ranges between (0.52-1.04) mSv (López et al., 2018). From the histogram, the cardiologists received the highest dose compared to that received by the nurses and the operators. There is a great variation of dose

for each cardiologist per procedure type due to the inconsistency in the number of procedures and their locations in the examination room.

For all the staff, CA and PCI procedures are the most contributors to the dose, since they are the highest number of procedures performed (diagnostic and therapeutic). From the histogram, cardiologist FOL, received (1.09, 2.18, 2.00) mSv whilst cardiologist AKA, received (1.10, 2.20, 2.00) mSv per NCRP, SWISS, and CHIDA algorithms respectively. These are the highest effective doses received because these workers are principal cardiologists and they performed most of the procedures. Nurse IHH serves as the main scrub nurse, hence receiving a relatively high dose as compared to the dose received by other nurses.

Although the nurses had high number of procedures (Table 16), they have low effective doses, that ranges between (0.54-1.61) mSv, which is indicative of their positions in the examination room (Maaño et al., n.d.). Also, from Table 16, CA is the highest number of procedures performed (952), followed by PCI of 167, CAPCI being 123 and 55 RHC.

Staff Effective Dose as Explained by Boxplot.

Boxplot was also used to study the staff radiation dose distributional characteristics and the level (magnitude) of dose during the various cardiology procedures namely, CA, PCI, CAPCI, and RHC at the Cath lab. For the diverse cardiac procedures performed at the Cath lab, boxplot was used in showing the dose distribution for the group of staff namely, cardiologists, operators, and nurses.

The boxplot provides a useful way to visualize the range and other characteristics of the radiation dose such as the median dose, lower and upper

doses, whiskers, and outlier dose in these groups of radiation workers. Generally, across the distribution (Figures 42-44) the data is skewed positively, since the medians across are closer to the lower quartile (Q1) with a few being normally distributed (both high and low doses) within the group of data set of cardiologist, nurses, and operators.

There is an elevated level of agreement in dose with each worker, as depicted by the comparative shortness of the boxplots in the three algorithms namely-Chida, NCRP and Swiss. However, the comparatively tall boxplots (Figures 42-44) for the staff, AGY, AKA, DOK and FOL suggest that these radiation workers have quite different dose variations which is an indication of the number and type of procedures performed; their locations in the examination room and their sensitivity to the radiation (Fardid R, Mirzadeh F, 2017a).

The variations in boxplots suggest that there is variation in dose between the groups since some are surgeons, nurses, and operators. The uneven nature (size) of the five sections of the boxplots, namely minimum dose, lower quartile (25% dose), median (50% dose), upper quartile (75% dose) and the maximum dose, shows the similarities and the variations in the dose of the occupationally exposed workers during the examinations.

The long upper whiskers such as for AGY, and DOK, figures 42 to 44 mean staff doses are varied amongst the most and least positive quartiles (maximum and minimum doses). From figures 42 to figure 44, the same applies for the median, with different distribution for the groups of staff as; [ABL, ADA, ANG, ASH, IIH, FOK, MIR]; [AGY, DOK]; [AKA]; [SAP] and [FOL] show that the median dose for these groups are close to the average and are of same (level) effect. The radiation dose for workers was less than 0.25 mSv per

the Chida and Swiss algorithms whilst for the NCRP algorithm, radiation dose was less than 0.1 mSv as depicted by the median total of the boxplots (Siiskonen et al., 2018).

The radiation dose to the staff per procedure with the radiation measuring device (TLD) over and under the protective apron, for dose optimization, was found to vary in value as per the nature of the respective boxplots, as shown in Figures 45 to 48. For CA, (Figure 45) the boxplots are comparatively short, meaning there is an elevated level (effect) of agreement in dose with each worker, with exception of staff DOK and FOL with relatively tall boxplots, suggesting these workers have quite different dose variations due to the volume and type of procedures performed.

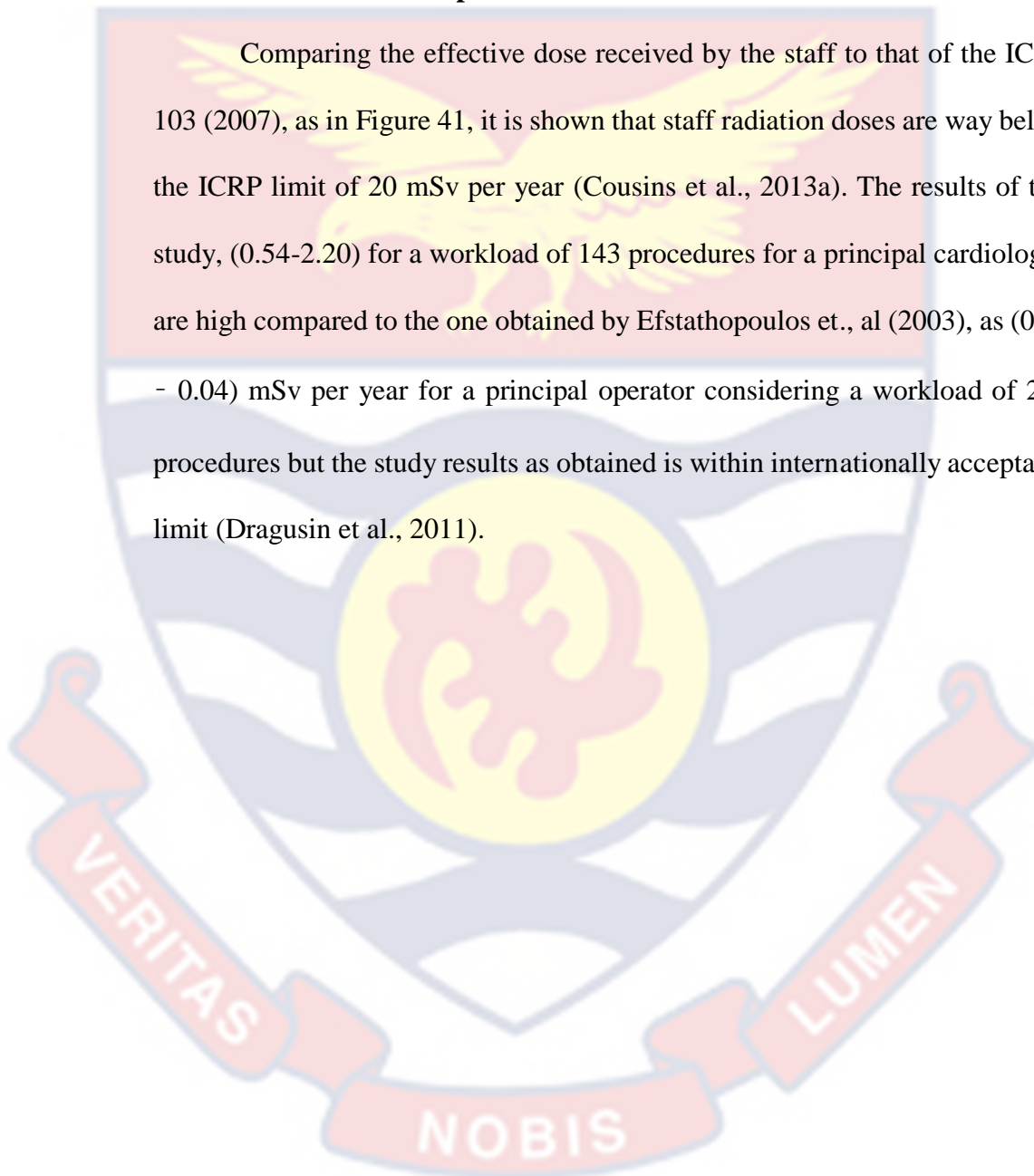
The uneven nature of the sections of the boxplots indicates the spread and similarities in the dose of the occupational workers. The median total for the CA procedure is just a little above 100 μ Sv. For PCI, (Figure 46) the boxplots are generally and comparatively tall, meaning the staff have varied doses, due to procedure types, the number of procedures, location in the examination room and individual sensitivity to radiation.

The median total across the distribution for PCI procedures is about 50 μ Sv. In the case of the combined procedure CAPCI, (Figure 47) the boxplots are comparatively short, which means staff doses agree with similar radiation dose effects (Siiskonen et al., 2018). The uneven distribution nature of the boxplots shows that the doses vary between 25, and 75% and the median with some whiskers (maximum and minimum dose) outside the 50% dose. The median total across the entire combined CAPCI procedures, indicative of the dose received by staff is about 110 μ Sv. During the RHC procedure, (Figure 48)

most of the staff received varied and different doses as shown by the tall nature of the boxplots with the median total being a little below 40 μSv indicative of the dose received during RHC procedures.

Staff effective Dose Compared with ICRP Limit

Comparing the effective dose received by the staff to that of the ICRP 103 (2007), as in Figure 41, it is shown that staff radiation doses are way below the ICRP limit of 20 mSv per year (Cousins et al., 2013a). The results of this study, (0.54-2.20) for a workload of 143 procedures for a principal cardiologist are high compared to the one obtained by Efsthopoulos et., al (2003), as (0.03 - 0.04) mSv per year for a principal operator considering a workload of 240 procedures but the study results as obtained is within internationally acceptable limit (Dragusin et al., 2011).



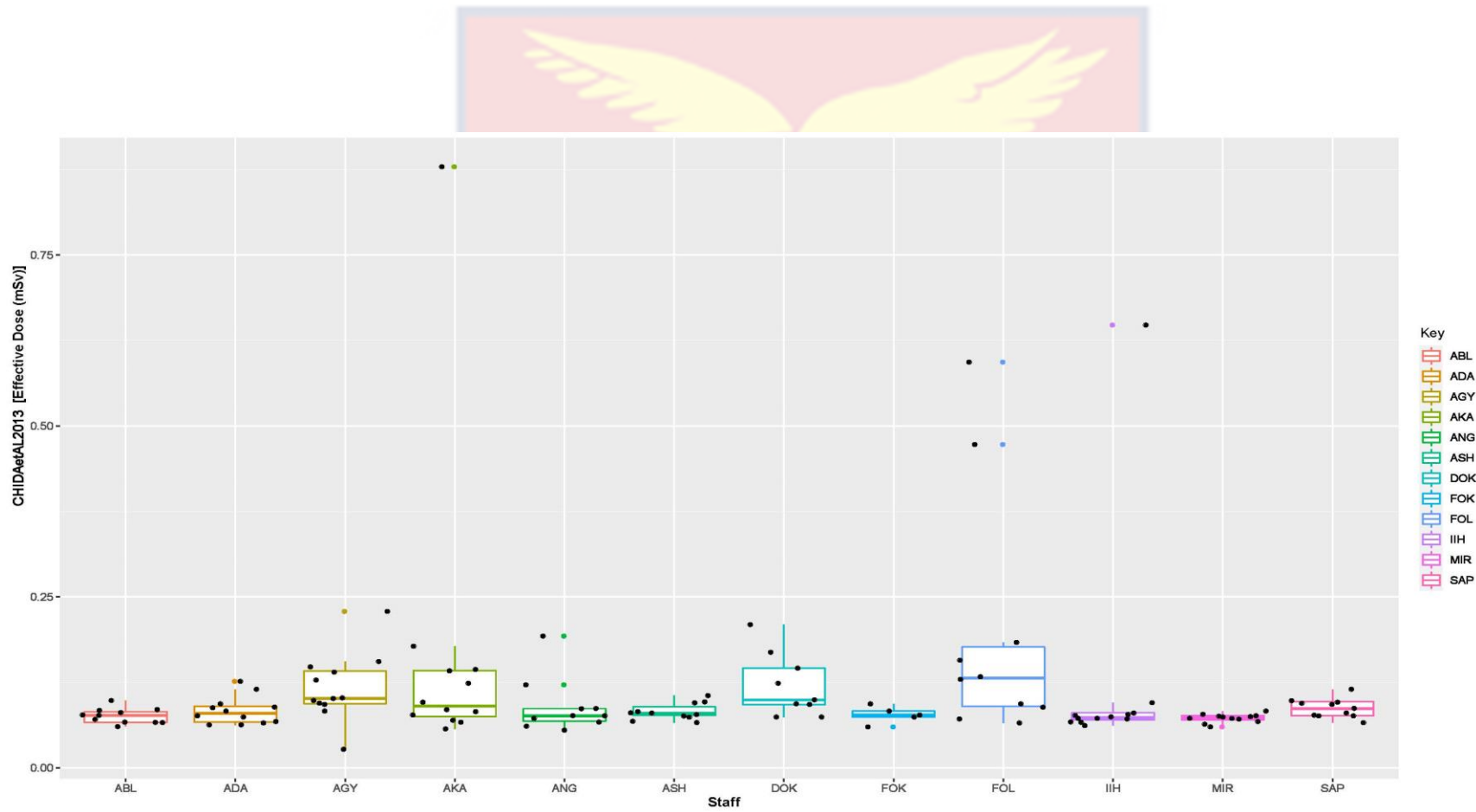


Figure 42: Staff radiation dose using Chida et al, 2013 algorithm. The box represents first, and third quartiles and the line in between indicate the median.

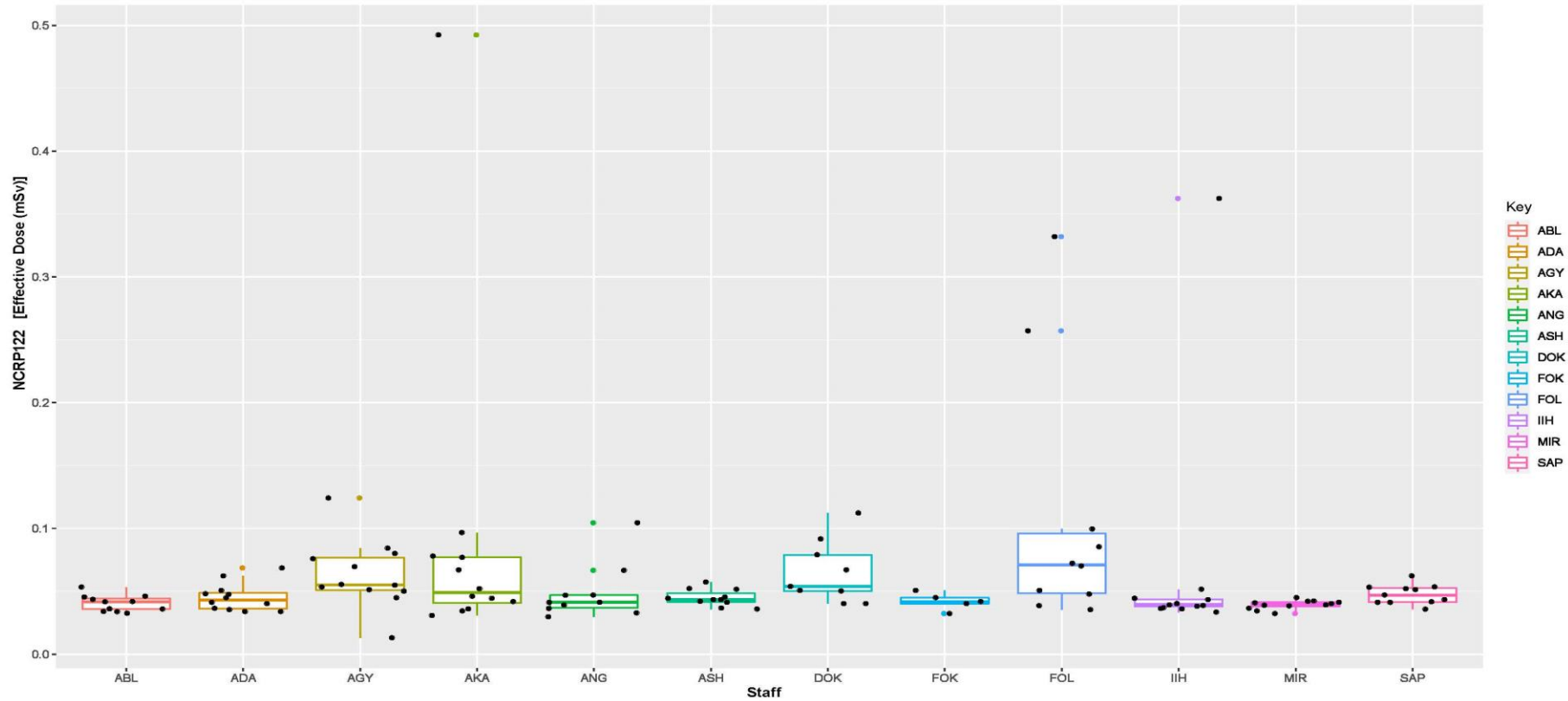


Figure 43: Staff radiation dose using NCRP 122, 1995 algorithm. The box shows the 25th and 75th percentiles with line between being the median.

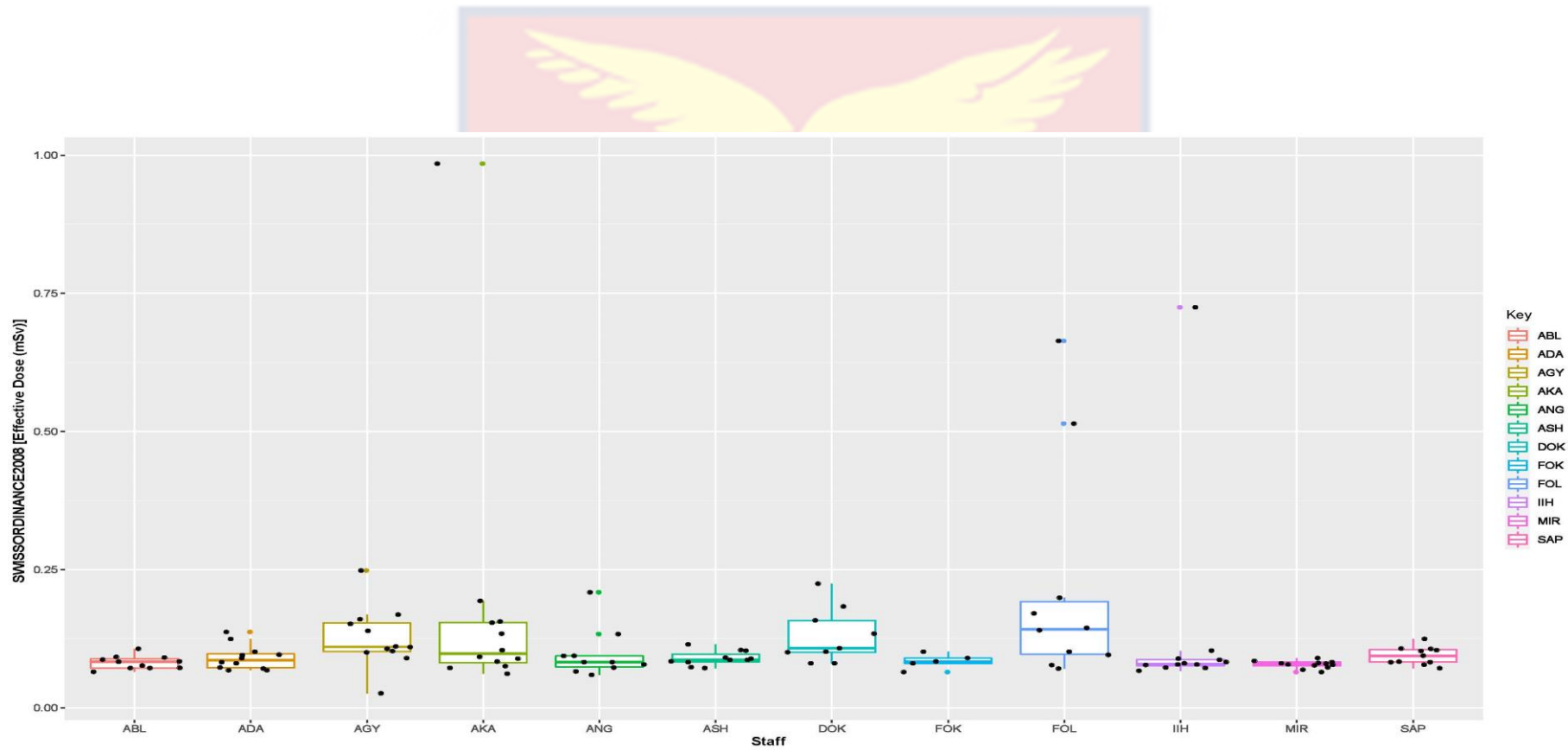


Figure 44: Staff radiation dose using Swiss et al, 2008 algorithm. The box represents the lower and upper quartiles whilst the line in between the median.

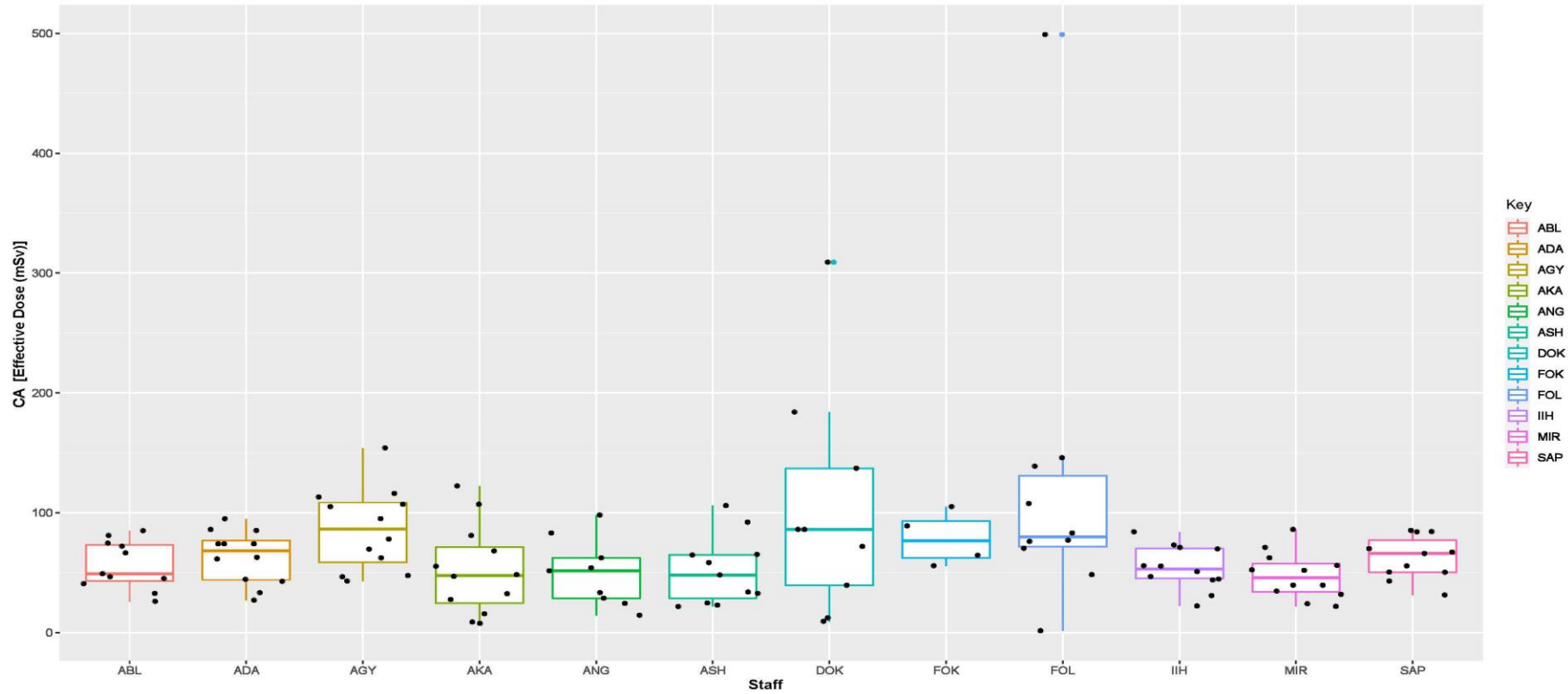


Figure 45: Staff radiation dose per CA Procedure. The box shows the first and third quartiles whilst the line in between the median.

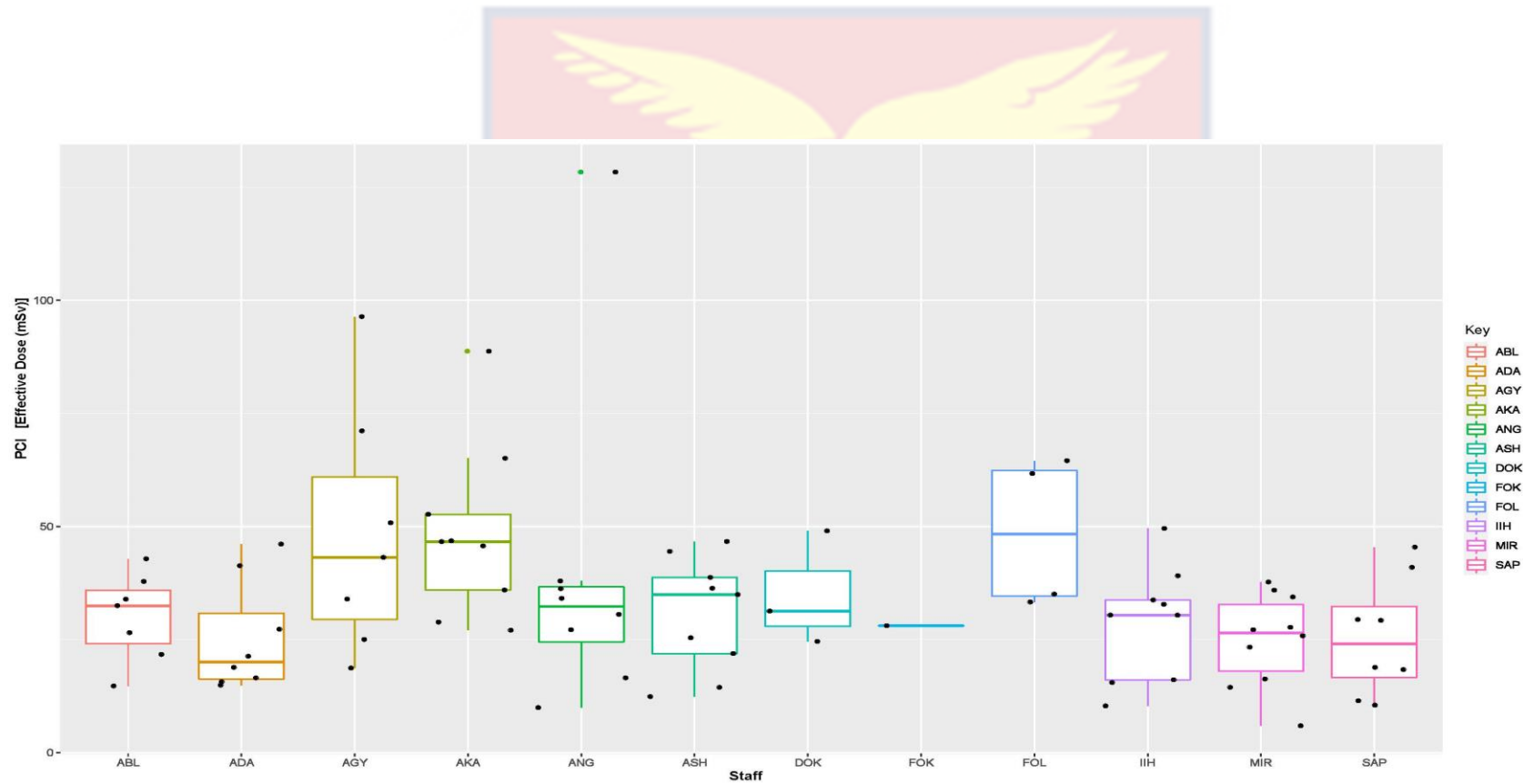


Figure 46: Staff radiation dose per PCI Procedure with the box showing the lower and upper quartiles, whilst the line in between is the median.

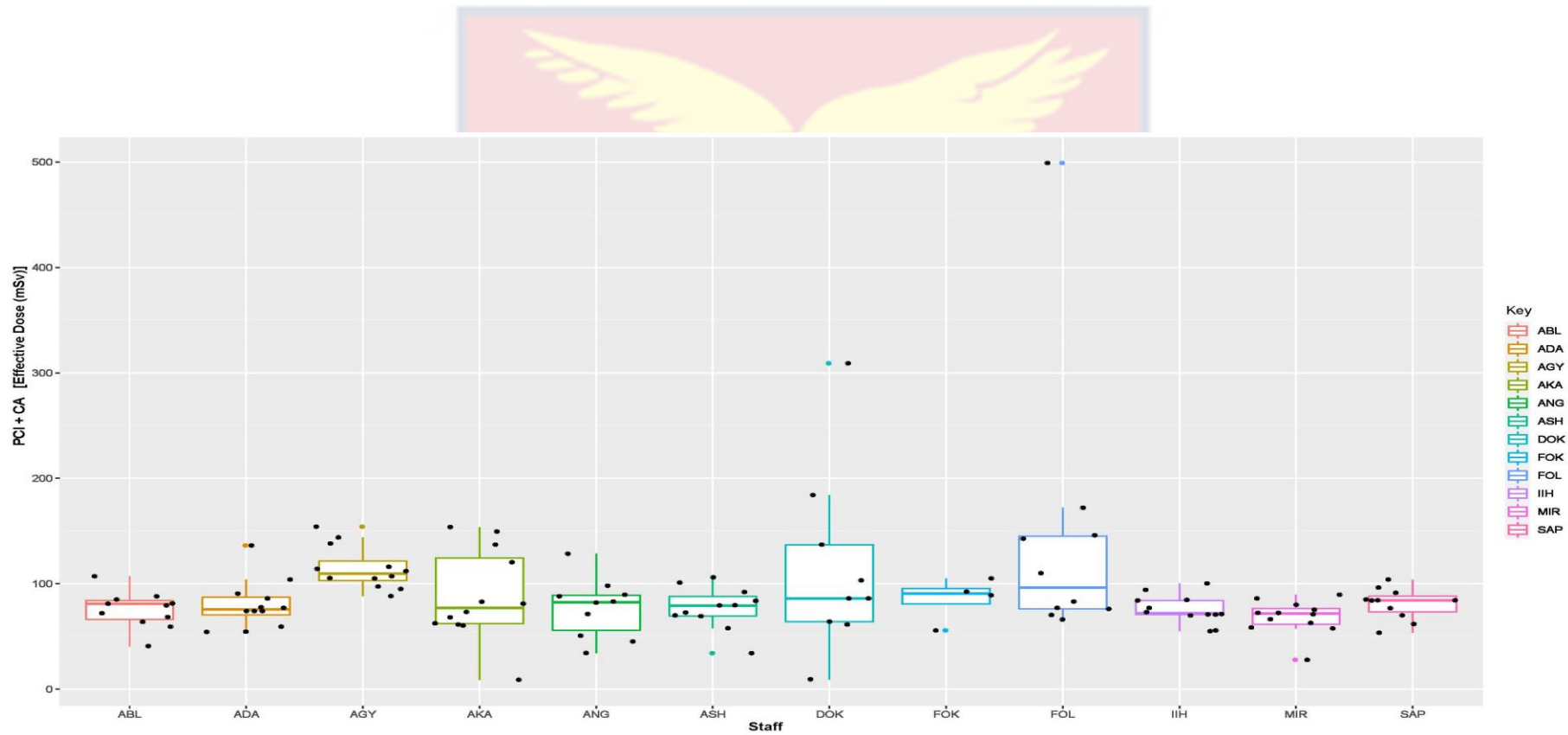


Figure 47: Staff radiation dose per combined CAPCI Procedure. The box represents the 25th and 75th percentiles with line in between being the median.

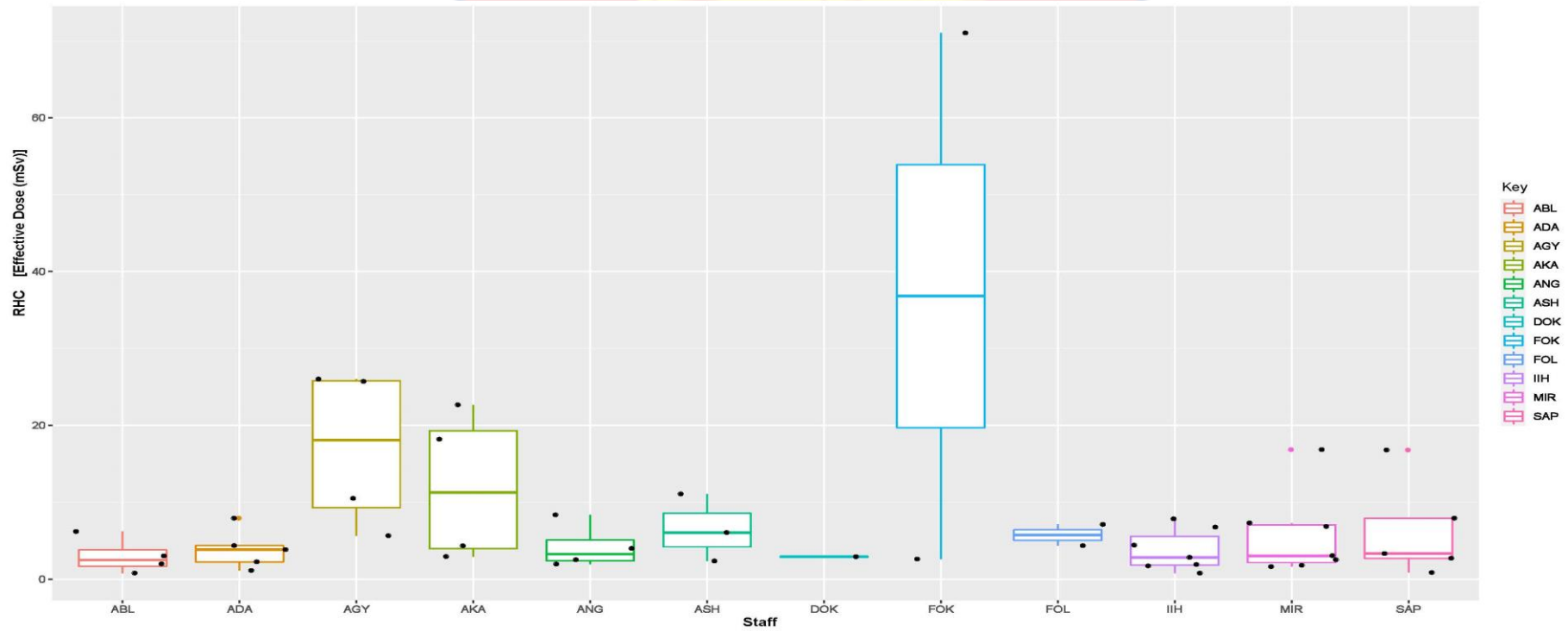


Figure 48: Staff radiation dose per RHC Procedure with the box representing the 25th and 75th percentiles and the line in between is the 50th percentile doses.

General Information on Radiation Protection and Safety in the Cath Lab

The occupationally exposed workers in the department confirm that they have received training on radiation protection during their general training. Radiation Protection was strengthened in the Cath lab after the Nuclear Regulatory Officer visited the lab for their routine work and emphasized the implementations of the requirements for radiation protection to be enhanced in the department and the senior matron was designated as the Radiation Protection Officer to oversee the radiation protection issues.

The department is well equipped with personal protective equipment, such as a lead curtain (0.5 mm) fixed on the patient bed, a screen of lead equivalent (0.5 mm) suspended from the ceiling, several thyroid collars, and aprons of equivalence lead 0.35 and 0.5 mm. There are no lead goggles and gloves available. All the workers have well-labelled TLD badges provided by Lumina Dosimetry Services.

Patient's information and dose details are well recorded and well-kept in digital form (computer, CDs, and external hard disk) and hard copies. Details of radiation safety in the department is shown in Table 17. The QC as well as radiation survey around the workplace are performed by the Nuclear Regulatory Officers during their inspection. This approach is not the best. The center should employ resident medical physicist to be responsible for QC and radiation protection.

This study was useful since it brought awareness of radiation exposure to the workers and had enhanced the practice of protective measures at the worker level and will contribute to the implementation of continuous personal monitoring in the departments.

Table 17: Radiation Protection and Safety in the Cath Lab

Protective measures	Cath lab
Tube Geometry	Under couch
Warning Light	Yes
Lead apron (0.35 mm)	Yes (100 %)
Thyroid shield (0.35)	Yes (100 %)
Lead glass	Yes
Lead gloves and goggles	No
Ceiling suspended screen	Yes
Medical Physicist	No
Refresher training	Yes
Quality Assurance	Yes
Radiation Protection Officer	Yes (Matron acts)
Quality Control	Yes

Source: Field Data 2019-2022

Risk Assessment to Staff (Occupationally Exposed Workers)

The probability of cancer-induced and heritable effect (or total detrimental risk) due to radiation exposure received by occupationally exposed workers in this study were calculated using ICRP 103 (2007) for individual risk coefficient and are presented in Figure 49.

The total detriment (cancer and heritable effects) or the estimated probability of health effects due to radiation to occupationally exposed workers in the Cath lab is low compared to the ICRP 2007 total detriment risk of 0.057 % and 0.042 % for the whole body and adult worker, respectively (Varghese et al., 2016).

However, the highest estimated risks by this study are for cardiologists [FOL (1.75×10^{-3} %)] and [AKA (1.76×10^{-3} %)], due to their roles as the

principal leads. Nurse, [IIH ($7.96 \times 10^{-4} \%$)] per the role, played as scrub nurse, had a risk level higher than that of other nurses.

Also, nurse, [MIR ($1.29 \times 10^{-4} \%$)] being the matron and present during almost all procedures shows a little higher risk value comparable to that of the other nurses. Averagely, estimated radiation risk by this study for cardiologists was ($1.76 \times 10^{-3} \%$), for nurses the value is ($7.96 \times 10^{-4} \%$) and for operators the estimated radiation risk was ($1.29 \times 10^{-4} \%$).

The estimated risk values obtained confirmed the indicative nature of the role each group of staff played during the procedures. The estimated radiation risks for the exposed workers are not significant but should not be ignored, since the Linear Non-Threshold (LNT) model assumes that every amount of radiation (no matter how small) carries with it the risk of cancer or heritable effect. Therefore, there is the need to enhance radiation protection actions to keep to ALARA principles and reduce the likelihood of stochastic effects.

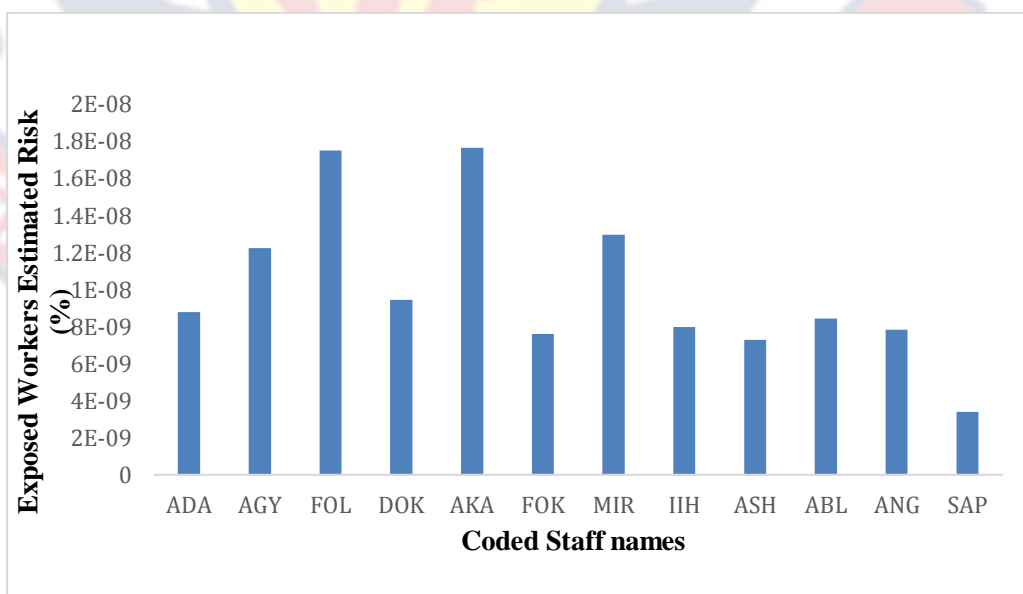


Figure 49: Total Risk (Detriment) of Occupationally Exposed Workers considered in the study.

Scattered Radiation to Occupationally Exposed Workers in the Examination Room

Figure 50 shows the result of scattered radiation in the examination room. The graph indicates that at all the kilovoltages between (60-120) kVp at which examinations were performed, the surgeons received the highest doses due to their locations (near patient and source of X-ray). The doses to their left and right positions are also high compared to the ones at the lead screen and store entrance.

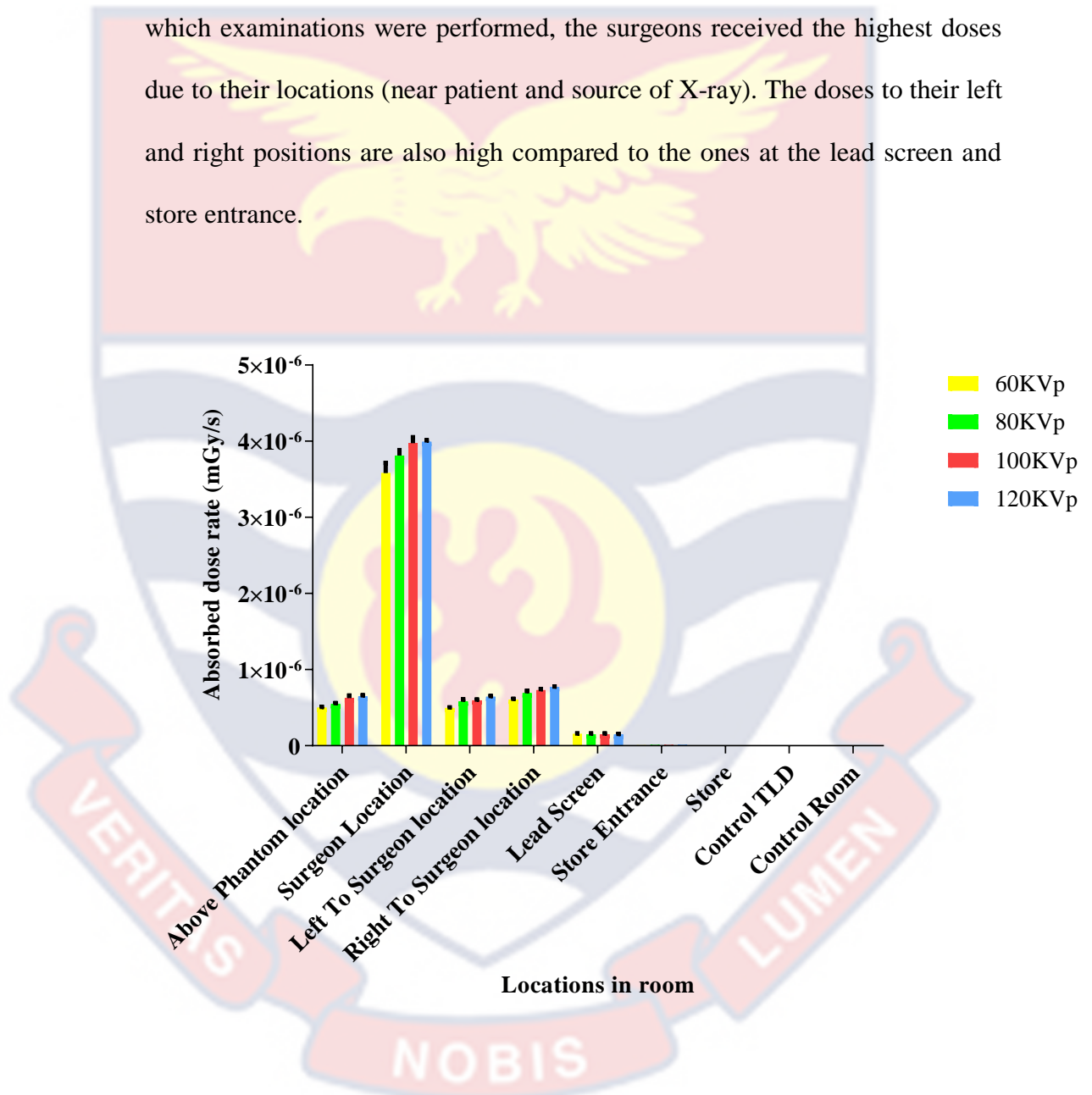


Figure 50: Result of Scattered Radiation in the Examination Room, showing vantage positions for kVp of between 60 to 120.

Comparison of this Study with other Studies

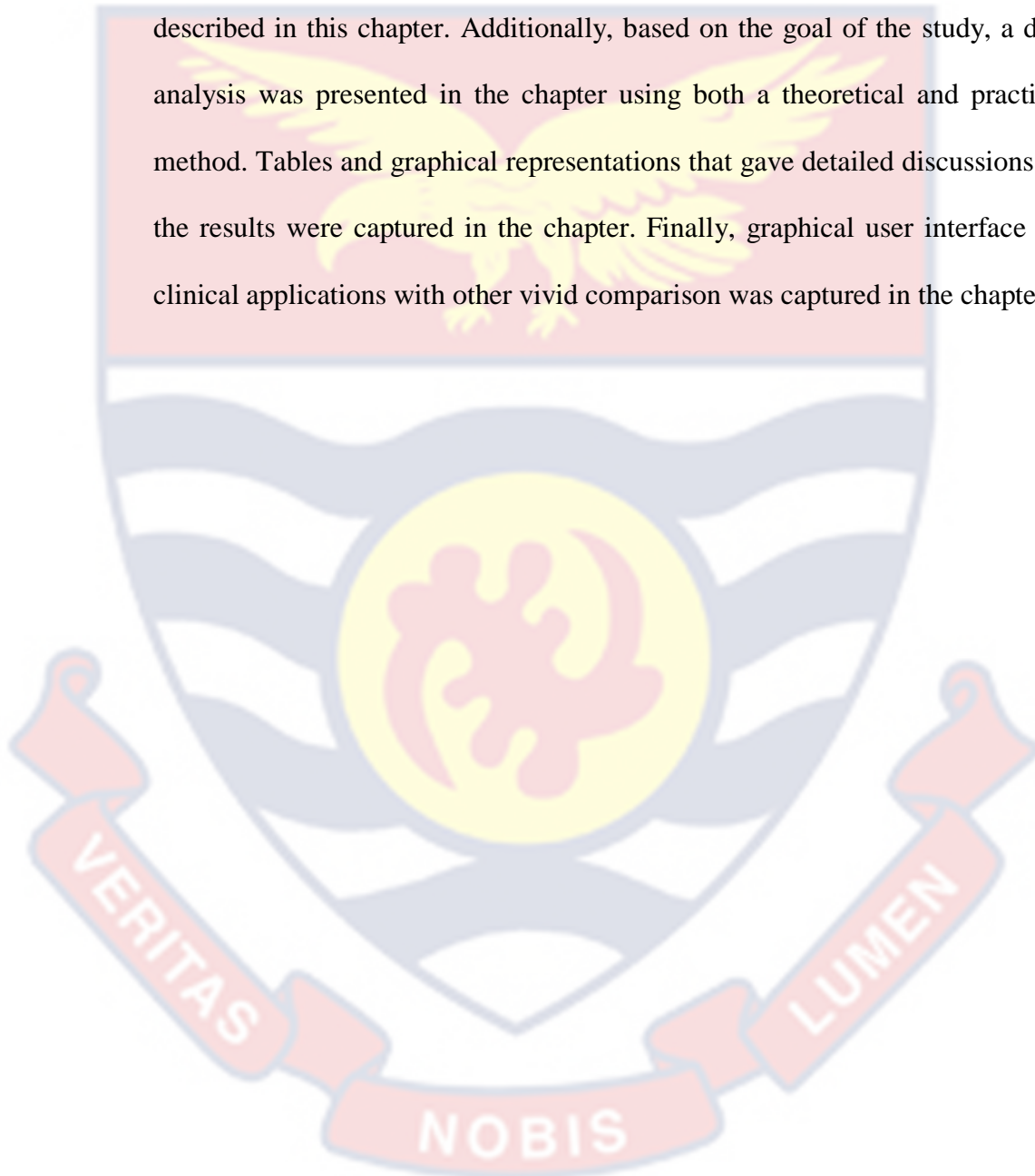
Published DRL from the past ten years. (Siiskonen et al., 2018)

Table 18: Comparison of Patient DAP with other works

Country	Reference level for DAP (Gycm ²)			
	CA	PCI	CAPCI	RHC
This study	43.39	104.13	84.03	34.57
Sentinel study (Fardid R, Mirzadeh F, 2017b)	45.00	85.00		
Sweden (Fardid R, Mirzadeh F, 2017b)	80.00			
UK (Fardid R, Mirzadeh F, 2017b)	29.00	50.00		
Belgium (Fardid R, Mirzadeh F, 2017b)	71.30	106.00		
Ireland (Fardid R, Mirzadeh F, 2017b)	42.00	84.00	107.00	
Croatia (Fardid R, Mirzadeh F, 2017b)	32.00	72.00		
Bulgaria (Fardid R, Mirzadeh F, 2017b)	40.00		140.00	
Switzerland (Fardid R, Mirzadeh F, 2017b)	102.00	125.00		
USA (Fardid R, Mirzadeh F, 2017b)	83.00	193.00	199.00	
Greece (Fardid R, Mirzadeh F, 2017b)	53.00	129.00		
France (Fardid R, Mirzadeh F, 2017b)	38.00	80.00		
Finland (Fardid R, Mirzadeh F, 2017b)	30.00		75.00	

Chapter Summary

In summary, this chapter covered the study's findings in both graphical and tabular form. The relationship between the numerous quantifiable quantities and parameters utilized for the computations and obtaining reliable results was described in this chapter. Additionally, based on the goal of the study, a data analysis was presented in the chapter using both a theoretical and practical method. Tables and graphical representations that gave detailed discussions on the results were captured in the chapter. Finally, graphical user interface for clinical applications with other vivid comparison was captured in the chapter.



CHAPTER FIVE

OVERVIEW, SUMMARY, CONCLUSION AND RECOMMENDATION

Overview

This chapter's framework is an extensive review of the key findings in connection to the stated goals of the study. The chapter draws vivid conclusions on the totality of the study. It concludes with pertinent conclusions and recommendations for the main stakeholders based on the key findings.

Summary

This research focused on five general areas namely: measurements of patient body parameters; measurements of patient dose area product for four cardiology procedures (CA, PCI, CAPCI, RHC) and the relationship with body parameters; measurements of staff whole body dose, $H_p(10)^*$; estimation of staff effective dose using algorithms and estimation of radiation risk to staff. The patient body parameters measured were height, weight, and body mass index based on age and gender variations. Additionally, exposure parameters such as kilovoltage peak (kVp), milliamperage current (mA), and fluoroscopy time (FT) were measured.

Minitab statistical software was used to model the patient's DAP and BMI to obtain the model equations. The model equations were validated through a statistical graphical tool as shown in appendices A1 to A4 for males and B1 to B4 for females models respectively. The modeled equations were programmed using Matlab app launcher to obtain a handy optimization tool for clinical applications. All the tabular and graphical representation of the data was summarized in chapter four of the study.

The effective dose obtained for the staff ranged as follows; (0.54-2.20) mSv for cardiologist, (0.45-1.61) mSv for nurses and (0.52-1.04) mSv for operators. The average estimated risk by the study were ($1.76 * 10^{-3} \%$), ($7.96 * 10^{-4} \%$) and ($1.29 * 10^{-4} \%$) for cardiologists, nurses, and operators respectively.

Conclusions

Average measured body parameters for male and female consisting of; weight, height, age, and BMI were obtained. Average DAP and fluoroscopy time (FT) were obtained for the various procedures for both males and females. (All results shown in chapter 4). The evaluations showed that females had larger BMI than their male counterparts since naturally women have more body fat and would therefore require higher radiation exposure than male during medical procedures. BMI and DAP for patients were significantly correlated. The findings suggest that patient body parameters are significant determinants of the amount of exposure patients receive during their medical treatment using ionizing radiation. The modelled equations in chapter four are designed and used to predict DAP for any BMI with a confidence level of 95 % as shown by the respective graphs for each procedure. In this research, patients measured body parameters, DAP, FT, and staff effective dose with the associated radiation detriment obtained agreed vividly with other reviewed international and institutional measured values.

This research results show that radiation dose to patients increases with patient BMI and FT. The study confirmed that patient radiation exposure during medical treatment is independent of gender but dependent on BMI. The challenge of high radiation exposure of patients during cardiac procedures as

outlined in the statement of the problem was addressed with supportive clinical decisive application software with the measurement of BMI and dose for radiation optimization in cardiac examinations at NCTC. Also, QC results prove that the angiography equipment is performing consistently.

Recommendations

Based on the study results, the following recommendations have been addressed to key stakeholders to help improve delivery of cardiology health care in Ghana.

Recommendations to the National Cardiothoracic Center, Korle-Bu

Teaching Hospital.

1. To assist in lowering the radiation exposure to patients, the facility is urged to acquire technology and apply methods for dose reduction. To guarantee adequate patient protection, training that is adequate and appropriate should be organized.
2. For a better Radiological Information System (RIS) in the center, data management units should be established and managed by competent and qualified occupational workers.
3. Due to the high radiation exposure during cardiac procedures, it is strongly recommended that the NCTC KBTH should consider employing a resident medical physicist to oversee the quality assurance, quality control and the entire radiation protection programme at the center.
4. This study showed that there is significant increase in radiation doses associated with obese patients, hence catheter laboratory staff should take active account of the patients' BMI in making conscious choices.

5. I proposed that the GUI developed from the models should be used for clinical applications and research in Ghana.

Recommendations to Regulatory Authority

1. The Regulatory Authority should have efficient regulatory control to guarantee the effectiveness of radiation protection for the workers and patients at the Cath lab.
2. The Regulatory Authority shall issue regulations and guidelines to help registrants and licensees meet with legal requirements for the management of medical exposure at the Cat lab.
3. To ensure that established and new catheterization facilities meet regulatory requirements, regular inspections should be conducted by the Regulatory Authority.

Recommendation for future works.

As a result of the four new (recently) established catheterization laboratories, inter comparison study should be conducted at these facilities that would be performing common cardiology procedures for the development and setting up of local reference levels in Ghana. Also, a future study should relate the image quality and dose as well as relationship between dose and other body indices with emphasis on pediatric.

REFERENCES

- Access, F. (2019). *Evaluation of patient and sta exposure with state of the art X - ray technology in cardiac catheterization: A randomized controlled trial*. *31*(6), 1–18.
- Balter, S., Fletcher, D. W., Kuan, H. M., & Miller, D. (2002). Techniques to estimate radiation dose to skin during fluoroscopically guided procedures α . United States Regulations 3 . Direct Dose Measurement Methods. *Report, July*, 1–10.
- Clerinx, P., Buls, N., Bosmans, H., & De Mey, J. (2008). Double-dosimetry algorithm for workers in interventional radiology. *Radiation Protection Dosimetry*, *129*(1–3), 321–327. <https://doi.org/10.1093/rpd/ncn148>
- Cousins, C., Miller, D. L., Bernardi, G., Rehani, M. M., Schofield, P., E., Einstein, A. J., Geiger, B., Heintz, P., Padovani, R., & Sim, K. H. (2013a). ICRP publication 120: Radiological Protection in Cardiology. *Annals of the ICRP*, *42*(1), 1–125. <https://doi.org/10.1016/j.icrp.2012.09.001>
- Cousins, C., Miller, D. L., Bernardi, G., Rehani, M. M., Schofield, P., E., Einstein, A. J., Geiger, B., Heintz, P., Padovani, R., & Sim, K. H. (2013b). ICRP publication 120: Radiological Protection in Cardiology. *Annals of the ICRP*, *42*(1), 1–125. <https://doi.org/10.1016/j.icrp.2012.09.001>
- Cusma, J. T., Bell, M. R., Wondrow, M. A., Taubel, J. P., & Holmes, D. R. (1999). Real-time measurement of radiation exposure to patients during diagnostic coronary angiography and percutaneous interventional procedures. *Journal of the American College of Cardiology*, *33*(2), 427–435. [https://doi.org/10.1016/S0735-1097\(98\)00591-9](https://doi.org/10.1016/S0735-1097(98)00591-9)

- Davros, W. J. (2007). *Fluoroscopy : basic science , optimal use , and patient / operator protection*. 44–54. <https://doi.org/10.1053/j.trap.2007.02.005>
- Dragusin, O., Bokou, C., Wagner, D., & Beissel, J. (2011). Optimization of Radiation Dose and Image Quality in Cardiac Catheterization Laboratories. *Advances in the Diagnosis of Coronary Atherosclerosis*. <https://doi.org/10.5772/20311>
- Edwin, F., Tettey, M., Aniteye, E., Tamatey, M., Sereboe, L., Entsua-Mensah, K., Kotei, D., & Baffoe-Gyan, K. (2011). The development of cardiac surgery in West Africa - The case of Ghana. *Pan African Medical Journal*, 9, 1–12. <https://doi.org/10.4314/pamj.v9i1.71190>
- Efstathopoulos, E. P., Katritsis, D. G., Kottou, S., Kalivas, N., Tzanalaridou, E., Giazitzoglou, E., Korovesis, S., & Faulkner, K. (2006). Patient and staff radiation dosimetry during cardiac electrophysiology studies and catheter ablation procedures: A comprehensive analysis. *Europace*, 8(6), 443–448. <https://doi.org/10.1093/europace/eul041>
- Eknayan, G. (2008). Adolphe Quetelet (1796-1874) - The average man and indices of obesity. *Nephrology Dialysis Transplantation*, 23(1), 47–51. <https://doi.org/10.1093/ndt/gfm517>
- Fallis, A. . (2013). No Title No Title. *Journal of Chemical Information and Modeling*, 53(9), 1689–1699. <https://doi.org/10.1017/CBO9781107415324.004>
- Fardid R, Mirzadeh F, R. H. (2017a). Occupational doses of cardiologists in cath labs and simulation method. *J Can Res Ther*, 13(6), 901–907. <https://doi.org/10.4103/0973-1482.192767>
- Fardid R, Mirzadeh F, R. H. (2017b). Occupational doses of cardiologists in

cath labs and simulation method. *J Can Res Ther*, 13, 901–907.

<https://doi.org/10.4103/0973-1482.192767>

Foti, C., Padovani, R., Trianni, A., Bokou, C., Christofides, S., Corbett, R. H.,

Kepler, K., Korečová, Z., Kosunen, A., Malone, J., Torbica, P., Tsapaki,

V., Vano, E., Vassileva, J., & Zdesar, U. (2008). Staff dosimetry in

interventional cardiology: Survey on methods and level of exposure.

Radiation Protection Dosimetry, 129(1–3), 100–103.

<https://doi.org/10.1093/rpd/ncn038>

Greffier, J., Van Ngoc Ty, C., Bonniaud, G., Moliner, G., Ledermann, B.,

Schmutz, L., Cornillet, L., Cayla, G., Beregi, J. P., & Pereira, F. (2017).

Assessment of peak skin dose in interventional cardiology: A comparison

between Gafchromic film and dosimetric software em.dose. *Physica*

Medica, 38, 16–22. <https://doi.org/10.1016/j.ejmp.2017.05.044>

Health Risks from Exposure to Low Levels of Ionizing Radiation. (2015). In

Health Risks from Exposure to Low Levels of Ionizing Radiation.

<https://doi.org/10.17226/11340>

Heidbuchel, H., Wittkamp, F. H. M., Vano, E., Ernst, S., Schilling, R., Picano,

E., Mont, L., Jais, P., De Bono, J., Piorkowski, C., Saad, E., & Femenia, F.

(2014). Practical ways to reduce radiation dose for patients and staff during

device implantations and electrophysiological procedures. *Europace*,

16(7), 946–964. <https://doi.org/10.1093/europace/eut409>

IAEA. (2010). Comprehensive Clinical Audits of Diagnostic Radiology

Practices: A Tool for Quality Improvement. *Human Health Series*, 4, 209.

ICRP. (2012). Annals of the ICRP 60. *International Commission on*

Radiological Protection, 1–125.

<https://doi.org/10.1016/j.icrp.2006.06.001>

Järvinen, H., Buls, N., Clerinx, P., Jansen, J., Miljanić, S., Nikodemová, D., Ranogajec-Komor, M., & D'Errico, F. (2008a). Overview of double dosimetry procedures for the determination of the effective dose to the interventional radiology staff. *Radiation Protection Dosimetry*, 129(1–3), 333–339. <https://doi.org/10.1093/rpd/ncn082>

Järvinen, H., Buls, N., Clerinx, P., Jansen, J., Miljanić, S., Nikodemová, D., Ranogajec-Komor, M., & D'Errico, F. (2008b). Overview of double dosimetry procedures for the determination of the effective dose to the interventional radiology staff. *Radiation Protection Dosimetry*, 129(1–3), 333–339. <https://doi.org/10.1093/rpd/ncn082>

Jones, J., & Goel, A. (2013). Flat panel detector. *Radiopaedia.Org*, 8–9. <https://doi.org/10.53347/rid-26365>

Jones, M. C., & Daly, F. (1995). Density Probability Plots. *Communications in Statistics - Simulation and Computation*, 24(4), 911–927. <https://doi.org/10.1080/03610919508813284>

Kato, M., Chida, K., Sato, T., Oosaka, H., Tosa, T., & Kadowaki, K. (2011). Evaluating the maximum patient radiation dose in cardiac interventional procedures. *Radiation Protection Dosimetry*, 143(1), 69–73. <https://doi.org/10.1093/rpd/ncq286>

Kim, K. P., Miller, D. L., De Gonzalez, A. B., Balter, S., Kleinerman, R. A., Ostroumova, E., Simon, S. L., & Linet, M. S. (2012). Occupational radiation doses to operators performing fluoroscopically-guided procedures. *Health Physics*, 103(1), 80–99. <https://doi.org/10.1097/HP.0b013e31824dae76>

- Kuon, E., Birkel, J., Schmitt, M., & Dahm, J. B. (2003). Radiation exposure benefit of a lead cap in invasive cardiology. *Heart*, 89(10), 1205–1210. <https://doi.org/10.1136/heart.89.10.1205>
- López, P. O., Dauer, L. T., Loose, R., Martin, C. J., Miller, D. L., Vañó, E., Doruff, M., Padovani, R., Massera, G., & Yoder, C. (2018). ICRP Publication 139: Occupational Radiological Protection in Interventional Procedures. *Annals of the ICRP*, 47(2), 1–118. <https://doi.org/10.1177/0146645317750356>
- Maaño, M. K., Sc, B., Morales, A. A., Sc, D., & Iii, D. V. E. (n.d.). *Estimation of Occupational Radiation Dose Levels of Interventional Cardiologists at the Philippine Heart Center*. 10–13.
- Memon, S., Larsen, T. R., & Mathew, J. (2018). patient population. *Baylor University Medical Center Proceedings*, 0(0), 1–4. <https://doi.org/10.1080/08998280.2018.1479598>
- Moladoust, H., Ghazanfari-Tehran, M., Nikseresht, V., Nadim, T., & Rad, M. A. (2015). Comparison of five developed algorithms to estimate staff effective dose in interventional cardiology: Are they interchangeable? *Journal of Medical Imaging and Health Informatics*, 5(3), 647–651. <https://doi.org/10.1166/jmihi.2015.1438>
- Nett, B. (2022). Ray Interactions, Illustrated Summary (Photoelectric, Compton, Coherent) for Radiologic Technologists and Radiographers. *How Radiology Works*, 1–12. <https://howradiologyworks.com/x-ray-interactions/>
- Nett, B. B. (n.d.). *X-Ray Interactions , Illustrated Summary (Photoelectric , Compton , Coherent) for Radiologic Technologists and Radiographers*

Overview of the Physics Behind X-Ray Interactions. 1–12.

Njantang, R. N. (1987). University Of Ghana. *Annals of Tropical Paediatrics*, 7(3), 154–154. <https://doi.org/10.1080/02724936.1987.11748497>

Octeville, C., & Sanitaria, F. (2019). *EXPERIMENTAL VALIDATION OF ALGORITHMS USED TO ESTIMATE EFFECTIVE DOSE DURING INTERVENTIONAL.* 1–8. <https://doi.org/10.1093/rpd/ncz136>

Ogden, C. L., Carroll, M. D., Kit, B. K., & Flegal, K. M. (2014). Prevalence of childhood and adult obesity in the United States, 2011-2012. *JAMA - Journal of the American Medical Association*, 311(8), 806–814. <https://doi.org/10.1001/jama.2014.732>

Owusu-Banahene, J., Darko, E. O., & Hasford, F. (2018). Body Mass Index and Percentage Body Fat Determination in Cancer Patients. *Open Journal of Radiology*, 08(04), 307–317. <https://doi.org/10.4236/ojrad.2018.84034>

Ramos, M., Montoro, A., Almonacid, M., Ferrer, S., Barquinero, J. F., Tortosa, R., Verdü, G., Rodríguez, P., Barrios, L. L., & Villaescusa, J. I. (2010). Radiation effects analysis in a group of interventional radiologists using biological and physical dosimetry methods. *European Journal of Radiology*, 75(2), 259–264. <https://doi.org/10.1016/j.ejrad.2009.03.035>

Risti, G. S. (n.d.). *THE DIGITAL FLAT-PANEL X-RAY DETECTORS.*

Salah, A., Taha, A., Diab, H., & Abdel Ghany, H. (2018). Investigation of Effect of Body Mass Index of Patient Radiation Dose During Interventional Cardiac processes. *Journal of Scientific Research in Science*, 35(part 1), 87–94. <https://doi.org/10.21608/jsrs.2018.26724>

Savva, A. (2010). *Personnel TLD monitors , their calibration and response by.* September.

- Serman, N., Goaz, P., & Pharoah, M. (2000). Production of X-rays and Interactions of X-rays with Matter. *Columbia University*, 11–20. http://www.columbia.edu/itc/hs/dental/sophs/material/production_xrays.pdf
- Shirazu, I., Mensah, Y. B., Schandorf, C., & Mensah, S. Y. (2017). Determination Of Standard Reference Body Indices For Clinical Application In Ghana. *International Journal of Scientific & Technology Research*, 6(02), 2. www.ijstr.org
- Siiskonen, T., Ciraj-Bjelac, O., Dabin, J., Diklic, A., Domienik-Andrzejewska, J., Farah, J., Fernandez, J. M., Gallagher, A., Hourdakis, C. J., Jurkovic, S., Järvinen, H., Järvinen, J., Knežević, Koukorava, C., Maccia, C., Majer, M., Malchair, F., Riccardi, L., Rizk, C., ... Vano, E. (2018). Establishing the European diagnostic reference levels for interventional cardiology. *Physica Medica*, 54. <https://doi.org/10.1016/j.ejmp.2018.09.012>
- Stratis, A. I., Anthopoulos, P. L., Gavaliatsis, I. P., Ifantis, G. P., Salahas, A. I., Antonellis, I. P., Tavernarakis, A. G., & Molfetas, M. I. (2009a). Patient dose in cardiac radiology. *Hellenic Journal of Cardiology*, 50(1), 17–25.
- Stratis, A. I., Anthopoulos, P. L., Gavaliatsis, I. P., Ifantis, G. P., Salahas, A. I., Antonellis, I. P., Tavernarakis, A. G., & Molfetas, M. I. (2009b). Patient dose in cardiac radiology. *Hellenic Journal of Cardiology*, 50(1), 17–25.
- Tsapaki, V. (2008). Body size-dependent patient effective dose for diagnostic radiography. *Radiation Measurements*, 43(2–6), 1008–1011. <https://doi.org/10.1016/j.radmeas.2007.11.028>
- Tsapaki, V. (2014). Eye lens dose estimation during interventional radiology and its impact on the existing radiation protection and safety program: In

the context with new International Commission on Radiological Protection guidelines. *Radiation Protection and Environment*, 37(2), 101–105.

<https://doi.org/10.4103/0972-0464.147291>

Valentin, J. (2000). Avoidance of radiation injuries from medical interventional procedures: ICRP Publication 85. *Annals of the ICRP*, 30(2), 7–67.

[https://doi.org/10.1016/S0146-6453\(01\)00004-5](https://doi.org/10.1016/S0146-6453(01)00004-5)

Valentin, J. (2007). *Annals of the ICRP*.

Vano, E., Ubeda, C., Miranda, P., Leyton, F., Durán, A., & Nader, A. (2011).

Radiation protection in pediatric interventional cardiology: An iaea pilot program in Latin America. *Health Physics*, 101(3), 233–237.

<https://doi.org/10.1097/HP.0b013e3182135fd1>

Varghese, A., Livingstone, R. S., Varghese, L., Kumar, P., Srinath, S. C.,

George, O. K., & George, P. V. (2016). Radiation doses and estimated risk from angiographic projections during coronary angiography performed using novel flat detector. *Journal of Applied Clinical Medical Physics*,

17(3), 433–441. <https://doi.org/10.1120/jacmp.v17i3.5926>

VIENNA, X. (2021). *Handbook of Basic Quality Control Tests for Diagnostic*

Radiology. 47. www.iaea.org/publications

WHO. (2011). Ionizing Radiation, Health Effects and Protective Measures.

Who, 1–5.

http://www.who.int/kobe_centre/emergencies/east_japan_earthquake/fact_sheet_ionizing_radiation_final.pdf?ua=1

X-RAY IMAGING IN AFRICA “ Enhancing Capacity Building of Medical Physicists to Improve Safety and Effectiveness of Medical Imaging .”

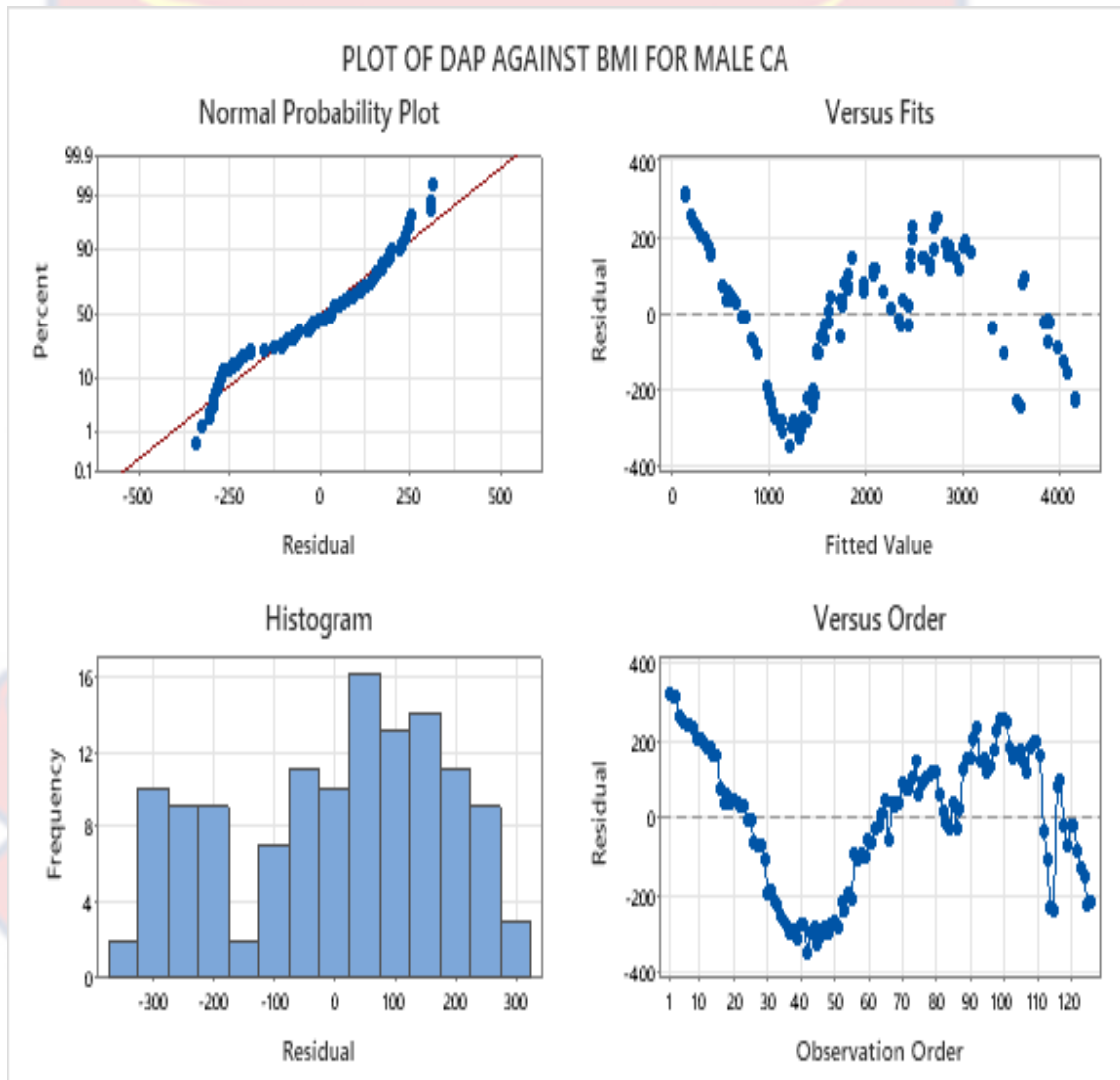
(2020). November, 1–65.

APPENDICES

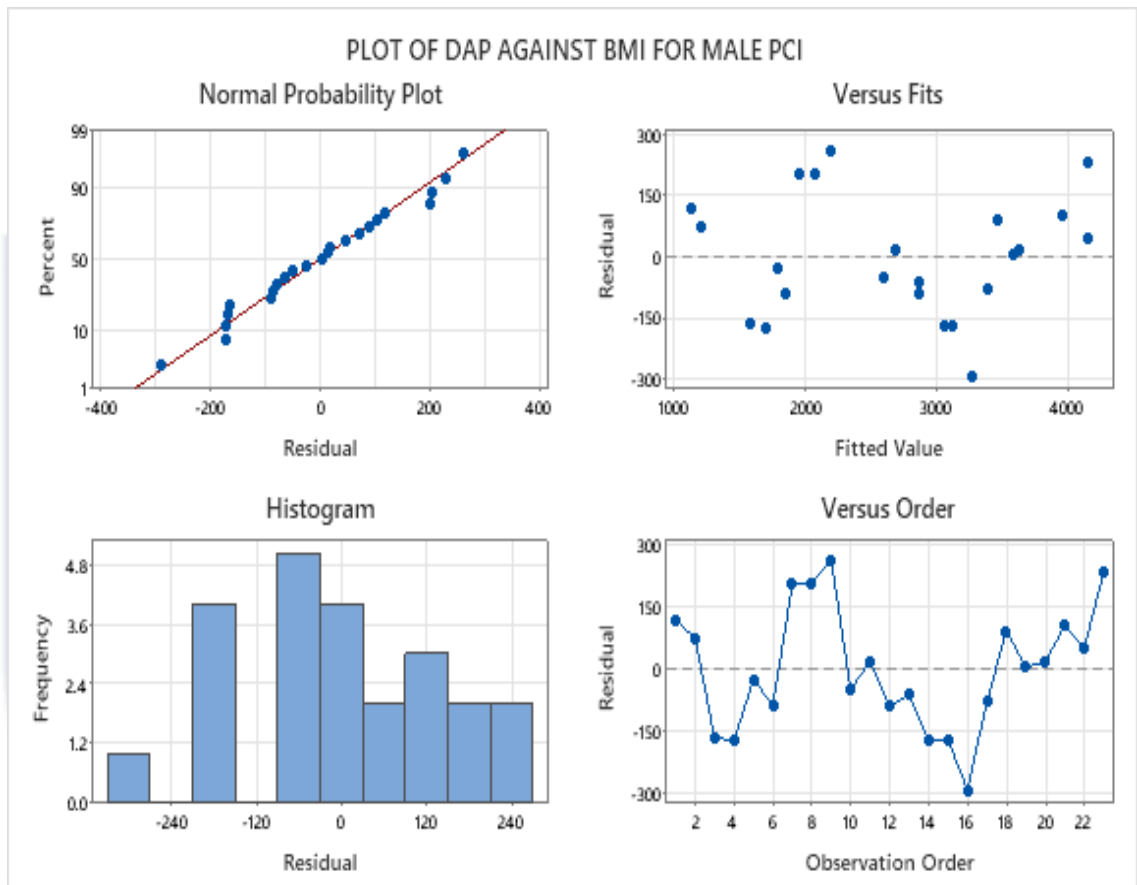
Appendix A

MODELLING DAP AND BMI FOR MALE PATIENTS

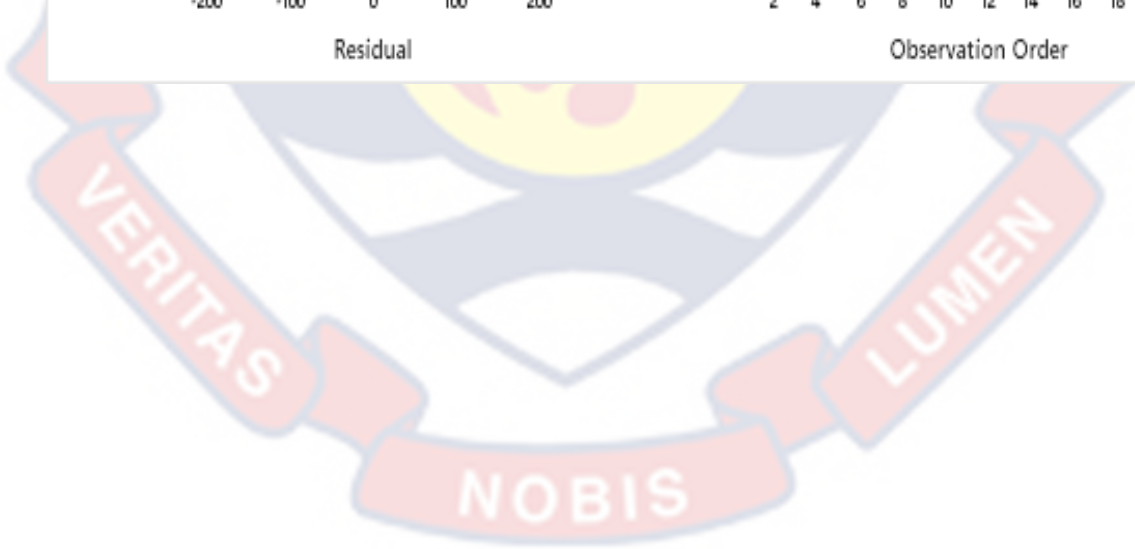
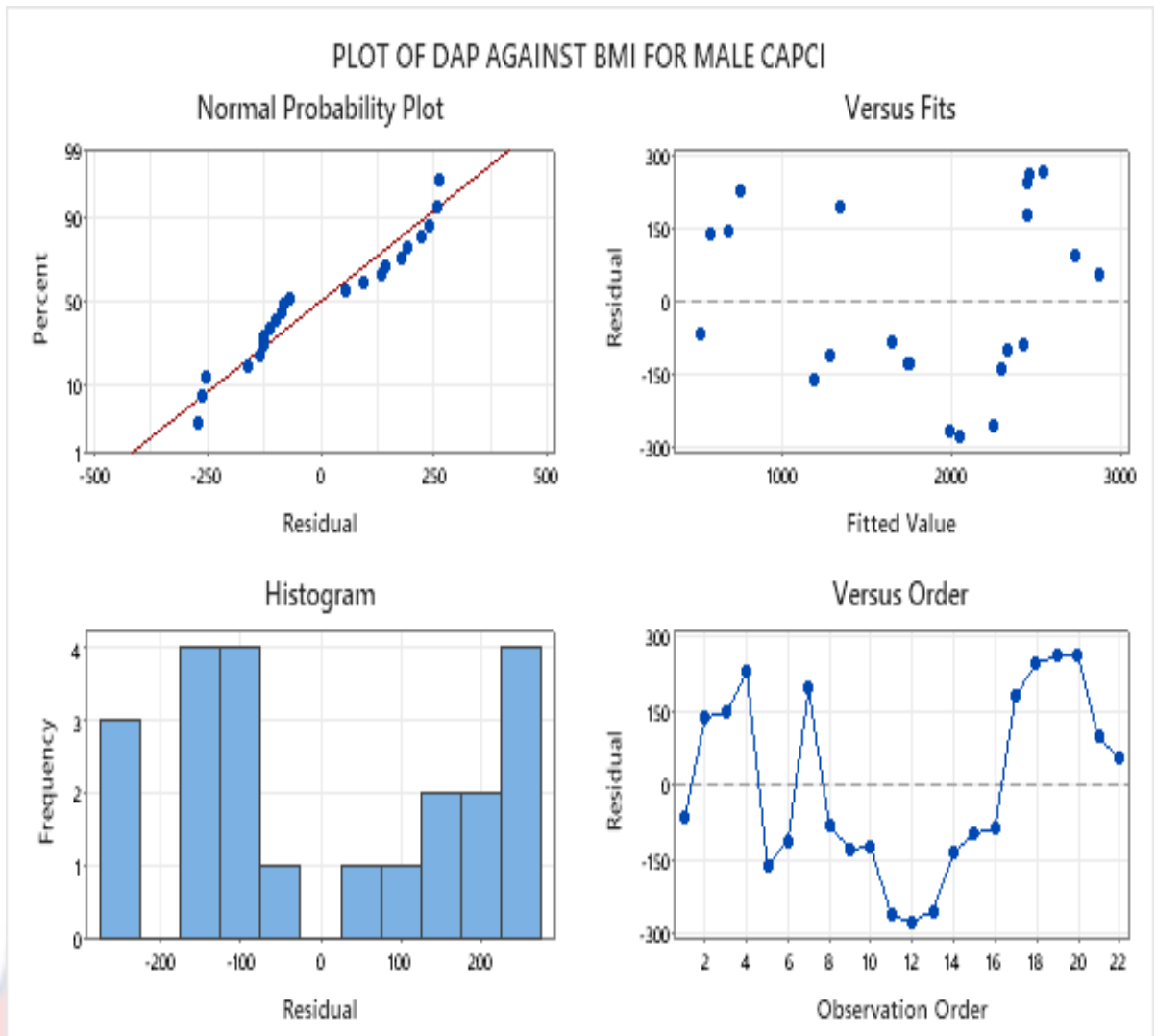
Appendix A-1: Linear DAP and BMI for male CA



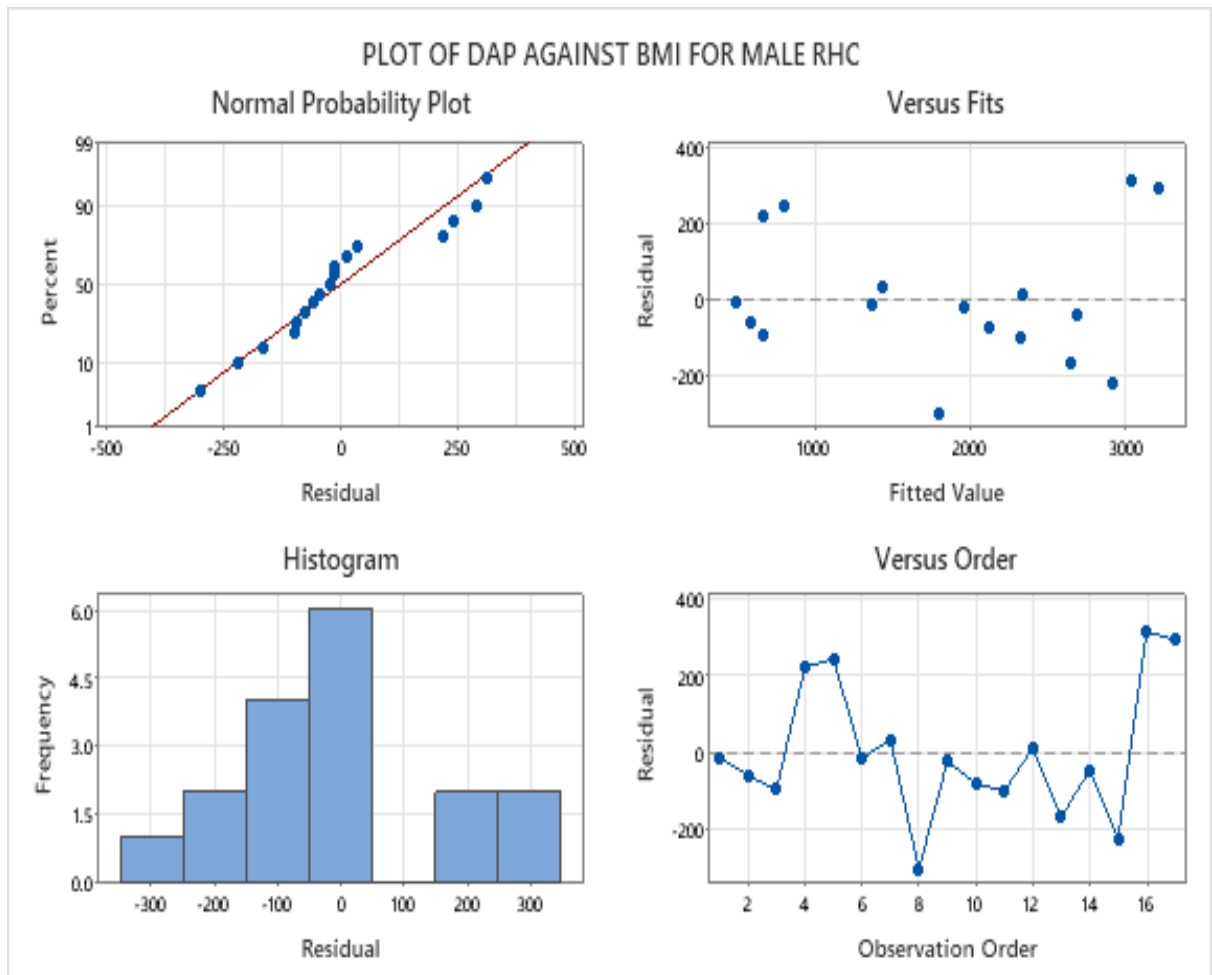
Appendix A-2: Linear DAP and BMI for male PCI



Appendix A-3: DAP and BMI for male combined CAPCI



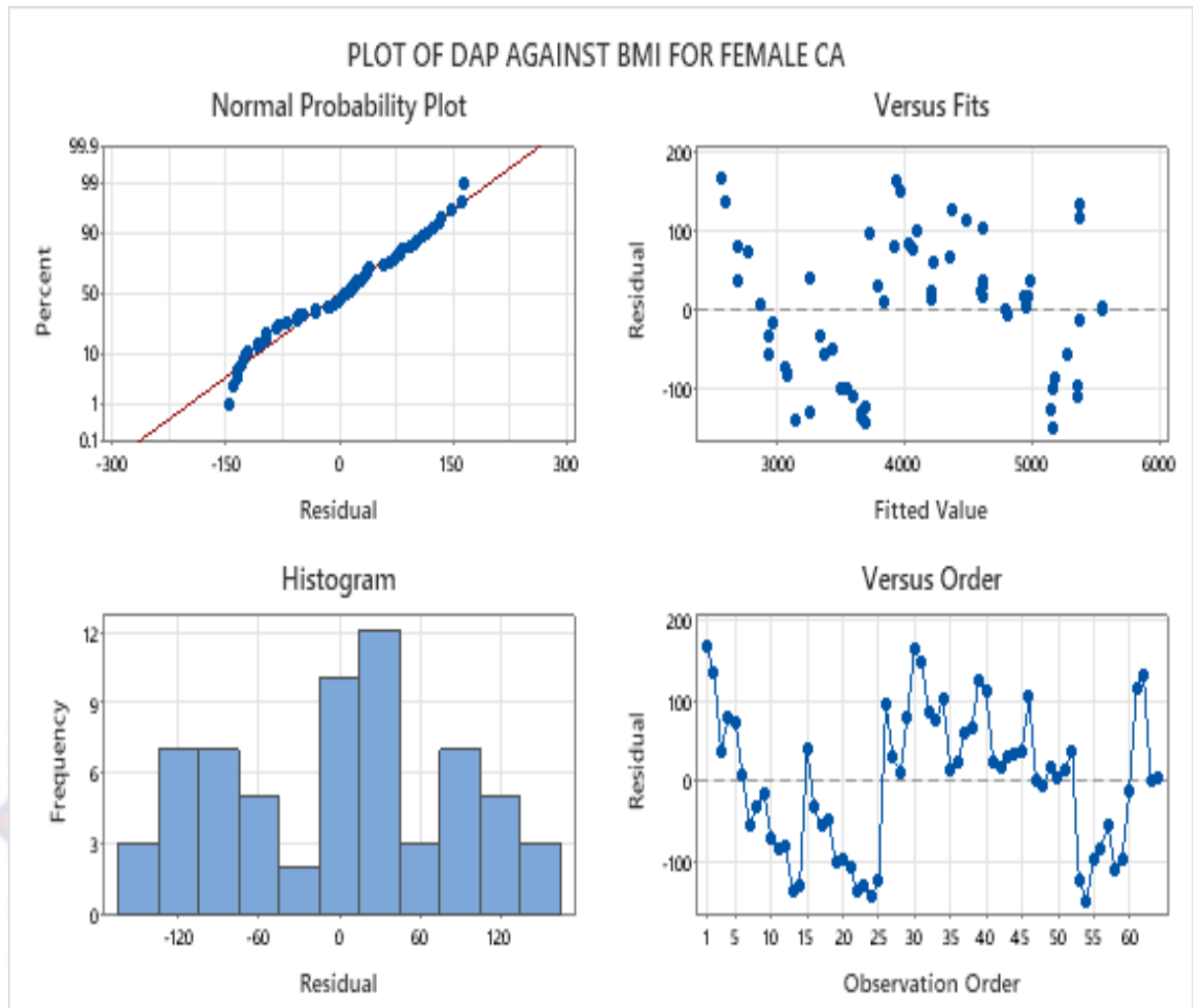
Appendix A-4: DAP and BMI for male RHC



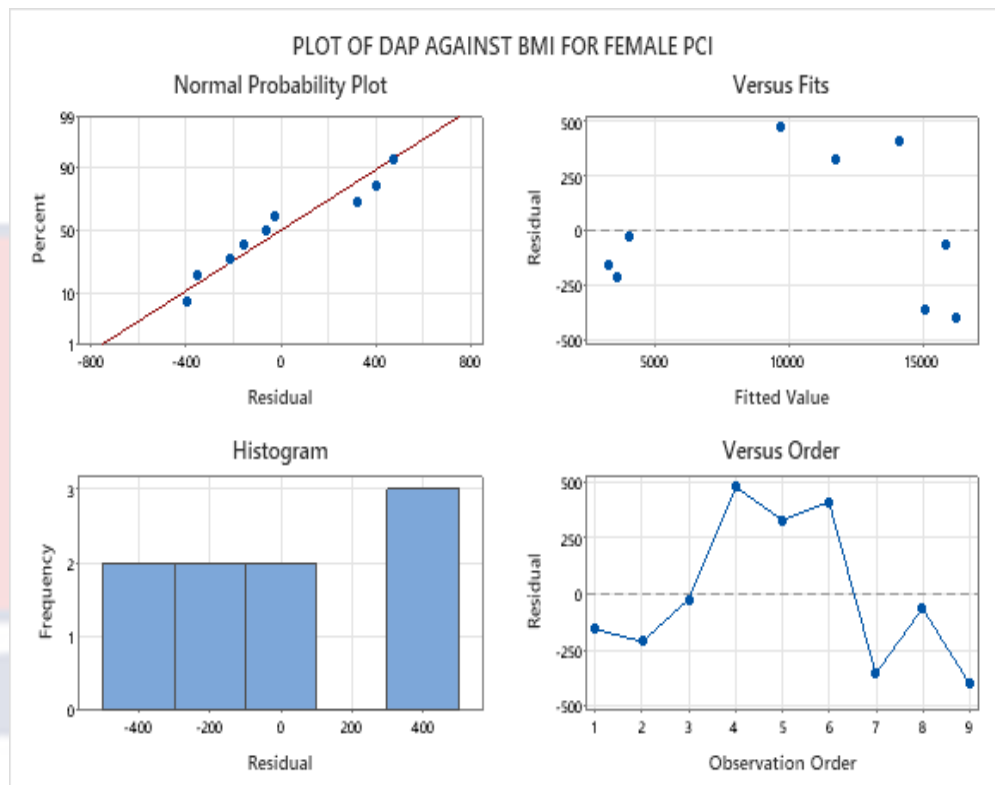
APPENDIX B

MODELLING DAP AND BMI FOR FEMALE PATIENTS

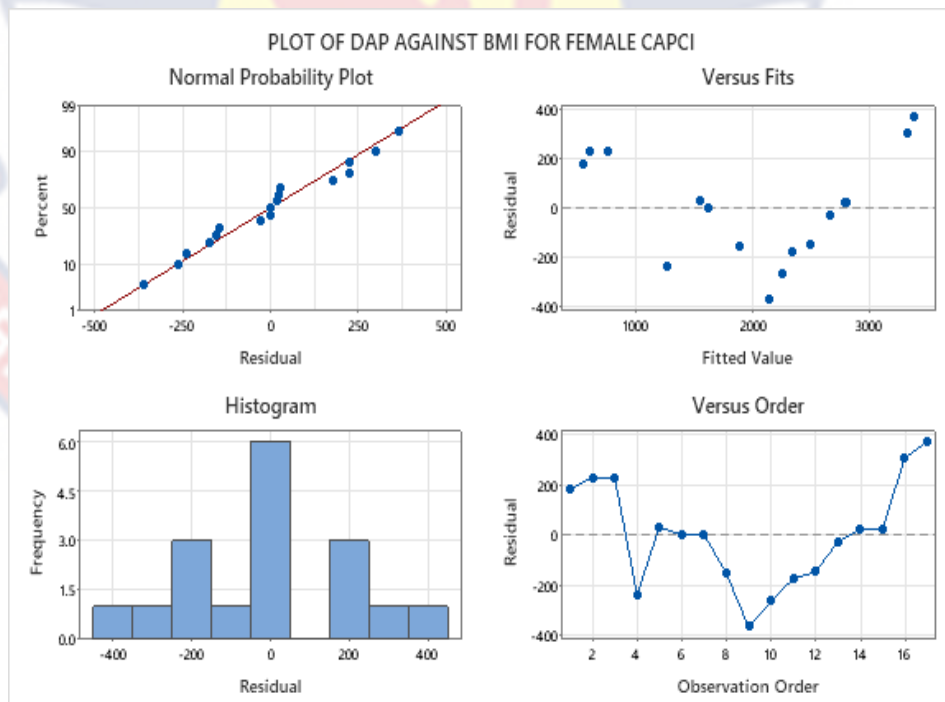
Appendix B-1: Linear DAP and BMI for female CA



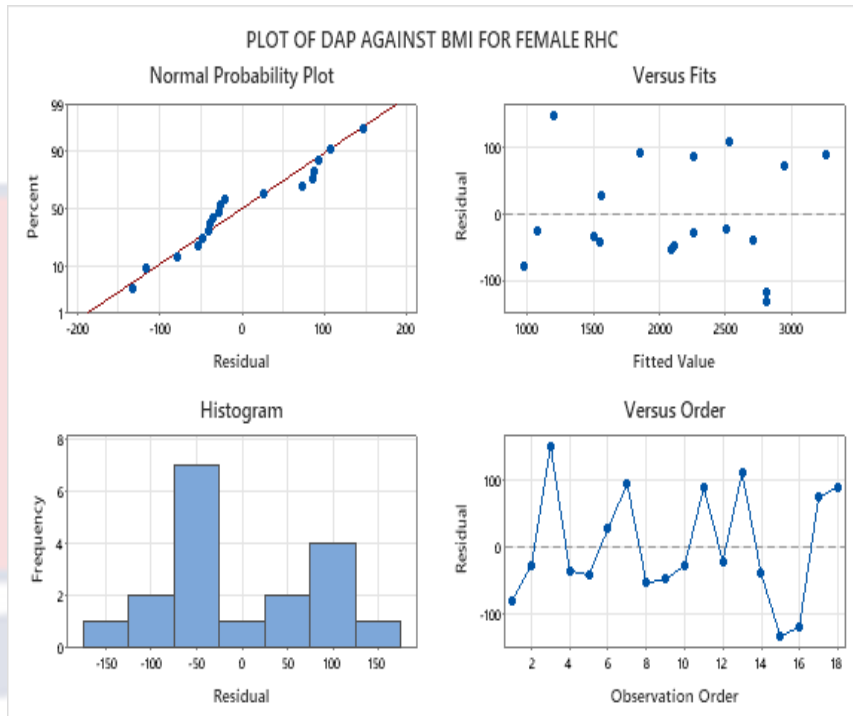
Appendix B-2: DAP and BMI for female PCI



Appendix B-3: DAP and BMI for female combined CAPCI



Appendix B-4: DAP and BMI for female RHC



APPENDIX C-1

ETHICAL CLEARANCE FROM UCC

UNIVERSITY OF CAPE COAST
INSTITUTIONAL REVIEW BOARD SECRETARIAT

TEL: 0558833443 / 0558833369
E-MAIL: irb@ucc.edu.gh
OUR REF: UCC/IRB/A/2016/0198
YOUR REF:
OMB NO: 0990-0279
IORG #: IORG0000006

10TH SEPTEMBER 2021

Mr. Emmanuel Akrobertu
Department of Physics
University of Cape Coast

Dear Mr. Akrobertu,

ETHICAL CLEARANCE – ID (UCCIRB/CANS/2020/04)

The University of Cape Coast Institutional Review Board (UCCIRB) has granted Provisional Approval for the implementation of your research titled **Radiation Dose, Image Quality and Risk assessment during Interventional cardiology Procedures: A Case at the National Cardiothoracic Centre, Korle Bu Teaching Hospital-Ghana**. This approval is valid from 10th September 2021 to 9th September 2022. You may apply for a renewal subject to submission of all the required documents that will be prescribed by the UCCIRB.

Please note that any modification to the project must be submitted to the UCCIRB for review and approval before its implementation. You are required to submit periodic review of the protocol to the Board and a final full review to the UCCIRB on completion of the research. The UCCIRB may observe or cause to be observed procedures and records of the research during and after implementation.

You are also required to report all serious adverse events related to this study to the UCCIRB within seven days verbally and fourteen days in writing.

Always quote the protocol identification number in all future correspondence with us in relation to this protocol.

Yours faithfully,

Samuel Asiedu Owusu, PhD
UCCIRB Administrator

ADMINISTRATOR
INSTITUTIONAL REVIEW BOARD
UNIVERSITY OF CAPE COAST

APPENDIX C-2

ETHICAL CLEARANCE FROM KBTH

In case of reply the number
And the date of this
Letter should be quoted

My Ref. No. KBTH/MB/193/22

Your Ref. No.



KORLE BU TEACHING HOSPITAL
P. O. BOX KB 77,
KORLE BU, ACCRA.

Tel: +233 302 667789/673834-6

Fax: +233 302 667759

Email: Info@kbth.gov.gh

pr@kbth.gov.gh

Website: www.kbth.gov.gh

10th March, 2022

EMMANUEL AKROBORTU
NUCLEAR REGULATORY AUTHORITY, HOUSES NO. 1 & 2
NEUTRON AVENUE, P.O. BOX AE 50, ATOMIC ENERGY
KWABENYA, ACCRA-GHANA

**INSTITUTIONAL APPROVAL: KORLE BU TEACHING HOSPITAL-SCIENTIFIC
AND TECHNICAL COMMITTEE/INSTITUTIONAL REVIEW BOARD (KBTH-
STC/IRB/00084/2020)**

Following approval of your study entitled "Statistical Assessment of Dose and Risk Evaluation during Interventional Cardiology Procedures: A Case Study at the National Cardiothoracic Centre, Korle-Bu Teaching Hospital-Ghana" by the Korle Bu Teaching Hospital-Scientific and Technical Committee/Institutional Review Board.

I am pleased to inform you that institutional approval has been granted for the conduct of your study in Korle Bu Teaching Hospital.

Please contact the Heads of Departments to discuss the commencement date of the study.

Please note that, this institutional approval is rendered invalid if the terms of the Institutional Reviewed Board/Scientific and Technical Committee approval are violated.

Sincere regards,

Dr. Ali Samba
Director of Medical Affairs
For: Chief Executive

In case of reply the number
And the date of this
Letter should be quoted

My Ref. No. KBTH/MB/168/22
Your Ref. No.



KORLE BU TEACHING HOSPITAL
P. O. BOX KB 77,
KORLE BU, ACCRA.

Tel: +233 302 667799/673034-6
Fax: +233 302 667759
Email: info@kbth.gov.gh
pr@kbth.gov.gh
Website: www.kbth.gov.gh

10th March, 2022

EMMANUEL AKROBORTU
NUCLEAR REGULATORY AUTHORITY, HOUSES NO. 1 & 2
NEUTRON AVENUE, P.O. BOX AE 50, ATOMIC ENERGY
KWABENYA, ACCRA-GHANA

**STATISTICAL ASSESSMENT OF DOSE AND RISK EVALUATION DURING
INTERVENTIONAL CARDIOLOGY PROCEDURES: A CASE STUDY AT THE
NATIONAL CARDIOTHORACIC CENTRE, KORLE-BU TEACHING HOSPITAL-
GHANA**

KBTH-IRB /00084/2020

Investigator: Emmanuel Akrobertu

The Korle Bu Teaching Hospital Institutional Review Board (KBTH IRB) reviewed and granted approval to the study entitled: "Statistical assessment of dose and risk evaluation during interventional cardiology Procedures: A Case Study at the National Cardiothoracic Centre, Korle-Bu Teaching Hospital-Ghana"

Please note that the Board requires you to submit a final review report on completion of this study to the KBTH-IRB.

Kindly, note that, any modification/amendment to the approved study protocol without approval from KBTH-IRB renders this certificate invalid.

Please report all serious adverse events related to this study to KBTH-IRB within seven days verbally and fourteen days in writing.

This IRB approval is valid till 30th January, 2023. You are to submit annual report for continuing review.

Sincere regards,

DR. DANIEL ANKRAH
VICE CHAIR (KBTH-IRB)
FOR: CHAIR (KBTH-IRB)

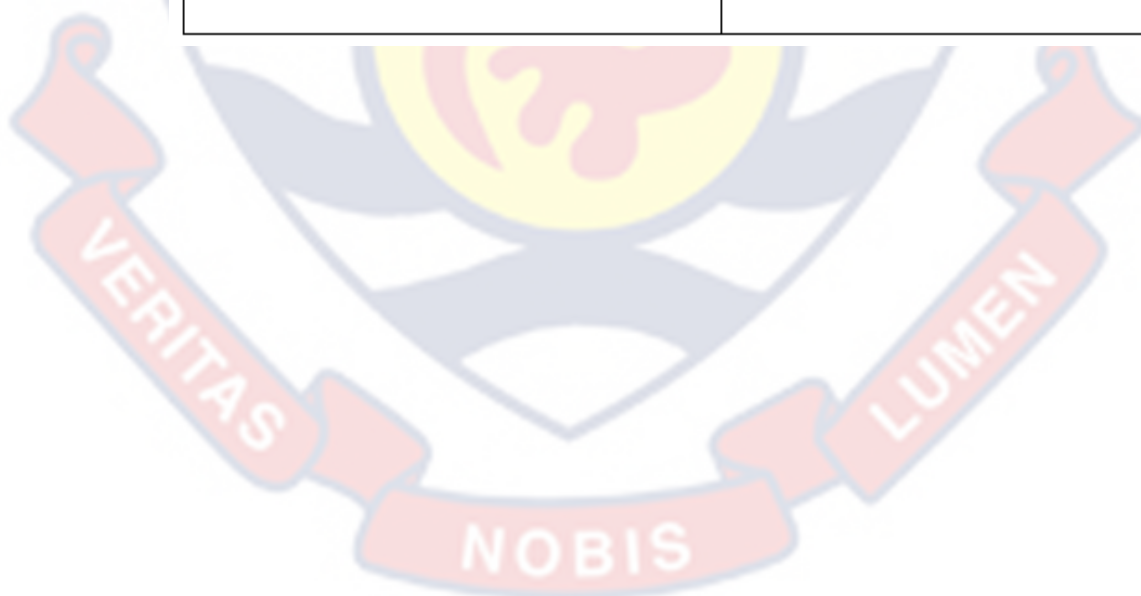
Cc: The Chief Executive Officer, KBTH
The Director of Medical Affairs, KBTH

NOBIS

APPENDIX D

Patient Dose Register

1. Patient's ID:	2. Patient's ID:
Sex:	Sex:
Procedure:	Procedure:
Weight:	Weight:
Age:	Age:
Height:	Height:
Dose/ <u>mGy</u> :	Dose/ <u>mGy</u> :
DAP dose/ <u>μGym^2</u> :	DAP dose/ <u>μGym^2</u> :
Time/Duration:	Time/Duration:
Tube Potential (<u>kVp</u>):	Tube Potential (<u>kVp</u>):
Tube Current (mA):	Tube Current (mA):
Filter <u>mmCu</u>):	Filter <u>mmCu</u>):
Date of Procedure:	Date of Procedure:
Name of Surgeon:	Name of Surgeon:
Names of Team Members:	Names of Team Members:
1.	1.
2.	2.
3.	3.
4.	4.
5.	5.



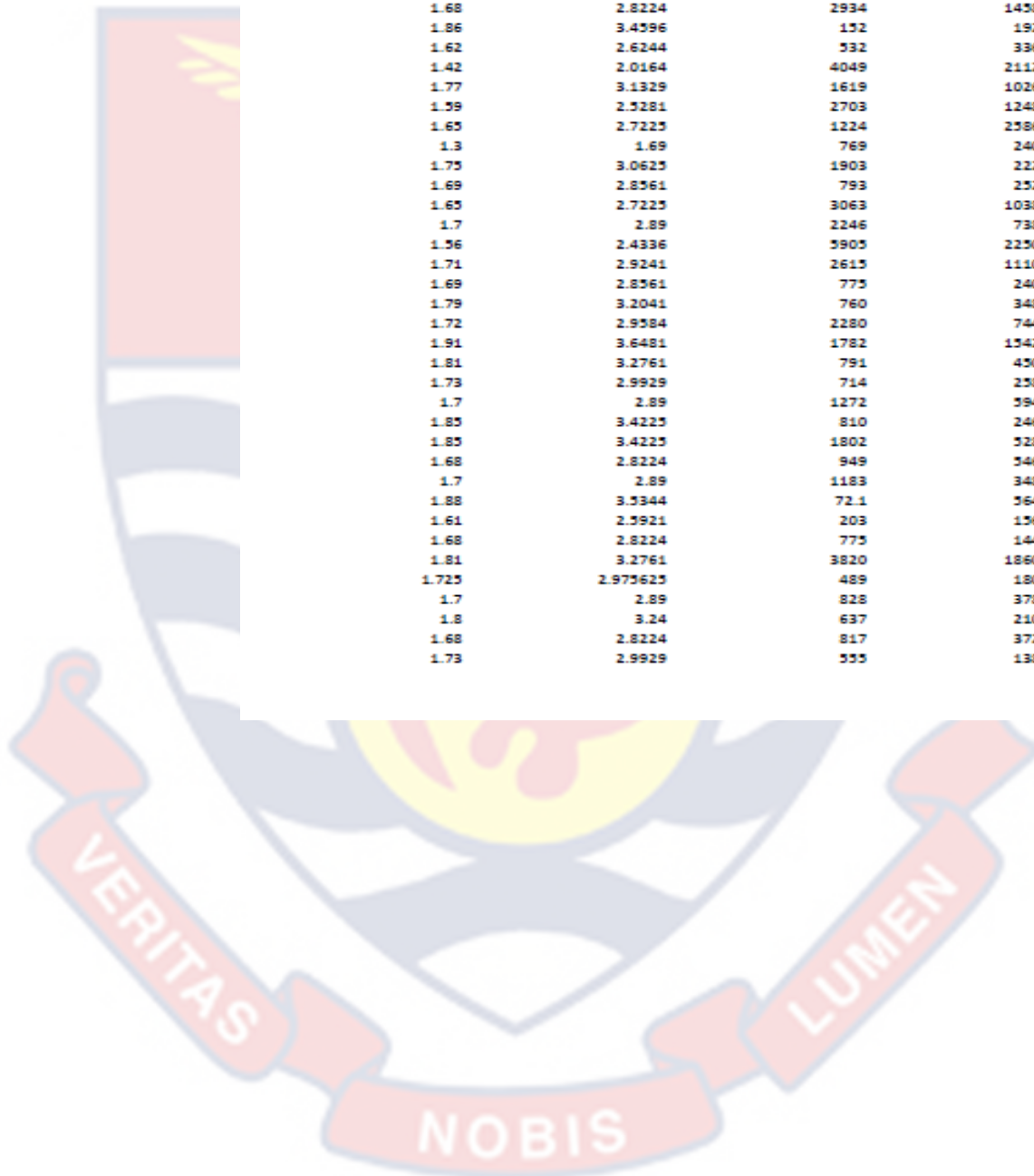
APPENDIX E

Raw Primary Data

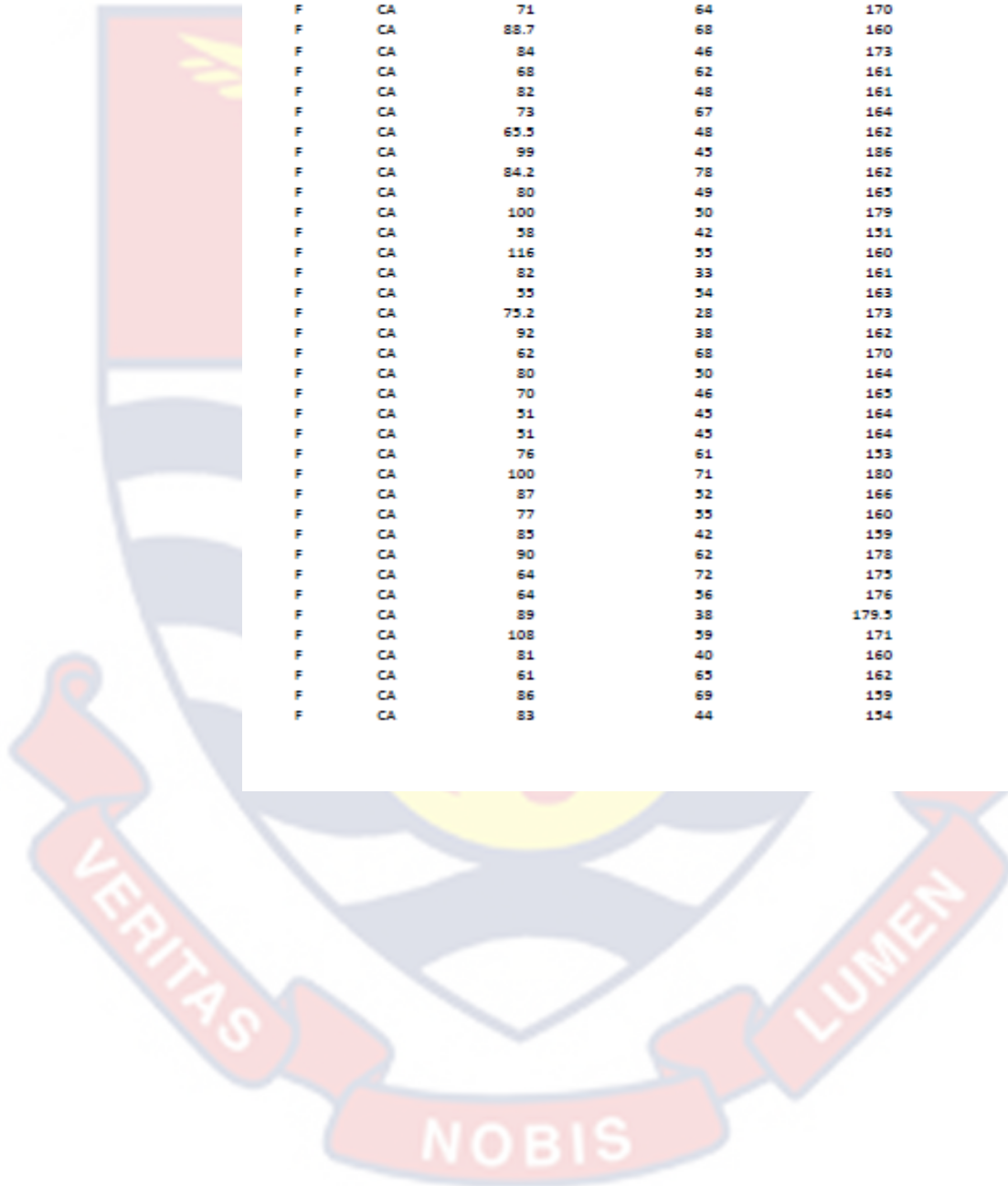
Gender	Procedure	Patient Weight (kg)	Patient Age (yrs)	Patient Height (cm)
M	CA	82	63	168
M	CA	105	69	169
M	CA	87	78	169
M	CA	71	71	168
M	CA	59	69	169
M	CA	72	66	162
M	CA	69	36	170
M	CA	92	65	175
M	CA	100	69	180
M	CA	69	36	136
M	CA	61	45	167.5
M	CA	99	63	168
M	CA	85	50	186
M	CA	110	48	162
M	CA	81	49	142
M	CA	95	50	177
M	CA	77	55	159
M	CA	80	65	165
M	CA	98	56	130
M	CA	110	64	175
M	CA	68	69	169
M	CA	84	69	165
M	CA	100	57	170
M	CA	70	49	156
M	CA	75	58	171
M	CA	69.4	46	169
M	CA	104	49	179
M	CA	78	58	172
M	CA	89.5	60	191
M	CA	78	36	181
M	CA	90	53	173
M	CA	96	60	170
M	CA	102.4	62	185
M	CA	120.7	49	185
M	CA	77.5	68	168
M	CA	76	53	170
M	CA	159.2	60	188
M	CA	68.2	56	161
M	CA	76	64	168
M	CA	81	78	181
M	CA	86.7	57	172.5
M	CA	67.6	81	170
M	CA	88	53	180
M	CA	68.9	74	168
M	CA	90.01	60	173

M	PCICA	75	75	164
M	PCICA	80	76	160
M	PCICA	66	71	162
M	PCICA	66	82	160
M	PCICA	74	58	169
M	PCICA	80	68	170
M	RHC	44	77	180
M	RHC	61	45	167.5
M	RHC	80	45	165
M	RHC	49	61	167
M	RHC	75	56	167
M	RHC	49	48	180
M	RHC	61.2	48	166
M	RHC	44	19	192
M	RHC	51	25	160
M	RHC	66	35	170
M	RHC	68	59	169

Patient Height (m)	Patient Height (m ²)	Patient Dose(μGym ²)	Procedure time (s)
1.68	2.8224	3315	1770
1.69	2.8561	1816	624
1.69	2.8561	622.7	474
1.68	2.8224	786	384
1.69	2.8561	2973	1140
1.62	2.6244	3209	1140
1.7	2.89	1521	2040
1.75	3.0625	1398	678
1.8	3.24	1267	744
1.36	1.8496	437	234
1.675	2.805625	70	288
1.68	2.8224	2934	1458
1.86	3.4596	152	192
1.62	2.6244	532	336
1.42	2.0164	4049	2112
1.77	3.1329	1619	1026
1.59	2.5281	2703	1248
1.65	2.7225	1224	2586
1.3	1.69	769	240
1.75	3.0625	1903	222
1.69	2.8561	793	252
1.65	2.7225	3063	1038
1.7	2.89	2246	738
1.56	2.4336	5905	2250
1.71	2.9241	2615	1110
1.69	2.8561	775	240
1.79	3.2041	760	348
1.72	2.9584	2280	744
1.91	3.6481	1782	1542
1.81	3.2761	791	450
1.73	2.9929	714	258
1.7	2.89	1272	594
1.85	3.4225	810	246
1.85	3.4225	1802	528
1.68	2.8224	949	546
1.7	2.89	1183	348
1.88	3.5344	72.1	564
1.61	2.5921	203	156
1.68	2.8224	775	144
1.81	3.2761	3820	1860
1.725	2.975625	489	180
1.7	2.89	828	378
1.8	3.24	637	210
1.68	2.8224	817	372
1.73	2.9929	555	138



Gender	Procedure	Patient We	Patient Age (yrs)	Patient Height (cm)	Patient Height (m)
F	CA	72		87	1.65
F	CA	71		89	1.59
F	CA	62		71	1.6
F	CA	68		60	1.82
F	CA	67		70	1.53
F	CA	85		62	1.628
F	CA	69		56	1.6
F	CA	75		70	1.61
F	CA	130		77	1.8
F	CA	71		64	1.7
F	CA	88.7		68	1.6
F	CA	84		46	1.73
F	CA	68		62	1.61
F	CA	82		48	1.61
F	CA	73		67	1.64
F	CA	65.5		48	1.62
F	CA	99		45	1.86
F	CA	84.2		78	1.62
F	CA	80		49	1.65
F	CA	100		50	1.79
F	CA	58		42	1.51
F	CA	116		55	1.6
F	CA	82		33	1.61
F	CA	55		54	1.63
F	CA	75.2		28	1.73
F	CA	92		38	1.62
F	CA	62		68	1.7
F	CA	80		50	1.64
F	CA	70		46	1.65
F	CA	51		45	1.64
F	CA	51		45	1.64
F	CA	76		61	1.53
F	CA	100		71	1.8
F	CA	87		52	1.66
F	CA	77		55	1.6
F	CA	85		42	1.59
F	CA	90		62	1.78
F	CA	64		72	1.75
F	CA	64		56	1.76
F	CA	89		38	1.795
F	CA	108		59	1.71
F	CA	81		40	1.6
F	CA	61		65	1.62
F	CA	86		69	1.59
F	CA	83		44	1.54



Patient Height (m ²)	DAP Dose(μGym ²)	DAP Dose(Gym ²)	Procedure time (s)	BMI (kg/m ²)
2.7225	4118.46	0.00411846	342	26.44628099
2.5281	3399.66	0.00339966	390	28.08433211
2.56	5490.32	0.00549032	1320	24.21875
3.3124	11754.2	0.0117542	1236	20.52892163
2.3409	5222.02	0.00522202	384	28.62147037
2.650384	11609.06	0.01160906	888	32.07082445
2.56	2729.7	0.0027297	294	26.933123
2.5921	4724.12	0.00472412	552	28.9340689
3.24	8651.83	0.00865183	234	40.12345679
2.89	4222.93	0.00422293	498	24.36747403
2.56	12.95	0.00001295	1152	34.6484375
2.9929	29238.99	0.02923899	1896	28.06642387
2.5921	7993.36	0.00799336	702	26.2335558
2.5921	70491	0.070491	840	31.634582
2.6896	6839.28	0.00683928	510	27.14138239
2.6244	8795.06	0.00879506	774	24.95808566
3.4596	9843	0.009843	564	28.61602497
2.6244	10532	0.010532	618	32.08352385
2.7225	6076.59	0.00607659	378	29.38475666
3.2041	6892	0.006892	528	31.21001217
2.2801	4497.64	0.00449764	576	25.43748081
2.56	7406.9	0.0074069	588	45.3125
2.5921	4951.64	0.00495164	192	31.634582
2.6569	6827.6	0.0068276	858	20.70081674
2.9929	6740.8	0.0067408	528	25.12613185
2.6244	8063.56	0.00806356	498	35.05563176
2.89	12365.92	0.01236592	900	21.4532872
2.6896	13304.79	0.01330479	1032	29.74419988
2.7225	6151.45	0.00615145	282	25.71166208
2.6896	1551.13	0.00155113	162	18.96192742
2.6896	1551.13	0.00155113	162	18.96192742
2.3409	4624.3	0.0046243	318	32.4661455
3.24	12060.92	0.01206092	744	30.86419753
2.7556	9146.5	0.0091465	978	31.37207142
2.56	4655.82	0.00465582	918	30.078125
2.5281	5361.92	0.00536192	468	33.62208773
3.1684	1813.7	0.0018137	180	28.40550436
3.0625	2079.8	0.0020798	126	20.89795918
3.0976	2426.58	0.00242658	150	20.66115702
3.222025	5897.26	0.00589726	270	27.62238034
2.9241	9959.59	0.00995959	462	36.93444137
2.56	1378	0.001378	492	31.640625
2.6244	3853.3	0.0038533	360	23.24340802
2.5281	4143.19	0.00414319	270	34.01764171
2.3716	5557.83	0.00555783	210	34.99747006

